An Islanding Model for Preventing Wide-Area Blackouts and the Issue of Local Solutions of the Optimal Power Flow Problem

Waqquas A. Bukhsh

Doctor of Philosophy
University of Edinburgh
2014

Declaration

I declare that this thesis was composed by myself and that the work contained therein is my own, except where explicitly stated otherwise in the text.

(*Waqquas A. Bukhsh*)

Declaration

The candidate confirms that the work submitted is his own, except where work which has formed part of jointly-authored publications has been included. The contribution of the candidate and the other authors to this work has been explicitly indicated below. The candidate confirms that appropriate credit has been given within the thesis where reference has been made to the work of others.

(*Waqquas Bukhsh*)

In this thesis chapter 3, 6 and 7 include some of the material that also appears in the jointly authored papers. The author has worked closely on all the material presented here from these papers. Reference to the jointly-authored papers are given for the material which is not included in the thesis.

- P. A. Trodden, W. A. Bukhsh, A. Grothey, and K. I. M. McKinnon, *Optimization-based Islanding of Power Networks using Piecewise Linear AC Power Flow*, Accepted for publication in IEEE Transactions on Power Systems, Nov. 2013
- W. A. Bukhsh, A. Grothey, Ken I. M. McKinnon and Paul A. Trodden, *Local solutions of the optimal power flow problem*, IEEE Transactions on Power Systems, vol. 28, No. 4, Nov. 2013
- P. A. Trodden, W. A. Bukhsh, A. Grothey, and K. I. M. McKinnon, *MILP formulation for controlled islanding of power networks*, International Journal of Electrical Power & Energy Systems, vol. 45, no. 1, pp. 501-508, 2013
- W. A. Bukhsh, A. Grothey, Ken I.M. McKinnon and Paul A. Trodden, *Local solutions of optimal power flow*, Tech. Rep. ERGO 11-017, Edinburgh Research Group in Optimization, School of Mathematics, University of Edinburgh, 2011.
- P. A. Trodden, W. A. Bukhsh, A. Grothey, and K. I. M. McKinnon, *MILP formulation for islanding of power networks*, Tech. Rep. ERGO 11-015, Edinburgh Research Group in Optimization, School of Mathematics, University of Edinburgh, 2011.

The test case archive for local solutions can be found on the following link:

http://www.maths.ed.ac.uk/OptEnergy/LocalOpt/,

where the relevant documentation is also to be found. The network data of some real world transmission networks can be found on the following link:

http://www.maths.ed.ac.uk/OptEnergy/NetworkData/.

Posters presented on this work in various conferences and workshops can be found here:

http://www.maths.ed.ac.uk/OptEnergy/Posters/

To Ami, Abu and Sarah.

Abstract

Optimization plays a central role in the control and operation of electricity power networks. In this thesis we focus on two very important optimization problems in power systems. The first is the optimal power flow problem (OPF). This is an old and well-known nonconvex optimization problem in power system. The existence of local solutions of OPF has been a question of interest for decades. Both local and global solution techniques have been put forward to solve OPF problem but without any documented cases of local solutions. We have produced test cases of power networks with local solutions and have collected these test cases in a publicly available online archive (http://www.maths.ed.ac.uk/optenergy/LocalOpt/), which can be used now by researchers and practitioners to test the robustness of their solution techniques. Also a new nonlinear relaxation of OPF is presented and it is shown that this relaxation in practice gives tight lower bounds of the global solution of OPF.

The second problem considered is how to split a network into islands so as to prevent cascading blackouts over wide areas. A mixed integer linear programming (MILP) model for islanding of power system is presented. In recent years, islanding of power networks is attracting attention, because of the increasing occurrence and risk of blackouts. Our proposed approach is quite flexible and incorporates line switching and load shedding. We also give the motivation behind the islanding operation and test our model on variety of test cases. The islanding model uses DC model of power flow equations. We give some of the shortcomings of this model and later improve this model by using piecewise linear approximation of nonlinear terms. The improved model yields good feasible results very quickly and numerical results on large networks show the promising performance of this model.

Lay Summary

The optimal power flow problem (OPF) is a well-studied optimization problem in power systems. This problem was first introduced by Carpentier in 1962, and since then various extensions of OPF and solution techniques to solve OPF have been proposed. The objective of OPF is to find a steady state operating point that minimizes the cost of electric power generation while satisfying operating constraints and meeting demand. The problem can be formulated as a nonlinear programming (NLP) problem, in which some constraints and possibly the objective function are nonlinear. Because of the nonlinearity there is a possibility that local solutions may exist for NLP problems. A local solution meets all the constraints but it is inferior in the objective value and there is no better solution close to it, but there may be a better solution further away. Thus a local solution obviously means spending more money on the fuel costs to meet the same demand in the electricity network. It is therefore important and desirable to seek global solution of OPF.

The issue of the possible existence of local optima to the OPF problem is an important one, but one that is not well covered in the literature. To best of our knowledge there were no documented cases of local solutions within reasonable voltage limits. In this thesis we provide networks for OPF problem with local solutions. All the cases are made available online in a archive, so that the researchers can use these as test cases to evaluate the robustness of their solution techniques. In this thesis we present the performance of a recent global optimization technique to solve OPF and compare it with a nonlinear relaxation of OPF problem we have developed. It is shown that this relaxation is more likely to yield good bounds to the global solution of OPF.

The second problem we discuss is the islanding of power systems. Power systems are designed to handle minor disturbances. But sometimes unpredictable events like wind storms or natural disasters happen and cause severe imbalance of generation and demand. Since power systems are not designed to handle such a situation, cascading outages can occur and lead to a large area blackout. Islanding is a control action that is used to restrict and minimize the affects of disturbance to a small area in network by electrically isolating it.

Here we propose an islanding model in a form of mixed integer linear programming

problem (MILP). The DC model of power flow equations is used in the islanding model. First we use the well known DC model of the power flow equations and show this has serious shortcomings, and then improve this model by using piecewise linear approximations of nonlinearities. Numerical experiments on variety of test networks are discussed, and we also discuss some issues involved in solving this problem in real time. Finally we conclude and give some future research directions.

Acknowledgements

I wish to express my deepest gratitude to my supervisor Ken McKinnon. This thesis would not have been possible had it not been Ken's kindness, patience and quality of teaching. All of which I really appreciate. I would also like to thank Andreas Grothey and Paul Trodden for many interesting discussions and insightful comments.

I am grateful for the financial support for my PhD from the EPSRC research grant and from the School of Mathematics.

I would like to thank all my colleagues and friends in the School of Mathematics, especially my office mates Feng and Yiming for the light hearted discussions.

I am indebted to my parents and siblings for their understanding, endless patience and encouragement when it was most needed. Thank-you to my wife Sarah, for her love, support and care. It is because of her I have been able to maintain a sustainable level of work/life balance throughout my PhD.

Finally thank you Edinburgh for making me feel at home. Sarah and I felt very welcomed in this lovely city and our time has been wonderful in so many different ways. Thank you to every one who helped, chatted and smiled.

Waqquas Bukhsh
(February 2014, Edinburgh)

Nomenclature

Sets

$\mathcal{B}$ Set of buses (nodes), indexed by b.

$\mathcal{L}$ Set of lines, indexed by l. It can also be indexed by bb' where the pair $(b, b') \in \mathcal{B} \times \mathcal{B}$ and denotes to and $from$ ends of transmission line.

$\mathcal{G}$ Set of generators, indexed by g.

$\mathcal{D}$ Set of loads, indexed by d.

$\mathcal{B}_l$ Set of buses connected by line l.

$\mathcal{L}_b$ Set of lines connected to bus b.

$\mathcal{G}_b$ Set of generators located at bus b.

$\mathcal{D}_b$ Set of loads located at bus b.

$\mathcal{B}^0$ Set of buses assigned to section 0.

$\mathcal{B}^1$ Set of buses assigned to section 1.

$\mathcal{L}^0$ Set of uncertain lines.

$\mathcal{B}^{\mathrm{G}}$ Set of generator buses.

Parameters

$\tau_{bb'}$ Off-nominal tap ratio of line (b, b') (if transformer).

β_d Loss penalty for load d.

$P_l^{\mathrm{L}+}$ Real power loss limit of line l.

$G_b^{\mathrm{B}}, B_b^{\mathrm{B}}$ Shunt conductance, susceptance at bus b.

$V_b^{\mathrm{LB}}, V_b^{\mathrm{UB}}$ Min., max. voltage magnitude at bus b.

$P_g^{\mathrm{LB}}, P_g^{\mathrm{UB}}$ Min., max. real power outputs of generator g.

$Q_g^{\mathrm{LB}}, Q_g^{\mathrm{UB}}$ Min., max. reactive power outputs of generator g.

$P_d^{\mathrm{D}}, Q_d^{\mathrm{D}}$ Real, reactive power demands of load d.

Θ_l, Θ_l^+ Max. angle across l if connected, disconnected.

$C_g(p_g^{\mathrm{G}})$ Generation cost function for generator g.

$G_{bb'}, B_{bb'}$ Conductance, Susceptance of line (b, b')

Variables

v_b, δ_b Voltage magnitude and phase at bus b.

$\theta_{bb'}$ $\delta_b - \delta_{b'}$, voltage phase difference between bus b and b'. Note $\theta_{bb'} = -\theta_{bb'}$.

$y_{bb'}$ $\cos\theta_{bb'}$. Note $y_{bb'} = y_{b'b}$.

$z_{bb'}$ $\sin\theta_{bb'}$. Note $z_{bb'} = -z_{bb'}$.

$\theta_l^{bb'}$ Voltage phase difference across a line l. Note $\theta_l^{bb'} = -\theta_l^{bb'}$.

$y_l^{bb'}$ $\cos\theta_l^{bb'}$. Note $y_l^{bb'} = y_l^{bb'}$.

α_d Proportion of load d supplied.

γ_b Binary. Section (0 or 1) assignment of bus b.

ζ_g Binary. Connection status of generator g.

$\rho_{bb'}$ Binary. Connection status of line l.

$v_l^b, v_l^{b'}$ Voltage magnitudes at either end of line l (which connects buses b and b').

$p_l^{bb'}, q_l^{bb'}$ Real, reactive power injection at bus b into line l (which connects buses b and b').

$p_g^{\mathrm{G}}, q_g^{\mathrm{G}}$ Real, reactive power outputs of generator g.

$p_d^{\mathrm{D}}, q_d^{\mathrm{D}}$ Real, reactive power supplied to load d.

Note that we use the convention of lower case for variables and upper case for parameters.

Contents

List of Tables

List of Figures

Chapter 1

Introduction

In the modern world, life without electricity is difficult to conceive. Most of our daily needs are met by electricity in one way or the other, and our life is becoming totally dependent on it. The ability to generate and transmit electricity, and invention of the machines to use it have changed our world in many different ways. The complex system responsible for generating, transmitting and distributing electricity is known as *power system*. The increased dependence of our lives on electricity demands a reliable and efficient power system to be in place.

The history of power system can be traced back to early 1880's; a few years after Thomas Edison invented the light bulb. Power system did not have an easy beginning. World's first power system, generating direct current (DC), started its operation on 4th September, 1882 at Pearl Street, USA. One hundred incandescent bulbs were illuminated on Wall Street using the DC current from Pearl street power station. This was a huge leap forward but there was a problem. Edison calculated that with his power system, he can only supply power within one square mile of the Pearl Street power station. That meant Edison's power system would never be economical to scale up. The next major break through was made by Nicola Tesla by introducing alternating current (AC) for transmission. Tesla showed that using AC current, power can be transferred over long distances. In July 1888, George Westinghouse bought Tesla's patents and started working on AC power systems. Edison believed that his DC transmission is much safer than the AC transmission. An era of rivalry between Edison and Westinghouse followed; which is remembered in history as the *war of currents*. In 1895, Westinghouse opened the first AC power station at Niagara falls. The Niagara falls power station was able to transport electricity more than 200 miles. This was the beginning of the new era of modern world. Till date electricity is transmitted on the principles pioneered by Tesla. Had we stuck with DC way of transmitting electricity, the world would be a very different place. Since 1895, power system has experienced tremendous evolution and with less than 120 years, it has lit up the whole world.

Normally electricity is produced far from populations centres, and is transported to consumers through transmission lines. Due to wide geographical distribution of consumers, transmission lines cover long distances, which makes power system a massive network. The enormous size of power system is not the only challenge for analysis and operation, but power system has some peculiar properties as well. Electricity can not be stored in large amount so the demand has to be matched to generation in real time. Also unlike gas networks, there are no valves to direct electricity, the flow of electricity is determined by the Kirchhoff's laws. These distinctive properties make power system a challenging yet interesting network to study.

In power system operation, the emphasize has always been on the generation side. Control resides with the generators and they react to the changes in demand. However in recent years, there is a focus on also putting control on the demand side of power system, and making the demands sensitive to the prices of electricity. However this is a question of ongoing research in power system and to date the control mainly resides with generators.

In this thesis we study two well known optimization problems which are concerned with the operation of power system. My aim in this chapter is to give the basic vocabulary and concepts, so that in the next chapters I can build upon these concepts. An effort has been made to keep the introductory material concise. Adequate references are made so that the reader can refer to the published material for further reading.

1.1 Structure of Power System

A power system is a complex interconnected network consisting of many components. Generally power system can be divided into the following four major components:

- Generators
- Transmission Network
- Distribution Network
- Demands

Electricity is secondary form of energy *i.e.*, it has to be converted from primary source. Generators are huge masses which rotate and convert mechanical energy into electrical energy. The source of mechanical energy depends on the type of generators. All conventional generators need some kind of fuel to operate. The most common fuels are coal, natural gas and nuclear. The use of these conventional fuels result in the emission of CO_2 gases which pollute the environment. Also there is a strong opposition to nuclear stations because of the high risks involved with the operation and waste

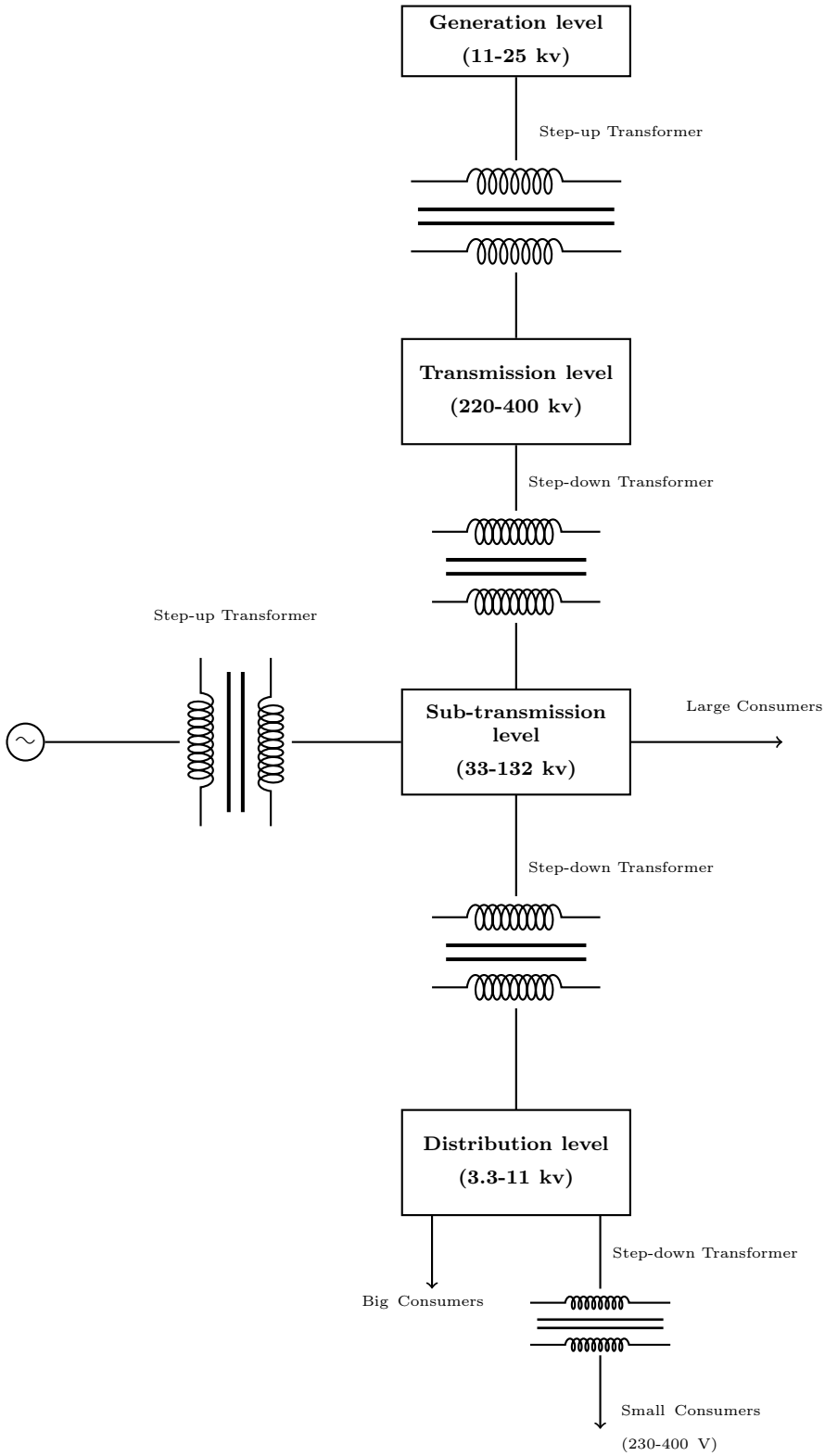

Figure 1.1: Structure of Power System

disposal. Due to these reasons a major part of power system research is focusing on environmental friendly fuels *e.g.*, wind and solar power.

The electricity produced by the generators is transmitted through transmission lines. These are the highways of electricity, connecting generators to the demands. A part of electrical power generated is lost in transmission lines, because of the resistive nature of the conductors. Power transferred through a transmission line is equal to current times the voltage. Therefore same amount of power can be transmitted by reducing the current and increasing the voltage in equal proportions. The power lost is equal to the current squared times the resistance, reducing the current we reduce the loss by the square. Because of this voltage is stepped up for transmission. For the distribution of electricity to customers, the voltage is stepped down because of the safety reasons, and also to increase the amount of current at the output (more current provides more torque for the electric motors). In the UK, the loss in the transmission network is around 2% [3] whereas, it is much higher in the distribution network (6% [4]).

The hierarchical structure of power system is shown in the Fig. 1.1. It shows that a power system consists of many different voltage levels. The *per unit* system is used to simplify the analysis of power system. A common set of base parameters is used to define all other quantities. The advantage of using per unit system is that the voltage bounds on each level can be defined in a similar way without the need of scaling. Let V, I, S and Z denotes the voltage, current, power and impedance respectively. The per unit conversion of these quantities is:

$$V_{pu} = \frac{V}{V_{base}}, \quad I_{pu} = \frac{I}{I_{base}}, \quad S_{pu} = \frac{S}{S_{base}}, \quad Z_{pu} = \frac{Z}{Z_{base}}.$$

We need two base values, and other base values can be calculated from them by the following relations:

$$I_{base} = \frac{S_{base}}{V_{base}}, \quad Z_{base} = \frac{V_{base}}{I_{base}}.$$

1.2 Role of Optimization in Power System Operation

Optimization plays an important role in various aspects of power system planning and operation. Optimization models are used for planning expansion of power system when the forecasts of demand and fuel prices are given. The problem is to find cost-effective additions to generation capacity of existing power system. Also maintenance and fuel scheduling is determined with the help of optimization models [5].

Power systems around the world are usually operated under *(N-1) criterion*. This basic principle of power system operation says that any single event leading to the failure of a single power system component should not endanger the security of the remainder

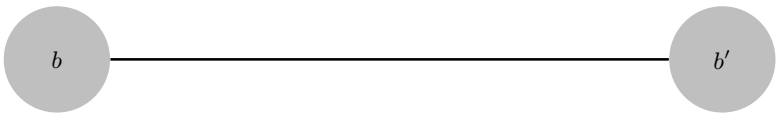

(a) Transmission line from b to b'

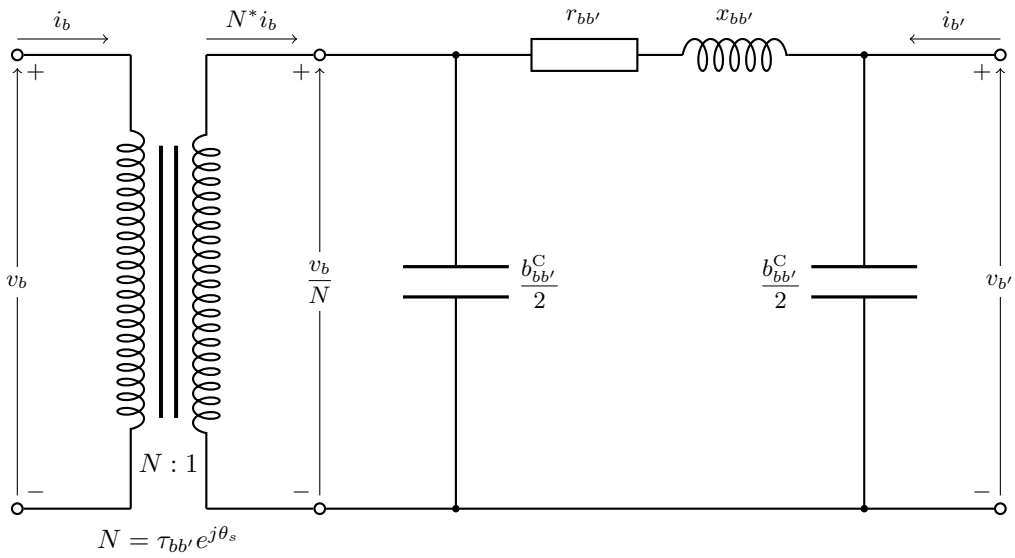

(b) π model of the transmission line

Figure 1.2: Transmission line model.

of the power system. In the UK the power system is operated under *(N-2) criterion*. An optimization model commonly known as security constrained optimal power flow (SCOPF) [6] is used to solve this problem. Optimization models are also used in real and short term time periods to determine the on/off state of the generators, and to optimize when to switch them on and off so as to generate among generation capacity to meet the current demand.

The optimization problems in power systems are not trivial. They have all the ingredients that makes them tough and challenging, like nonconvexity, huge network size and the complexity of the nonlinear Kirchhoff's laws that makes them tough and challenging.

1.3 Mathematical Model of the Power System

Mathematical models of the flow of electricity are used in power systems for control and planning purposes, and form basis of all the analysis. Simulation packages based on these models help engineers to control the power system. Also due to economic considerations and physical constraints, often these models are used within optimization problems. In this section we will derive the network equations of power system.

In power systems terminology nodes are called *buses* and edges are called *lines*. Consider a transmission line from bus b to b' as shown in the Fig. 1.2(a). The transmission

line is represented by an equivalent circuit in Fig. 1.2(b), commonly known as π model of a transmission line. Let $r_{bb'}$ and $x_{bb'}$ denotes the resistance and reactance of the transmission line, and let $b^{\mathrm{C}}_{bb'}$ denotes the line charging susceptence and in the π model of transmission line half of it is lumped at each end of the line. Let $\tau_{bb'}$ denotes the tap ratio and θ_s denotes the phase angle shift of the transformer. To simplify the derivation we assume that the phase shift due to the transformer is zero. The impedance of the line (b, b') is denoted and defined by $\mathbf{z}_{bb'} = r_{bb'} + jx_{bb'}$. The inverse of impedance is known as admittance and it is defined as $\mathbf{y}_{bb'} = g_{bb'} + jb_{bb'}$, where

$$g_{bb'} = \frac{r_{bb'}}{r^2_{bb'} + x^2_{bb'}}, \qquad b_{bb'} = \frac{-x_{bb'}}{r^2_{bb'} + x^2_{bb'}}.$$

Let $\mathbf{v}_b$ and $\mathbf{v}_{b'}$ denotes the complex voltage at buses b and b' respectively. Let $\mathbf{i}_{bb'}$ and $\mathbf{i}_{b'b}$ denote the current going into the line bb' out of b and b' respectively. These are given by the following equations;

$$\tau_{bb'}\mathbf{i}_{bb'} = \frac{\mathbf{v}_b}{\tau_{bb'}}\frac{jb^{\mathrm{C}}_{bb'}}{2} + (\frac{\mathbf{v}_b}{\tau_{bb'}} - \mathbf{v}_{b'})(g_{bb'} + jb_{bb'}), \tag{1.1a}$$

$$\mathbf{i}_{b'b} = \mathbf{v}_{b'}\frac{jb^{\mathrm{C}}_{bb'}}{2} + (\mathbf{v}_{b'} - \frac{\mathbf{v}_b}{\tau_{bb'}})(g_{bb'} + jb_{bb'}). \tag{1.1b}$$

Current flowing into line bb' out of bus b is $\tau_{bb'}\mathbf{i}_{bb'}$ and the voltage at bus b is $\frac{\mathbf{v}_b}{\tau_{bb'}}$. This is because we have considered transformer at b end of the line. When there is no transformer between the buses b and b' then $\tau_{bb'} = 1$. The equations (1.1) can be rewritten in the following form:

$$\tau_{bb'}\mathbf{i}_{bb'} = \left(g_{bb'} + j(b_{bb'} + \frac{b^{\mathrm{C}}_{bb'}}{2})\right)\frac{\mathbf{v}_b}{\tau_{bb'}} - (g_{bb'} + jb_{bb'})\mathbf{v}_{b'}, \tag{1.2a}$$

$$\mathbf{i}_{b'b} = \left(g_{bb'} + j(b_{bb'} + \frac{b^{\mathrm{C}}_{bb'}}{2})\right)\mathbf{v}_{b'} - (g_{bb'} + jb_{bb'})\frac{\mathbf{v}_b}{\tau_{bb'}}. \tag{1.2b}$$

We rewrite the equations (1.2) in the following form:

$$\mathbf{i}_{bb'} = \hat{\mathbf{Y}}_{bb'}\mathbf{v}_b + \mathbf{Y}_{bb'}\mathbf{v}_{b'}, \tag{1.3a}$$

$$\mathbf{i}_{b'b} = \mathbf{Y}_{b'b}\mathbf{v}_b + \hat{\mathbf{Y}}_{b'b}\mathbf{v}_{b'}, \tag{1.3b}$$

where

$$\tau_{bb'}^2 \hat{\mathbf{Y}}_{bb'} = \hat{\mathbf{Y}}_{b'b} = \left(g_{bb'} + j(b_{bb'} + \frac{b_{bb'}^{\mathrm{C}}}{2}) \right),$$
$$\mathbf{Y}_{b'b} = \mathbf{Y}_{bb'} = (G_{bb'} + jB_{bb'}),$$
$$g_{bb'} = -\tau_{bb'} G_{bb'} = -\tau_{bb'} G_{b'b} = G_{b'b'},$$
$$b_{bb'} + 0.5 b_{bb'}^{C} = B_{b'b'},$$
$$-b_{bb'} = \tau_{bb'} B_{b'b} = \tau_{bb'} B_{bb'}.$$

Our next task is to generalize these equations to a network with n^{B} buses. To generalize this we make use of a fundamental law in circuit analysis known as Kirchhoff's current law (KCL). KCL states that at any point in the circuit the total current entering is exactly equal to the total current leaving the point. The point may be considered any where in the circuit. Applying KCL at bus b we have:

$$\mathbf{i}_b = \sum_{b' \in \mathcal{B}_b} \mathbf{i}_{bb'} = \mathbf{v}_b \sum_{b' \in \mathcal{B}_b} \hat{\mathbf{Y}}_{bb'} + \sum_{b' \in \mathcal{B}_b} \mathbf{Y}_{bb'} \mathbf{v}_{b'} \tag{1.4}$$

where $\mathcal{B}_b$ is the set of all buses connected to bus b, and $\mathbf{i}_b$ is the total current from bus b flowing into the lines connected to it, and therefore according to KCL also the net current injected into bus b from outside the network. Note that $\sum_{b' \in \mathcal{B}_b} \hat{\mathbf{Y}}_{bb'}$ is called the self admittance of the bus b, and we denote it by $\mathbf{Y}_{bb} = \sum_{b' \in \mathcal{B}_b} \hat{\mathbf{Y}}_{bb'}$.

Now applying KCL on each bus of the network we can have the following set of equations:

$$\mathbf{i}_1 = \mathbf{Y}_{11} v_1 + \mathbf{Y}_{12} v_2 + \ldots + \mathbf{Y}_{1n^{\mathrm{B}}} v_{n^{\mathrm{B}}}, \tag{1.5a}$$
$$\mathbf{i}_2 = \mathbf{Y}_{21} v_1 + \mathbf{Y}_{22} v_2 + \ldots + \mathbf{Y}_{2n^{\mathrm{B}}} v_{n^{\mathrm{B}}}, \tag{1.5b}$$
$$\vdots \quad \vdots \quad \vdots \quad \ddots \quad \vdots$$
$$\mathbf{i}_b = \mathbf{Y}_{b1} v_1 + \mathbf{Y}_{b2} v_2 + \ldots + \mathbf{Y}_{bn^{\mathrm{B}}} v_{n^{\mathrm{B}}}, \tag{1.5c}$$
$$\vdots \quad \vdots \quad \vdots \quad \ddots \quad \vdots$$
$$\mathbf{i}_{n^{\mathrm{B}}} = \mathbf{Y}_{n1} v_1 + \mathbf{Y}_{n2} v_2 + \ldots + \mathbf{Y}_{n^{\mathrm{B}} n^{\mathrm{B}}} v_{n^{\mathrm{B}}}. \tag{1.5d}$$

Equation (1.5) can be written in vector form as:

$$\mathbf{I} = \mathbf{Y}\mathbf{V}, \tag{1.6}$$

where $\mathbf{I}$ and $\mathbf{V}$ are $n^{\mathrm{B}} \times 1$ complex matrices, *i.e.*,$\mathbf{I} = [\mathbf{i}_1, \mathbf{i}_2, ..., \mathbf{i}_{n^{\mathrm{B}}}]$, and $\mathbf{V} = [\mathbf{v}_1, \mathbf{v}_2, ..., \mathbf{v}_{n^{\mathrm{B}}}]$, and the $n^{\mathrm{B}} \times n^{\mathrm{B}}$ admittance matrix of the network is given as:

$$\mathbf{Y} = \begin{pmatrix} \mathbf{Y}_{11} & \mathbf{Y}_{12} & \cdots & \mathbf{Y}_{1n^{\mathrm{B}}} \\ \mathbf{Y}_{21} & \mathbf{Y}_{22} & \cdots & \mathbf{Y}_{2n^{\mathrm{B}}} \\ \vdots & \vdots & \ddots & \vdots \\ \mathbf{Y}_{n^{\mathrm{B}}1} & \mathbf{Y}_{n2} & \cdots & \mathbf{Y}_{n^{\mathrm{B}}n^{\mathrm{B}}} \end{pmatrix}.$$

The diagonal entries of the admittance matrix describe the self admittance at each bus and the off diagonal entries describe the mutual admittance of the corresponding buses.

Complex power is defined as the product of voltage and complex conjugate of current. The real part of complex power is known as *real power*, and the imaginary part of complex power is known as *reactive power*. Real power is responsible for delivering the energy and it is the quantity for which we pay. The reactive power can be thought of a by-product of this process. The complex power injected into bus b from outside the network, denoted by $\mathbf{s}_b^{\mathrm{inj}}$, is given by:

$$\mathbf{s}_b^{\mathrm{inj}} = p_b^{\mathrm{inj}} + j q_b^{\mathrm{inj}} = \mathbf{v}_b \mathbf{i}_b^*, \tag{1.7}$$

where p_b^{inj} and q_b^{inj} are the real and reactive power injections, respectively, at bus b. Using the value of $\mathbf{i}_b$ from equation (1.5d) in equation (1.7), we have the following:

$$p_b^{\mathrm{inj}} = \mathcal{R}\left(\mathbf{v}_b \sum_{b'=1}^{n^{\mathrm{B}}} \mathrm{Y}_{bb'}^* \mathbf{v}_{b'}^*\right), \tag{1.8a}$$

$$q_b^{\mathrm{inj}} = \mathcal{I}\left(\mathbf{v}_b \sum_{b'=1}^{n^{\mathrm{B}}} \mathrm{Y}_{bb'}^* \mathbf{v}_{b'}^*\right). \tag{1.8b}$$

Now we express the complex voltage $\mathbf{v}_b$ in the polar form as: $\mathbf{v}_b = v_b\,(\sin\theta_b + j\cos\theta_b)$, where v_b is the voltage magnitude and θ_b is the voltage angle (also known as power factor angle). It is the angle by which voltage leads the current, *i.e.* $\theta_b = 0$ would mean voltage and current are in-phase.

Using the polar form of voltage in equations (1.8), and writing admittance of the lines in terms of conductance and susceptance, we get the following equations for real and reactive power:

$$p_b^{\text{inj}} = \sum_{b' \in \mathcal{B}_b} \left(v_b^2 G_{bb} + v_b v_{b'} (G_{bb'} \cos(\theta_b - \theta_{b'}) + B_{bb'} \sin(\theta_b - \theta_{b'})) \right), \tag{1.9a}$$

$$q_b^{\text{inj}} = \sum_{b' \in \mathcal{B}_b} \left(-v_b^2 B_{bb} + v_b v_{b'} (G_{bb'} \sin(\theta_b - \theta_{b'}) - B_{bb'} \cos(\theta_b - \theta_{b'})) \right), \tag{1.9b}$$

where $\mathcal{B}_b$ is the set of buses connected by a line to bus b. The equations (1.9) are known as power flow or load flow equations.

1.4 Load Flow Problem

Let the set of generators be $\mathcal{G}$,and let $\mathcal{G}_b$ and $\mathcal{D}_b$ be the set of generators and demands at bus b. Also let p_g^{G} and q_g^{G} be the real and reactive power generation, respectively, at the bus g. Also let P_d^{D}, and Q_d^{D} be the real and reactive demand, respectively, at the bus d. The real and reactive power balance equations at bus $b \in \mathcal{B}$: are given as:

$$p_b^{\text{inj}} = \sum_{g \in \mathcal{G}_b} p_g - \sum_{d \in \mathcal{D}_b} P_d^{\text{D}}, \tag{1.10a}$$

$$q_b^{\text{inj}} = \sum_{g \in \mathcal{G}_b} q_g - \sum_{d \in \mathcal{D}_b} Q_d^{\text{D}}. \tag{1.10b}$$

We can substitute the values of p_b^{inj}, q_b^{inj} from Eq. (1.9a-1.9b) in the Eq. (1.10a-1.10b) respectively to get $2n^{\text{B}}$ nonlinear equations, in $2(n^{\text{G}} + n^{\text{B}})$ variables.

If we fix all the demands, and the voltages at all generator buses, and the generator outputs at all generators buses expect one (referred to as the slack bus), and also fix the phase angle at the slack bus, then we get a system of $2n^{\text{B}}$ nonlinear equations in $2n^{\text{B}}$ variables. This system can then be solved for the remaining variables by numerical methods. This is the load flow problem [7] and it is well known that the load flow problem can have 0,1 or multiple solutions [8, 9].

1.5 Nonlinear Optimization and Issue of Local Solutions

In this section we take a step back from power system and discuss the issues involved in solving nonconvex optimization problems. Inevitably many real life problems lie in the domain of nonconvex optimization.

Convexity is a beautiful and a very useful attribute for an optimization problem. But unfortunately most of the real life problems can not be posed as convex optimization problems. This is because of the nonconvex laws governing the physical phenomenons. Also often the linear/convex relaxations of nonconvexities are not tight, and fail to yield

good bounds. The main issues involved in solving nonconvex optimization problems are as follows:

- Difficult to know the geometry of the feasible region.
- Possibility of many local solutions, with considerable different objective values.
- No universally applicable optimization techniques.

While solving an optimization problem it is often advantageous to know the geometry of the feasible region. This knowledge helps in picking up the right optimization technique off the shelf. For example, if a nonconvex problem consists of only one connected component then random search with a local optimization technique might help. Interestingly there are no straightforward way of knowing the number of connected components of a nonconvex program.

Gradient based optimization techniques (also known as local optimization methods) are guided downhill in the attraction basin by the local information of derivative. If the nonconvex problem has more than one attraction basins then the gradient based techniques can not differentiate between local and global solutions. There are global optimization techniques which have been developed to tackle non convex problems but global optimization techniques take a considerable amount of time and computational effort and should only be used if the problem has known local solutions.

It is possible for a nonconvex problem to have a unique solution, *e.g.*, consider the optimization problem: $\min_{\substack{-5\leq x\leq 5,\\ -2\leq y\leq 2}} (-e^{-x^2-y^2} + y^2)$. This problem is nonconvex but it has a global optimal solution at $(x, y) = (0, 0)$ and no local solutions, as shown in Fig. 1.3. In general, especially in higher dimensions, for nonconvex problems it is not possible to give a certificate of global optimality to a solution. In [10] some uniqueness results are discussed for nonconvex optimization problems.

Convex relaxations are often used to obtain lower bounds for the objective function of nonlinear minimization problems. A branch and bound approach (B&B) can be used to subdivide the feasible region and improve the quality of the lower bound by solving a convex relaxation on each leaf of the B&B tree. This technique has been used in power systems optimization problems in [11]-[12]. However the test cases used by the authors did not have any known local solutions.

Another popular approach to solve nonconvex NLP and MINLP problems is to use heuristics or evolutionary algorithms. A set of initial guesses (or feasible solutions if known) are generated and are ranked based on the objective function. Some of the best initial guesses are selected to take part in the evolutionary process, which yields the next generation(set) of guesses. This process continues until the termination point is reached. Some famous evolutionary algorithms are simulated annealing, genetic algorithms and

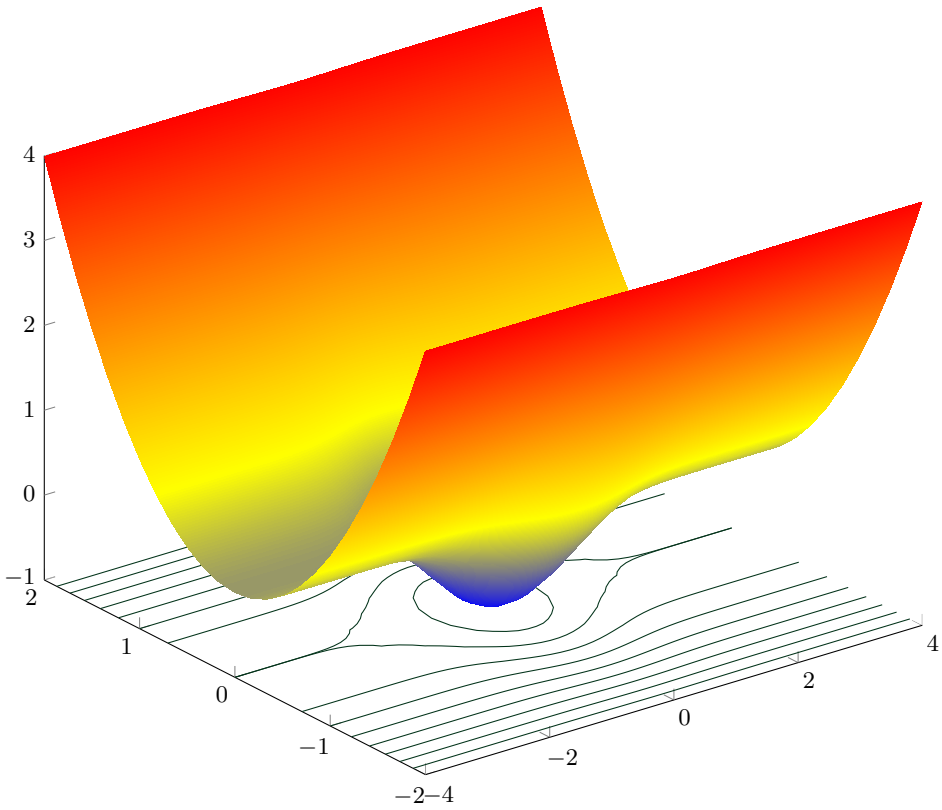

Figure 1.3: Nonconvex optimization problem with unique solution.

particle swarm optimization. These algorithms are easy to implement and can exploit the modern computation power. However finding the global optimal solution is not guaranteed using these methods. These methods have been applied to the optimization problems in power systems [13].

1.6 Motivation, contributions and layout of this thesis

This thesis focuses on two very important power system optimization problems. First we focus our attention on optimal power flow problem (OPF). It is an old and well known optimization problem in power system. Existence of local solutions of OPF has been a documented long standing issue. We have settled this issue by providing variety of test cases with local optima of OPF. These test cases include small test networks which are constructed in-house, and other test cases which are derived from standard test networks. Overall we have made an effort to keep all the parameters realistic in these test cases. These are publicly available on the web so that the researchers and practitioners can test the robustness of their solution techniques on our test cases. We have also tested the numerical performance of a recent global optimization technique on our test cases with local solutions.

Secondly we present a nonlinear relaxation of the optimal power flow problem. The

proposed relaxation is not convex so it is not possible to guarantee to find its global solution, however empirical tests show that in practice it does gives very good valid bounds on the global solution of the OPF problem.

Thirdly, we discuss the islanding problem of the power system. This is relatively a new problem. We have developed an integer programming model for islanding and tested our model on standard test cases. Initially we use the DC model of the power flow equations and discuss the advantages and shortcomings of this approach. Later on we improve the DC model by using piecewise linear approximation of the nonlinear terms. Numerical results show the promise of our islanding model.

The OPF and islanding problem share some features. The most important characteristic common to both is the existence of Kirchhoff's laws, which are nonconvex equality constraints and govern the flow of electricity in power system. Thus developing a robust and efficient solution method for OPF is relevant to islanding problem as well.

The thesis is divided into eight chapters. The current chapter sets the scene by covering basic vocabulary, and gives the model of a transmission line. In second chapter, we give formulation of OPF problem in polar coordinates, discuss alternate formulations and relate OPF to load flow problem. In chapter 3 we give examples of the local solutions of the OPF problem, and the performance of a SDP approach on our test cases. Chapter 4 presents a nonlinear relaxation of the OPF problem and we test this relaxation on variety of test cases. In Chapter 5, we give steady state models of controls in power systems. These control models are used in subsequent chapters. In chapter 6, we give an islanding model of power systems. The islanding model uses DC model of power flow equations. We discuss the robustness of our approach and also give the limitations of the DC model. In chapter 7 we improve on the DC model by proposing a new method of approximating nonconvex power flow equations. The conclusions are given in chapter 8.

Chapter 2

Optimal Power Flow Problem: Formulation

2.1 Introduction to the Optimal Power Flow Problem

Optimal power flow problem(OPF) is a well studied optimization problem in power systems. This problem was first introduced by Carpentier in 1962 [14]. The objective of OPF is to find a steady state operating point that minimizes the cost of electric power generation while satisfying operating constraints and meeting demand. The problem can be formulated as a nonlinear programming (NLP) problem, in which some constraints and possibly the objective function are nonlinear.

The OPF sits in the heart of power systems operation. It is used for scheduling generators, long and short term planning and for network expansion studies. The OPF problem has been extended in various ways. For example security constrained OPF [6] and risk based OPF [15] deal with the problem of ensuring the network operates securely. It is important to note that the issues involved in solving OPF in principle also exist for the extensions of OPF.

2.2 Formulation of OPF in the Polar coordinates

The OPF problem can be formulated in different ways. In polar coordinates the variables are the voltage magnitude v_b and phase angle θ_b at each bus, real and reactive generation, p_g^{G} and q_g^{G}, at each generator bus respectively, and the real and reactive power flows.

Consider a power system network with the b_0 as the reference (or slack) bus. Parameters v_b^{LB} and v_b^{UB} are the lower and upper bounds on variable v_b, the voltage at bus b; parameters P_g^{LB} and P_g^{UB} are the bounds on variable p_g^{G}, the real power output of generator g; parameters Q_g^{LB} and Q_g^{UB} are the bounds on variable q_g^{G}, the reactive

power output of generator g; and parameters P_d^{D} and Q_d^{D} are the real and reactive power consumed by load d, which are assumed to be independent of voltage. Variables $p_{bb'}^{\mathrm{L}}$ and $q_{bb'}^{\mathrm{L}}$ are the real and reactive power flowing into line (b, b') from bus b, and parameter $S_{bb'}^{\max}$ is the apparent power line rating of the line (b, b').

The OPF problem is to minimize the cost of generation while supplying all the load and satisfying the bus voltage limits, the apparent power line limits and the real and reactive generator output power limits. It can be written as:

$$\min \sum_{g \in \mathcal{G}} f(p_g^{\mathrm{G}}), \tag{2.1a}$$

subject to

$$\left.\begin{aligned} \sum_{g \in \mathcal{G}_b} p_g^{\mathrm{G}} &= \sum_{d \in \mathcal{D}_b} P_d^{\mathrm{D}} + \sum_{b' \in \mathcal{B}_b} p_{bb'}^{\mathrm{L}} + G_b^{\mathrm{B}} v_b^2, \\ \sum_{g \in \mathcal{G}_b} q_g^{\mathrm{G}} &= \sum_{d \in \mathcal{D}_b} Q_d^{\mathrm{D}} + \sum_{b' \in \mathcal{B}_b} q_{bb'}^{\mathrm{L}} - B_b^{\mathrm{B}} v_b^2, \end{aligned}\right\}, \forall\ b \in \mathcal{B}, \tag{2.1b}$$

$$\left.\begin{aligned} p_{bb'}^{\mathrm{L}} &= v_b^2 G_{bb} + v_b v_{b'} (G_{bb'} \cos(\theta_b - \theta_{b'}) + B_{bb'} \sin(\theta_b - \theta_{b'})), \\ q_{bb'}^{\mathrm{L}} &= -v_b^2 B_{bb} + v_b v_{b'} (G_{bb'} \sin(\theta_b - \theta_{b'}) - B_{bb'} \cos(\theta_b - \theta_{b'})), \end{aligned}\right\}, \forall\ (b, b') \in \mathcal{L}, \tag{2.1c}$$

$$\theta_{b_0} = 0, \tag{2.1d}$$

$$V_b^{\mathrm{LB}} \leq v_b \leq V_b^{\mathrm{UB}}, \quad \forall\ b \in \mathcal{B}, \tag{2.1e}$$

$$\left.\begin{aligned} P_g^{\mathrm{LB}} &\leq p_g \leq P_g^{\mathrm{UB}}, \\ Q_g^{\mathrm{LB}} &\leq q_g \leq Q_g^{\mathrm{UB}}, \end{aligned}\right\}, \forall\ g \in \mathcal{G}, \tag{2.1f}$$

$$p_{bb'}^{\mathrm{L}}{}^2 + q_{bb'}^{\mathrm{L}}{}^2 \leq (S_{bb'}^{\max})^2, \quad \forall\ (b, b') \in \mathcal{L}, \tag{2.1g}$$

where (2.1a) is the objective function, equations (2.1b) are Kirchhoff's Current Law (KCL) enforcing real and reactive power balance, (2.1c) are Kirchhoff's Voltage Law (KVL), (2.1d) removes the degeneracy in the bus voltage angles by fixing it to zero at the arbitrary reference bus, (2.1e)–(2.1f) are constraints on voltage and power generation, and (2.1g) are the line flow constraints, which are enforced on both ends of the line.

The constraints (2.1d)–(2.1g) are convex, and usually the generator costs are convex (linear or quadratic). However (2.1b) are nonlinear equality constraints and therefore nonconvex. Consequently the polar coordinate formulation is nonconvex. With a slight redefinition of $p_{bb'}^{\mathrm{L}}$ and $q_{bb'}^{\mathrm{L}}$ it is possible to transfer the nonlinear terms in the KCL to the KVL equations leaving the KCL equations linear. It is also possible to eliminate equations (2.1c) and instead use them to eliminate $p_{bb'}^{\mathrm{L}}$ and $q_{bb'}^{\mathrm{L}}$ from (2.1c) and (2.1g). However neither of these reformulations change the solutions in terms of the bus voltages and angles and generator outputs. Any angle in polar formulation of OPF can be changed by a multiple of 2π without changing the other variables, so these give

equivalent solutions and are not counted as distinct solutions.

2.3 Alternate formulations of the OPF

2.3.1 OPF in the rectangular coordinates

In the rectangular OPF formulation the bus voltages are represented by the real and imaginary voltage components [7], *i.e.* $\mathbf{v}_b = v_b^{\mathcal{R}} + jv_b^{\mathcal{I}}$. The real and reactive power flows are quadratic functions of real and imaginary parts of the voltage. This results in the generator limits, the fixed loads and the apparent power line limits being nonconvex constraints, and in addition the lower limits of bus voltage magnitudes are nonconvex. Hence the rectangular formulation is also nonconvex.

The rectangular formulation of OPF is given as:

$$\min \sum_{g\in\mathcal{G}} f(p^{\mathrm{G}}), \tag{2.2a}$$

subject to

$$\left.\begin{aligned} \sum_{g\in\mathcal{G}_b} p_g^{\mathrm{G}} &= \sum_{d\in\mathcal{D}_b} P_d^{\mathrm{D}} + \sum_{b'\in\mathcal{B}_b} p_{bb'}^{\mathrm{L}} + G_b^B\left((v_b^{\mathcal{R}})^2 + (v_b^{\mathcal{I}})^2\right), \\ \sum_{g\in\mathcal{G}_b} q_g^{\mathrm{G}} &= \sum_{d\in\mathcal{D}_b} Q_d^{\mathrm{D}} + \sum_{b'\in\mathcal{B}_b} q_{bb'}^{\mathrm{L}} - B_b^B\left((v_b^{\mathcal{R}})^2 + (v_b^{\mathcal{I}})^2\right), \end{aligned}\right\}, \forall\, b\in\mathcal{B}, \tag{2.2b}$$

$$\left.\begin{aligned} p_{bb'}^{\mathrm{L}} &= \left((v_b^{\mathcal{R}})^2 + (v_b^{\mathcal{I}})^2\right) G_{bb} + B_{bb'}(v_{b'}^{\mathcal{R}} v_b^{\mathcal{I}} - v_b^{\mathcal{R}} v_{b'}^{\mathcal{I}}) + G_{bb'}(v_b^{\mathcal{R}} v_{b'}^{\mathcal{R}} + v_b^{\mathcal{I}} v_{b'}^{\mathcal{I}}), \\ q_{bb'}^{\mathrm{L}} &= -\left((v_b^{\mathcal{R}})^2 + (v_b^{\mathcal{I}})^2\right) B_{bb} + G_{bb'}(v_{b'}^{\mathcal{R}} v_b^{\mathcal{I}} - v_b^{\mathcal{R}} v_{b'}^{\mathcal{I}}) - B_{bb'}(v_b^{\mathcal{R}} v_{b'}^{\mathcal{R}} + v_b^{\mathcal{I}} v_{b'}^{\mathcal{I}}), \end{aligned}\right\}, \forall\, (b,b')\in\mathcal{L}, \tag{2.2c}$$

$$v_{b_0}^{\mathcal{I}} = 0, \tag{2.2d}$$

$$\left(V_b^{\mathrm{LB}}\right)^2 \le (v_b^{\mathcal{R}})^2 + (v_b^{\mathcal{I}})^2 \le \left(V_b^{\mathrm{UB}}\right)^2, \quad \forall\, b\in\mathcal{B}, \tag{2.2e}$$

$$\left.\begin{aligned} P_g^{\mathrm{LB}} &\le p_g \le P_g^{\mathrm{UB}}, \\ Q_g^{\mathrm{LB}} &\le q_g \le Q_g^{\mathrm{UB}}, \end{aligned}\right\}, \forall\, g\in\mathcal{G}, \tag{2.2f}$$

$${p_{bb'}^{\mathrm{L}}}^2 + {q_{bb'}^{\mathrm{L}}}^2 \le (S_{bb'}^{\max})^2 \quad \forall\, (b,b')\in\mathcal{L}. \tag{2.2g}$$

2.3.2 OPF formulation in the IV

In the current and voltage (**IV**) formulation of the OPF, complex voltages and complex currents are the variables at the buses. The complete formulation is given as:

$$\min \sum_{g \in \mathcal{G}} f(p^{\mathrm{G}}), \tag{2.3a}$$

subject to

$$\mathbf{I} = \mathbf{Y}\mathbf{V}, \tag{2.3b}$$

$$\left.\begin{aligned} \sum_{g \in \mathcal{G}_b} p_g^{\mathrm{G}} &= \sum_{d \in \mathcal{D}_b} P_d^{\mathrm{D}} + v_b^{\mathcal{R}} i_b^{\mathcal{R}} + v_b^{\mathcal{I}} v_b^{\mathcal{R}}, \\ \sum_{g \in \mathcal{G}_b} q_g^{\mathrm{G}} &= \sum_{d \in \mathcal{D}_b} Q_d^{\mathrm{D}} + v_b^{\mathcal{I}} i_b^{\mathcal{R}} - v_b^{\mathcal{R}} i_b^{\mathcal{I}}, \end{aligned}\right\}, \forall\ b \in \mathcal{B}, \tag{2.3c}$$

$$\left.\begin{aligned} i_{bb'}^{\mathcal{R}} &= G_{bb'}(v_b^{\mathcal{R}} - v_{b'}^{\mathcal{R}}) - B_{bb'}(v_b^{\mathcal{I}} - v_{b'}^{\mathcal{I}}), \\ i_{bb'}^{\mathcal{I}} &= B_{bb'}(v_b^{\mathcal{R}} - v_{b'}^{\mathcal{R}}) + G_{bb'}(v_b^{\mathcal{I}} - v_{b'}^{\mathcal{I}}), \end{aligned}\right\}, \forall\ (b, b') \in \mathcal{L}, \tag{2.3d}$$

$$v_{b_0}^{\mathcal{I}} = 0, \tag{2.3e}$$

$$\left(V_b^{\mathrm{LB}}\right)^2 \leq (v_b^{\mathcal{R}})^2 + (v_b^{\mathcal{I}})^2 \leq \left(V_b^{\mathrm{UB}}\right)^2, \quad \forall\ b \in \mathcal{B}, \tag{2.3f}$$

$$\left.\begin{aligned} P_g^{\mathrm{LB}} \leq p_g \leq P_g^{\mathrm{UB}}, \\ Q_g^{\mathrm{LB}} \leq q_g \leq Q_g^{\mathrm{UB}}, \end{aligned}\right\}, \forall\ g \in \mathcal{G}, \tag{2.3g}$$

$$i_{bb'}^{\mathcal{R}}{}^2 + i_{bb'}^{\mathcal{I}}{}^2 \leq (i_{bb'}^{\max})^2 \quad \forall\ (b, b') \in \mathcal{L}. \tag{2.3h}$$

The complex current and voltage are related by a linear equality constraint (2.3b). The Kirchhoff's current law is given by the equality constraints (2.3c), which are nonlinear and nonconvex functions of real and imaginary voltage and current respectively. The real and reactive flow of current in a line is give by the equality constraints (2.3d). The voltage magnitude constraint is given by the constraint (2.3f). Because of the nonlinear equality constraints in (2.3c) and the left hand inequality in the constraint (2.3f), this formulation of OPF is also nonconvex. In the rectangular coordinates and in the **IV** formulation, the bus voltages are represented by their real and imaginary components. Since the voltage magnitudes must be positive for a feasible solution the mapping between polar and rectangular coordinates is one to one and continuous in the neighbourhood of any feasible point. Consequently local solutions in polar coordinates give rise to local solution in rectangular coordinates(and in **IV** formulation) and vice versa, so the number of local optima in rectangular coordinates is the same as the number of non-equivalent local solutions in polar coordinates. We have implemented these three formulations in AMPL [16] and have checked the validity of the previous statement numerically. The computational performance of some NLP solvers on these three techniques is given in [17], but no local solutions have been found for OPF by this paper.

In transmission networks the changes in real power are strongly coupled to the

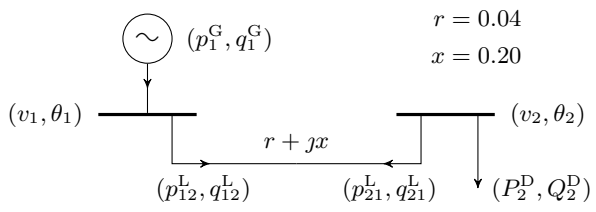

Figure 2.1: WB2 2-bus system.

changes in voltage angle while the changes in reactive power are strongly coupled to the changes in voltage magnitude. The polar formulation of OPF exhibits this property and that is the reason of its predominant use in literature. From here on we will only consider the polar formulation of the load flow equations and the OPF problem.

2.4 Relation of the OPF to the load flow problems

We have defined the load flow problem in Section 1.4. Here we give the relation of OPF to the load flow problem. Provided a load flow solution satisfies all the line limits and the bounds on voltages and generator outputs imposed in OPF it will be a feasible solution for OPF. We shall now present a simple load flow example with multiple solutions, and in the following chapter extend this to illustrate one reason for local solution of OPF existing.

Consider the 2-bus network shown in Fig. 2.1. Bus 2 is the load bus, and bus 1 is the generator bus and slack bus, and for it we set $v_1 = 0.95$ and $\theta_1 = 0$. If we know the load at bus 2 then it is possible to find the remaining variables $(p_g, q_g, v_2, \theta_2)$. There are at most two possible load flow solutions. Fig. 2.2 shows these solutions when the load at Bus 2 is $(P_2^{\mathrm{D}}, Q_2^{\mathrm{D}}) = t(350, -350)$ for $t > 0$. Note the load here is capacitative and so reactive power is *injected* from the load into bus 2. For a load corresponding to $t < 1.004$ there are two alternative solutions. The solid branch corresponds to lower real power generation (the better case) and to higher voltage at bus 2, and the dotted branch corresponds to higher real power generation and lower voltage. Moreover, we can see that as the load increases the two solutions get closer and eventually coalesce at a point. Beyond this there are no solutions – *i.e.,* the line loading limit has been reached.

In power system, normally the feasible range of voltage magnitudes at any bus is taken as $\pm 10\%$ of the nominal voltage *i.e.* 1 p.u. In this example the solutions come together at a voltage that is feasible, however if the load is changed from capacitative to inductive the voltage at the coalescing point drops to an infeasibly low value. The solution space of a general 2-bus system is discussed in [18].

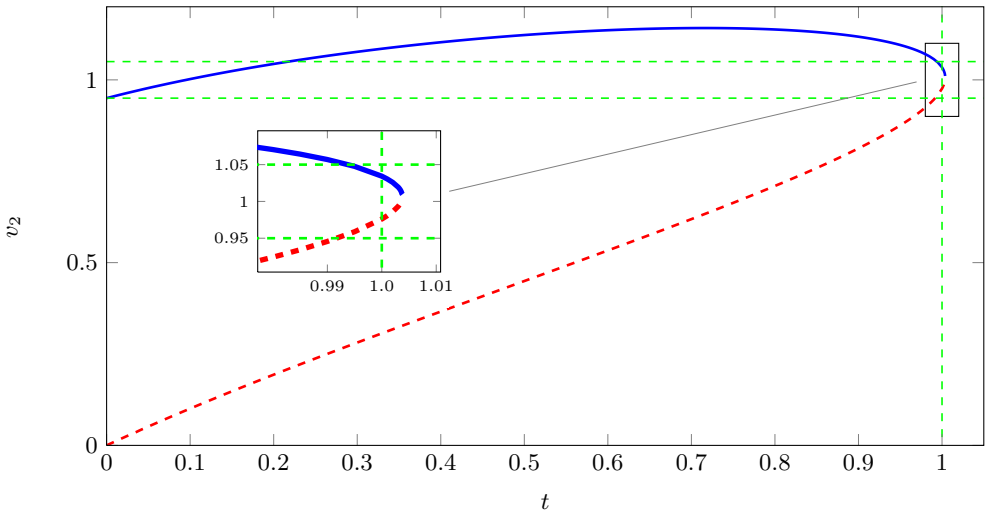

(a) Voltage at bus 2

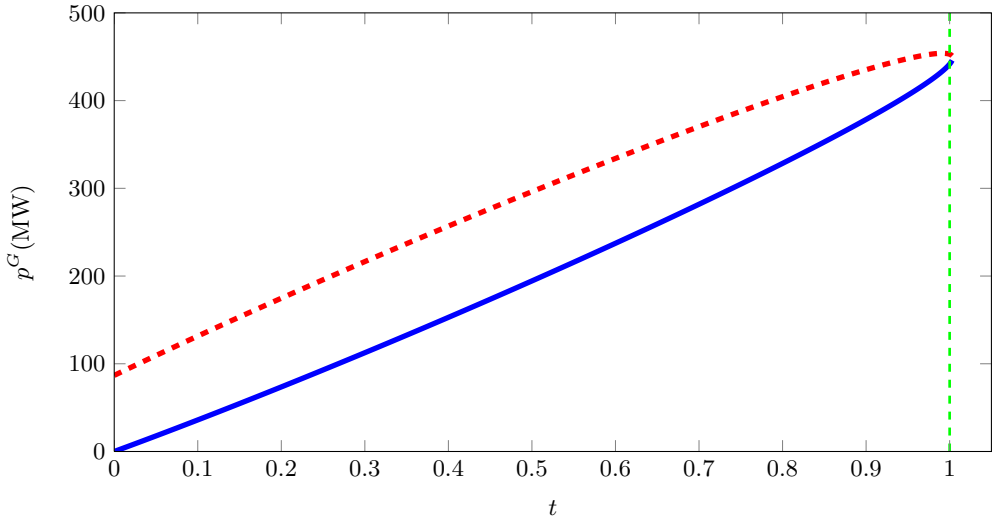

(b) Real Power generation at bus 1

Figure 2.2: Alternate load flow solutions as the demand parameter, t, varies.

2.5 Solution of the OPF problem

The first solution method for the OPF problem was proposed by Dommel and Tinney [19] in 1968, and since then numerous other methods have been proposed. A good literature survey of classical optimization techniques as applied to OPF over the last 30 years is given in [20, 21]. None of these methods are guaranteed to find the global minimum if a local one exists. Following is a brief discussion of three solution techniques which are commonly used to solve OPF problems.

2.5.1 Solving the OPF as an NLP by Local Optimization Techniques

OPF can be solved as NLP using local optimization techniques. The theory of local optimization techniques is quite rich and we will not go into the details of it. However the

NLP solvers are readily available, therefore a dedicated implementation is not necessary to solve the OPF.

We have implemented the polar formulation of OPF problem in AMPL [16]. The NLP solvers like SNOPT [22], KNITR0 [23], IPOPT [24] *etc.* can be called from the AMPL model to solve the OPF.

2.5.2 LP relaxations of the OPF

The nonlinearities in OPF can be linearized in variety of ways. When integer variables are introduced to a problem involving the power flow equations the overall formulation becomes a mixed integer nonlinear programming problem (MINLP). This motivates forming a linear or piecewise linear approximation to the power flow equations, as this change the problem to a MILP for which efficient solution methods are available.

One of the most common linearizations of OPF is so called DCOPF. This linearization uses what is called the DC model of the AC power flow equations (1.9a-1.9b). In the DC model we assume that voltage magnitudes at all buses are 1 *i.e.*, $v_b = 1, \forall \ b \in \mathcal{B}$, and small angle approximations are valid *i.e.*, $\sin(\theta_b - \theta_{b'}) \approx (\theta_b - \theta_{b'})$ and $\cos(\theta_b - \theta_{b'}) \approx 1$, and finally $b_{bb'} >> g_{bb'} \approx 0$. Using these assumptions the equations (1.9a-1.9b) become:

$$p_b^{\text{inj}} = B_{bb'}(\theta_b - \theta_{b'}), \tag{2.4a}$$

$$q_b^{\text{inj}} = 0. \tag{2.4b}$$

In DCOPF, the reactive power and voltage variables get eliminated, and the real power flow through a transmission line becomes linear function of phase angle difference across the line. DCOPF is an LP and can be solved very efficiently. However there is a trade off in accuracy. The error in approximation becomes bigger in the networks where phase angle differences are not small and voltages are not clustered in the neighbourhood of 1 p.u. Due to this reason DC model usually behaves poorly in stressed networks and networks with large transmission losses. Some of the shortcomings of DC model are given in [25] and the references therein.

2.5.3 SDP Approach to solve the OPF problem

In [26] the authors give an interesting semi-definite program (SDP) formulation which is a relaxation of the OPF problem. They show that if there is no duality gap a globally optimal solution to the OPF can be recovered from the SDP dual, and they give a condition, which can be tested after solving the SDP dual, that guarantees there is no duality gap. It is however not obvious just from the properties of a general network

	LP	NLP		SDP
Objective Values	DCOPF	OPF (`fmincon`)	OPF(`MIPS`)	`sedumi`
	350.00	946.58	1082.33	946.53

Table 2.1: Solution of 5 bus OPF problem as LP, NLP and as an SDP

whether or not there will be a duality gap and it is not clear how often the method works in practice. Sufficient conditions for there to be no duality gap that rely only on network properties are given in [27] and [28]. These apply to tree networks and networks with lossless loops and require fixed voltage magnitudes, limits on the angle difference across lines and/or significant flexibility in the real and reactive power balance at buses. However these conditions are not met in general networks. Some of the shortcomings of the SDP approach are discussed in [29]. In [11] examples are given of modified IEEE test cases where the SDP recovery strategy fails, and a branch and bound strategy using the SDP formulation for the relaxations is proposed that find the global optima in these cases. However none of these cases have documented local OPF solutions.

We will use the SDP method for comparison purposes later in this thesis. The mathematical details of the SDP formulation of OPF are lengthy and are not relevant to the findings of our work. So we leave the details out and the complete formulation can be found in [26]. We have implemented this approach in YALMIP [30], and solved the SDP with `sedumi` [31] as a solver.

We conclude this chapter by giving an illustrative example of solving OPF problem with above mentioned techniques. Consider a five bus network as shown in Fig. 2.3. This network consists of two generators, three demand buses and six transmission lines. The demands and the line parameters are shown in the Fig. 2.3. We use $\pm 5\%$ voltage bounds and there are no bounds on the real and reactive power generation of the generators. The objective function of OPF for this network is $4p_1^{\mathrm{G}} + p_5^{\mathrm{G}}$, *i.e.*, the generator at bus 1 is four times more expensive than the generator at bus 5.

We solve the OPF problem as an NLP by a well known publicly available tool MATPOWER [32]. Table 2.1 gives the results. The LP relaxation of OPF yields a poor bound (170% less than the best NLP solution). MATPOWER with `fmincon` as a solver finds the best solution, whereas MATPOWER with `MIPS` as a solver converges to the local solution. The sufficient condition of zero duality gap for SDP method is not met however the bound found by this approach is very good.

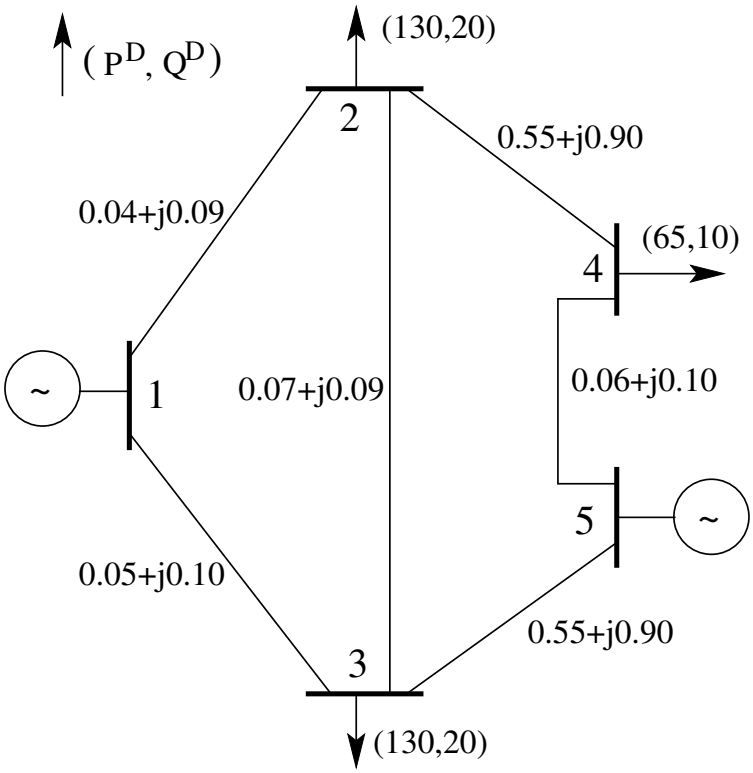

Figure 2.3: Five Bus System

Chapter 3

Local Solutions of the Optimal Power Flow Problem

3.1 Why local solutions of the OPF are important?

The objective of OPF is to minimize the cost of power generation. A local solution (and not global) obviously means spending more money on the fuel costs to meet the same demand. Therefore it is important and desirable to seek global solution of OPF. Also with the recent privatization of electricity markets, convergence to local solution raises the question of fairness in the electricity market. Individual companies might argue that the electricity market is unfair if the contracts are awarded based on the local solution of OPF.

The issue of the possible existence of local optima to the OPF problem is an important one, but one that is not well covered in the literature. A recent literature survey [33] of OPF covers evolutionary algorithms as well as classical local nonlinear techniques. Evolutionary algorithms are global optimization techniques that attempt to find global optima. Global techniques are much slower than the local ones so should only be used for problems where local optima may exist. The authors of [34] discuss the role of metaheuristic techniques to solve the OPF problem and give the possible convergence to local solutions as a major drawback of classical optimization techniques applied to OPF. However, none of these surveys give any reference to examples of local optima of OPF or estimate how often these occur in practice.

In the usual polar coordinate formulation of OPF the major nonlinearity in the constraints is in Kirchhoff's voltage laws (KVL), which gives the flow of power in a transmission line as a nonlinear function of bus voltages and phase angles. The presence of the nonlinear equality constraints results in the feasible region of the OPF problem being nonconvex [35] and hence raises the possibility of the existence of local OPF solutions. However in the 1997 paper [36] one of the authors states that in practice

OPF solutions are unique, and this remains a common perception.

In order to support the current research interest in optimization techniques for OPF problem, it is important to have test cases with known local optima. It is well known that the power flow equations can have solutions with very low voltages at some buses. By relaxing the voltage bounds in standard test networks we have found corresponding low voltage local solutions for the OPF problem (see [37] for details). These low voltage solutions however are not of practical interest and are excluded in OPF problems by reasonable voltage bounds. In this chapter, we give examples of local solutions of OPF within reasonable voltage bounds: all examples either have $\pm 5\%$ bounds or the same bounds as the standard cases from which they are derived (where the most extreme voltages are within $\pm 10\%$). The modifications made to the standard test cases are either to reduce demand or change the generator power limits. All other system properties are unchanged. Some of the changes in generator power limits are significant, but in no cases are the optimal generator outputs unrealistic. The data for the test cases, their network diagrams and all the local solutions we have found are available in the online archive [38].

3.2 Constructed OPF networks with local optima

In this section we present examples, WB2, WB3 and WB5, of simple radial and meshed/loop networks we have constructed to illustrate local optima. These examples have no line limits and have voltage limits within $\pm 5\%$ off-nominal, and WB2 and WB3 have no generator limits. However all the optimal solutions have reasonable generator outputs and line flows. We also document local optima in a contrasting example, LMBM3, which is the 3-bus example in [29] but with a different line limit.

3.2.1 Local solutions in 2-,3- and 5-bus networks

Consider first a 2-bus OPF example, WB2, based on the network in Fig. 2.1 with t fixed at the value 1.0, which gives fixed real and reactive loads of 350.0 MW and -350.0 Mvar respectively. This is close to the nose of the curve in Fig. 2.2. In Section 2.4, the slack bus voltage was fixed at $v_1 = 0.95$ to obtain Fig. 2.2. In OPF problems this voltage is one of the degrees of freedom, and in a one generator example it is the only degree of freedom. Now set the voltage limits on both buses to $[0.95, 1.05]$.

The feasible region is shown by the thick lines in Fig. 3.1. It consists of two disconnected sections. The objective is the real power generated, p^{G}, and the global minimum is at S_1 on the solid (blue) curve, at which point $v_1 = 0.952$. Higher values of v_1 would reduce the objective but would cause v_2 to rise above 1.05, which is its upper limit. On the dotted (red) section of the feasible region the optimal point is S_2. This is a local

optima as it is the best point in its neighbourhood. Both solutions are given in Tab. 3.1.

This 2-bus example shows that OPF problems can have local solutions with reasonable voltages. However as with the load flow case this relies on there being a net injection of reactive power at the load. This could be due to a fixed capacitor, or a generator with positive lower bound on reactive power generation. A more common cause of excess reactive power is cables injecting reactive power when their flow is low. This motivates the next example.

A 3-bus network, WB3, in which bus 2 and bus 3 are connected via a cable is shown in Fig. 3.2. The cable is identical to one in the 24-bus IEEE test case. Loads are in MW and Mvar and neither is capacitative. Results are given in Tab. 3.2: S_1 is the global solution and S_2 is the local solution.

In each of the above examples the objective values are proportional to the real power output of the single generator, and in both cases the local and global optimum are very close. This is because the difference in cost is due only to the different power losses in the lines and these losses are small compared to the power transferred.

To get a bigger difference in the objective values there needs to be more than one generator with different costs. In the 5 bus network in Fig. 2.3 the generator at bus 1 is four times more expensive than the generator at bus 5 (giving the objective function $4p_1^G + p_5^G$). Each generator has a lower limit on its reactive power output of -30 Mvar, and this is active at one generator in both local and global solution. Table 3.3 gives two OPF solutions, S_1 is the global solution with objective value of 946.58, and S_2 is the local solution with the 14% higher objective value of 1082.33.

In the above examples, in all the standard test cases and in the cases derived from them in this chapter, the line limits are large and are inactive at all optimal solutions. Also in most cases with local optima there is an excess of reactive power in the network. In contrast, the 3-bus example LMBM3 in [29], shown in Fig. 3.3, has an apparent power limit $S_{32}^{\max}$ on line 3–2 but no other line limits. There are no positive or negative limits on the reactive power outputs of the generators at buses 1 and 2 or the synchronous condenser at bus 3. The real power output of the generators can be any non-negative

	Cost	Bus	v (p.u.)	θ (deg)	p^{G} (MW)	q^{G} (Mvar)
S_1	877.78	1	0.952	0.00	438.89	94.44
		2	1.050	−57.14		
S_2	905.73	1	0.950	0.00	452.86	164.32
		2	0.976	−64.94		

Table 3.1: OPF Solutions for the WB2 2-bus problem.

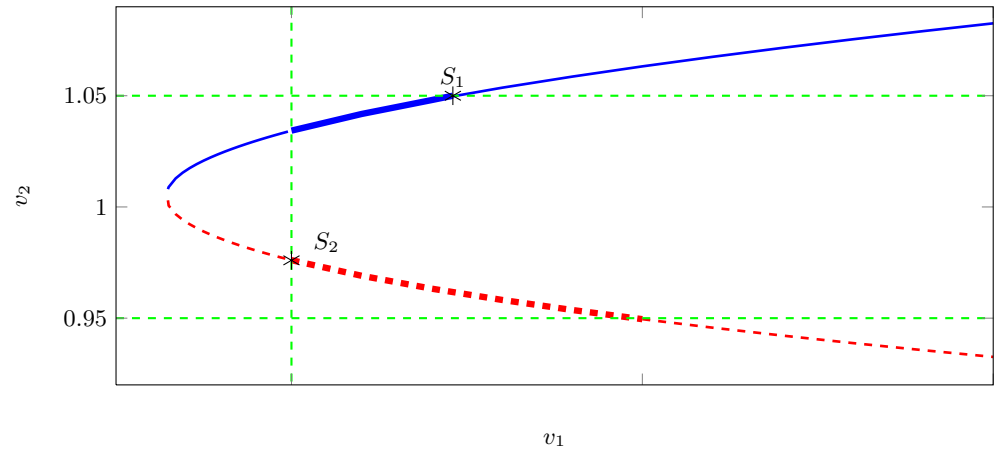

(a) Voltage at bus 2

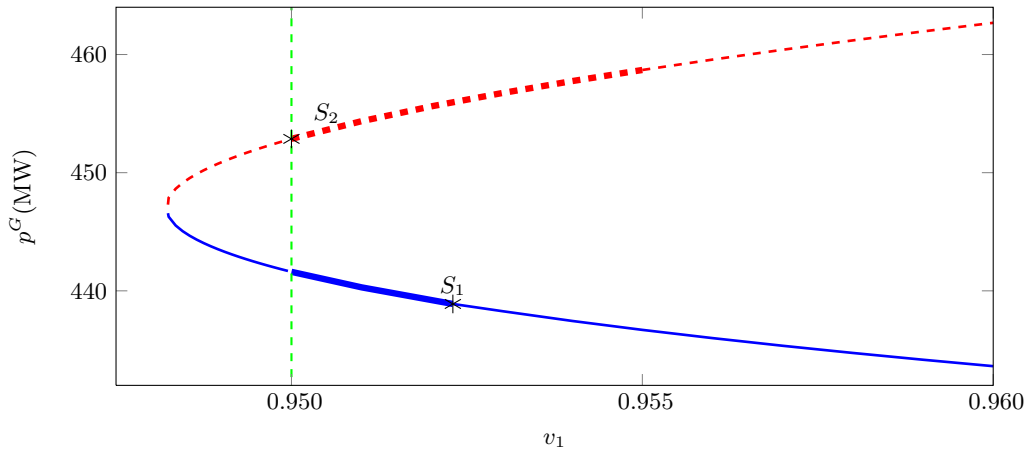

(b) Real Power generation at bus 2

Figure 3.1: WB2 2-bus system. Dependency of bus 2 voltage, v_2, and generator real power p^{G} on bus 1 voltage v_1. Feasible region shown by thick lines.

value (and is 0 for the synchronous condenser). Voltage limits are ±10% off-nominal. The cost of generator g is $C^{\mathrm{L}}p_g^{\mathrm{G}}+C^{\mathrm{Q}}(p_g^{\mathrm{G}})^2$, independent of reactive power output. Since there is unlimited reactive power available at every bus, the reactive power constraints are redundant and the results are independent of the reactive loads. When $S_{32}^{\max} = 186$ there are 5 optimal solutions; see Tab. 3.4. If the voltage limits are tightened to ±5% the perturbation of S_3 becomes infeasible leaving 4 solutions.

3.2.2 Local solutions in loop networks

In power transmission networks there is usually more than one path between pairs of buses, and such networks contain loops. It has been shown that for networks containing loops there can be multiple load flow solutions corresponding to different integer multiple of 2π for the phase shift round the loop [39, 40], and this phenomenon has been repeatedly observed to occur in real power systems [40]. We now present an example

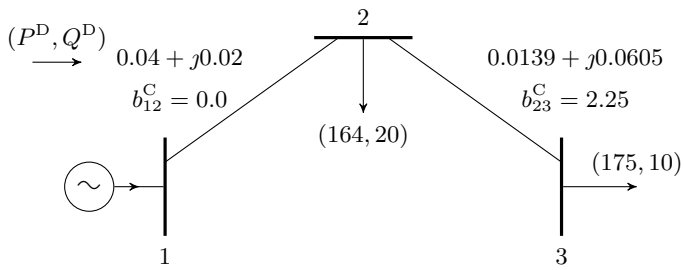

Figure 3.2: WB3 3-bus system.

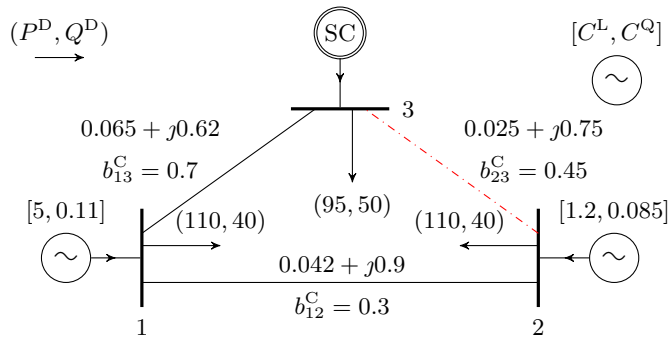

Figure 3.3: LMBM3 3-bus system.

of this that gives rise to local OPF solutions.

The network shown in Fig. 3.4 consists of single loop with an even number n of buses. The loads are at the even buses and the generators at the odd. Every load is the same and every line has the same impedance. If all generators have identical real and identical reactive power outputs, then in the solution of the load flow the voltage magnitudes at all generator buses are equal and the voltage magnitudes at all load buses are equal. For each integer value of m there is a solution with voltage angle at bus k

	Cost	Bus	v (p.u.)	θ (deg)	p^{G} (MW)	q^{G} (Mvar)
S_1	417.25	1	0.951	0.00	208.62	8.93
		2	0.950	−27.25		
		3	0.981	−30.36		
S_2	418.14	1	0.950	0.00	209.07	−20.79
		2	1.011	−26.36		
		3	1.050	−29.23		

Table 3.2: OPF Solutions for WB3 3-bus problem with cable.

	Bus	v (p.u.)	θ (deg)	p^{G} (MW)	q^{G} (Mvar)
	1	1.047	0.00	181.43	124.09
	2	0.957	−3.46		
S_1	3	0.950	−3.21		
	4	0.984	37.65		
	5	1.050	45.48	220.87	−30.00
	1	1.014	0.00	246.05	29.27
	2	0.954	−3.49		
S_2	3	0.950	−3.24		
	4	1.014	38.60		
	5	1.050	46.76	98.15	−30.00

Table 3.3: Two OPF Solutions for the 5 bus problem

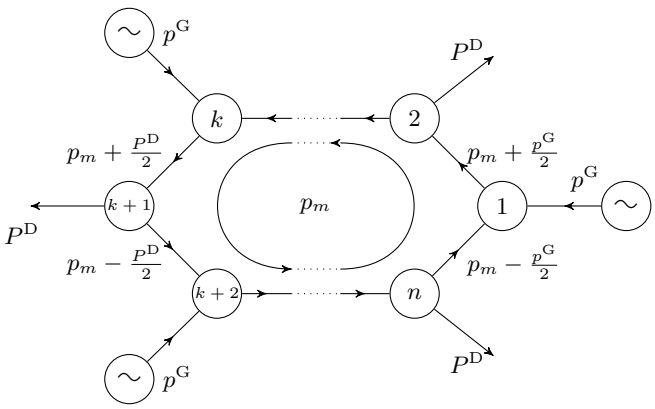

Figure 3.4: Solutions in n-bus loop network (showing only real flows).

given by

$$\theta_k = \begin{cases} \frac{2\pi m}{n}(k-1) & k = 1, 3, \ldots, n-1 \\ \frac{2\pi m}{n}(k-2) + \alpha & k = 2, 4, \ldots, n \end{cases} \tag{3.1}$$

where α is the voltage angle at bus 2. The corresponding real power flows are shown in Fig. 3.4. If $m = 0$ then the circulating flow, p_m, is 0, the voltage angles at the generator buses are all 0 and the angles at the load buses are all α. If $m \neq 0$ then p_m is nonzero and there is a circulating flow.

In the corresponding OPF problem different generators can have different outputs. If all the generators have the same cost then it is optimal (verified computationally in Sec. 3.3) for all generators to have the same output. Hence the above flows are optimal. Fig. 3.4 with $p_m = 0$ is the global solution. When $p_m \neq 0$ there is a circulating flow which results in extra line losses, so this gives a local solution. For the network where

	Total Cost	Bus	v (p.u.)	θ (deg)	p^{G} (MW)
		1	1.100	0.00	128.46
S_1	5694.54	2	1.100	9.00	188.22
		3	1.100	−11.64	0.00
		1	0.900	0.00	124.78
S_2	6833.94	2	0.900	128.59	223.07
		3	0.900	−35.81	0.00
		1	1.033	0.00	186.45
S_3	7684.42	2	0.900	125.81	178.68
		3	0.900	−69.79	0.00
		1	0.900	0.00	181.17
S_4	7966.67	2	0.900	32.18	194.54
		3	0.900	−132.22	0.00
		1	0.900	0.00	231.75
S_5	9677.11	2	1.100	−108.01	168.32
		3	1.047	173.27	0.00

Table 3.4: OPF Solutions for LMBM3 3-bus system with $S_{32}^{\max} = 186$.

$n = 22$, $z = 0.01 + \jmath 0.05$, $(P^{\mathrm{D}}, Q^{\mathrm{D}}) = (204.25, 43)$, $\pm 5\%$ voltage limits and all generators with the same cost, the $m = 0$ case gives the global solution and $m = \pm 1$ cases give the only local solutions, which are 31% more expensive. Tab. 3.5 gives the solutions. If the voltage bounds are widened to $\pm 10\%$ off-nominal the $m = \pm 2$ case is also feasible and the local optima are 28% and 132% more expensive than the global solution.

	Bus	v (p.u.)	α (deg)	p^{G} (MW)	q^{G} (Mvar)
S_1	k odd	1.050		206.31	53.30
	k even	1.029	−2.60		
S_2	k odd	1.015		269.519	369.28
	k even	0.950	13.33		

Table 3.5: Two OPF Solutions for the 22-bus loop network.

3.3 Searching for local OPF solutions

In this section we report the results of a computational search for local OPF solutions in standard test networks and in slightly modified versions of them, as well as in the cases described in Sec. 3.2. The standard cases tested were the IEEE 14-, 24-, 30-, 57-, 118- and 300-bus cases as specified in the archive [41] and the 9 and 39 bus case from the MATPOWER test library [32]. In these examples most of the voltage limits are either 5% or 6% above or below nominal and all limits are within 10%. In our modifications of the standard cases the only change to the voltage limits is to tighten the limits in the 39 bus case from ±6% to ±5%.

It is important to be aware that an NLP solver may converge to a point that is not a local optimum, either by reaching (or by chance being started at) a stationary but non-optimal point or simply through an unreported solver error. For example MATPOWER with MIPS or `fmincon`-IPM falsely identifies a local optimum in the network in [42]. In order to avoid mistakenly classifying a point as a local optimum we check that the first order optimality conditions are satisfied and also that several NLP solvers converge to it when started from several random points in a small box surrounding it. The optimization systems used were MATPOWER [32] using `fmincon` with default settings, and the NLP solvers IPOPT, KNITRO and SNOPT each called from an AMPL model. For the problems in this chapter we found no cases where any of these solvers converged to a solution that was non-optimal.

A second common mode of failure for any nonlinear solver is for it to converge to an infeasible point. This occurs in some of the cases reported later, however were such a case to occur in a real world OPF case then it would be identified and the search repeated from a different starting point. This is therefore not such a serious problem as finding a local optimum without realizing there is a better global solution.

To find local solutions we generated a random point within the bounds of each variable using a uniform distribution, and solved the OPF problem starting from this initial point. For each test case this process was repeated over 2000 times. There is however no guarantee even with such a large number of searches that all optima have been found.

When applied to the examples in Sec. 3.2 the method found all the reported solutions (and no others). When applied to the unmodified standard test cases no local solutions were found, and this was true also if the quadratic terms in the objective were omitted. However after scaling down the demand, modifying the generator bounds or tightening the voltage bounds the local optima described below were found. Full specifications of all the solutions are available at [38].

	1	2	3	4
Objective Value	3087.84	3398.03	4246.48	4265.15
Loss (MW)	6.40	6.36	5.03	5.01

Table 3.6: Four OPF Solutions for the 9 bus network

3.3.1 9-bus case

When the reactive power generation lower bounds on all three generators were raised from −300 Mvar to −5 Mvar and all loads scaled to 60%, then 4 optimal solutions were found. The cost of the worst local solution is 37% more than the cost of global solution. The objective values of all the four solutions found are given in Tab. 3.6. It is interesting to note that the cheapest solution is incurring the highest line loss.

3.3.2 39-bus case

When the loads were halved and the voltage limits tightened from ±6% to ±5%, two OPF solutions were found. The local solution cost was 115% above the global solution. When in addition only the linear cost coefficients were used, 16 solutions were found. These solutions have very different generation levels, however they are all within 0.5% in objective value. The reason for this is that the generators have identical cost functions so in the linear case, the difference in the objective values is due only to the different losses in the network.

3.3.3 118-bus case

When the generators' real and reactive power bounds were all relaxed by scaling them by a factor of 7, then three optimal solutions were found. The cost of the local solutions were 38% and 51% greater than the global solution.

3.3.4 300-bus case

The 300-bus case was modified as in the 9-bus case (*i.e.,* the lower limits on generator reactive power are changed to −5 Mvar and load scaled down to 60%). This change in the generator bounds tightens some and relaxes others. Then 7 optimal OPF solutions were found, and the worst local solution had a cost 2.5% above the global solution.

3.3.5 Starting point in local search

In all the above cases random starting points were used to find different local optima. If solving an OPF problem only once then it is more natural to start from a flat start: *i.e.,* the point with all voltage angles 0, all bus voltage magnitudes 1 and all generator

injections at the mid point of the bounds. From a flat start IPOPT found the global optimum in all the cases in this chapter, but MATPOWER with MIPS (the default solver) converged to a local optimum for WB5. To investigate further we took the modified 9-, 39-, 118- and 300-bus cases (which have local optima) and for each generated 200 cases by randomly perturbing their costs. This yielded 649 cases with local optima and for these cases we tested how often the global minimum was found starting from the flat start and from random points. This showed that the flat start was significantly better than random points: from a flat start IPOPT converged to a local but not global minima in 2.6% of cases and to an infeasible point in 0.3% of cases, compared to 23.2% and 1.4% respectively from the random points.

3.4 Reasons for local optima

In this section we analyse reasons for the occurrence of the local optima reported in Sec. 3.2 and 3.3. All the examples of local optima in this chapter have one or more of the following features: disconnected feasible region, loop flow, an excess of real or reactive power, or large voltage angles differences across lines. Each of these features is discussed below.

Local optima of optimization problems may lie within a connected part of the feasible region or be in different disconnected parts. When the feasible region is disconnected then the optima within each region must be a local optima for the whole problem, so there are at least as many optima as disconnected feasible regions.

A disconnected feasible region occurs because of the interaction of the nonlinear KCL and KVL equations with the remaining constraints (which are convex). It can be seen from Fig. 3.1 that the feasible space of the 2 bus case is disconnected, and this is due to the interaction of the lower voltage limit on v_1 with the other constraints. If this lower limit is relaxed to below 0.948, then the solid and dotted curves in Fig. 3.1 join within the feasible region. The feasible region is then connected and the local optimum disappears. A similar analysis shows this is also the reason for the local optima in the 3-bus example.

Whenever there is a loop in a network there is the possibility of load flow solutions analogous to alternative solutions in the loop network example of Sec. 3.2.2. Fig. 3.5 shows the complex bus voltages in rectangular coordinate for the loop (solid) and non-loop (dotted) solutions of the loop network of Fig. 3.4 with $n = 22$ and with $\pm 5\%$ off-nominal voltage limits. The edges correspond to lines in the network. In the non-loop optimal solution the voltages at generator buses are all the same and the voltages at the load buses are all the same, so there are only two distinct bus voltages on the plot and all the edges coincide. For the loop flow there is a closed connected path

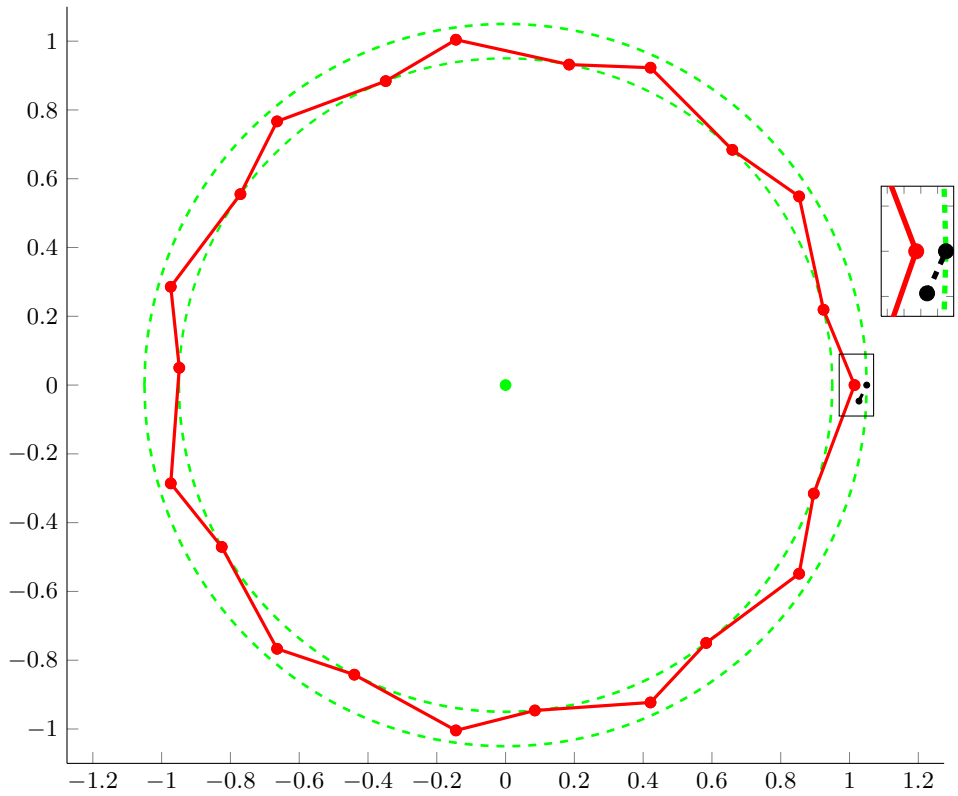

Figure 3.5: Real and imaginary voltages (in p.u.) for the 2 solutions of the 22-bus loop case. The loop flow solution has red solid lines and the non loop flow has the black dashed line. The two circles show the ±5% voltage limits.

surrounding the origin whereas for the non-loop flow this is not the case. If the bus voltages are moved continuously from their values in the loop flow to their values in the non-loop flow (with the straight edges following) there must be a stage where the closed path moves from surrounding to origin to not surrounding it. At that stage the origin lies on one of the (straight) edges and so the angle across the corresponding line is π.

This is the point of maximum line loss and in most practical cases this will be excluded by a some constraint, for example on apparent power, that limits the phase angle difference across the line. When such constraints exists then the loop and non-loop flows are in disconnected parts of the feasible region (and so local optima must exist). Even if there are no constraints that limit line angles, it is likely that other constraints on generation level or voltage will prevent line angles passing through π. This is the situation in the 22-bus loop network (which has loops with phase cycles of 2π and 4π) and the 118-bus case (in which the more expensive local solution has loops with a 2π phase cycle, see Fig. 3.7). As a result these are disconnected from the global optima.

In LMBM3 the voltage plots Fig. 3.6 of S_3 and S_5 surround the origin but the voltage plots of S_1, S_2 and S_4 do not. The feasible region has two disconnected parts, with all except S_3 in one of them. When S_5 is moved continuously to S_1, then line

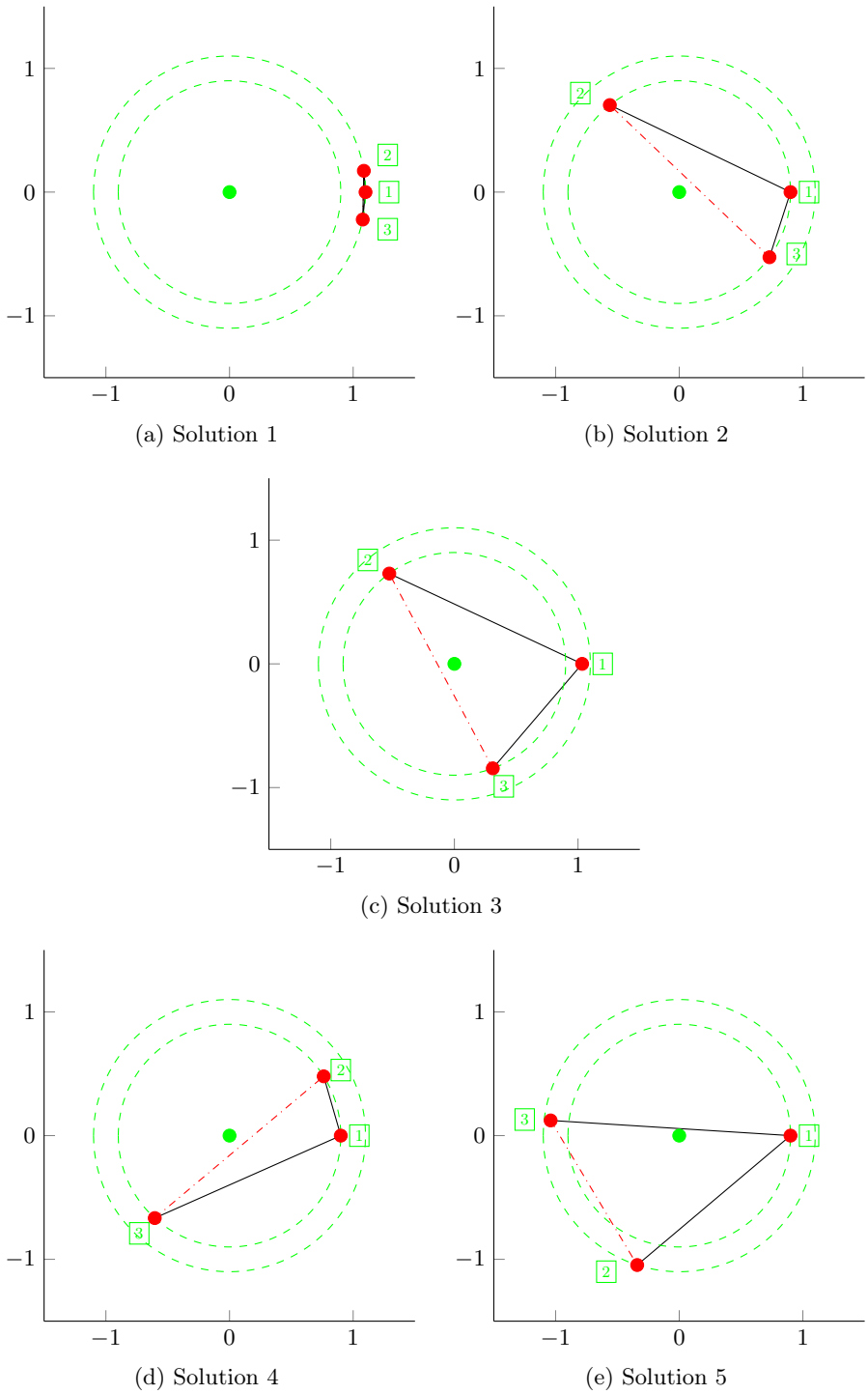

(a) Solution 1

(b) Solution 2

(c) Solution 3

(d) Solution 4

(e) Solution 5

Figure 3.6: Five Local Solutions of LMBM3

1–3 passes through π, but this is possible because line 1–3 has no limit. However the combination of the line limit on 3–2 and the bus voltage limits make it impossible to move continuously from S_3 to a feasible solution with a line angle of π on either of the other lines, so the feasible region is disconnected.

In the other cases of local optima it is not obvious whether or not they lie in the

same connected region. To check this we used the following method to find a continuous path connecting the local optima.

Let $\mathcal{F}$ be the OPF feasible region in the space of all OPF variables, let S be an OPF solution and let $\mathcal{H}(u_i^*)$ be a (very small) hypercube centered on u_i^*. Starting at an initial point u_1^* solve

$$u_{i+1}^* = \arg \min_{u \in \mathcal{H}(u_i^*) \cap \mathcal{F}} \|u - S\|^2$$

iteratively until a point u^* is reached where there is no further reduction in the distance from S. If at this point $u^* = S$, a path has been found between u_1^* and S, showing that points u_1^* and S lie in the same connected region. If however $u^* \neq S$ a path was not found. This will always occur if u_1^* and S are in different disconnected regions, but it could also occur even if they are in the same region as a result of the path getting trapped in a local minimum of the distance to S. We chose u_1^* to be the central point of the constraints (as found by solving the OPF problem by interior point without an objective).

If a path is found the local optima must lie in the same connected part of the feasible region. Paths were found between S_1, S_2, S_4 and S_5 in LMBM3 and between all the local optima in each of the 39- and 300-bus cases, so showing they lie in the same connected region. However in all other cases no path was found between the local optima. This is consistent with the previous analysis of WB2, WB3, LMBM3, and the 22-bus loop and 118-bus cases which we know have disconnected feasible regions. This leaves WB5 and the 9-bus case as the only uncertain cases.

In Sec. 3.2 we noted that in WB2 a local solution within reasonable voltage limits required the load to be capacitative (which injects reactive power), and in WB3 a cable was needed (which also generates reactive power). Also in WB5 the lower limits on generator reactive power output were active. No local solutions were found in the 9-, 39- and 300-bus networks with the default loads, but were found once the loads were reduced and/or the generator reactive power lower limits were increased. Since loads normally absorb reactive power, reducing loads leaves more reactive power in the network. Also lower loads lead to lower line flows and this results in less reactive power being absorbed by lines and eventually results in most lines becoming sources of reactive power. These two effects together can result in an excess of reactive power in the network and reactive power marginal prices that are negative.

When there is an excess of reactive power it would improve the solution if lines were able to absorb more reactive power. However in a line with phase angle $\Delta\theta$ the reactive power absorbed and the real power lost are each proportional to $1 - \cos(\Delta\theta)$. It is therefore not possible by varying only voltage angles to increase the reactive power absorbed in a line without also increasing the real power lost. In situations where the reactive power excess is not high there is no advantage in increasing both the absorption

and loss, however when the reactive power excess is high this can be an advantage. There is then an advantage in having a high value of $1 - \cos(\Delta\theta)$, which occurs with either small or large $\Delta\theta$, and this dichotomy is a potential cause of local optima.

A related though rarer situation is when there is an excess of real power in the network with corresponding negative real power marginal prices (making it worthwhile to pay consumers to increase their demand or suppliers to reduce their generation). This occurs for example in the local optima of WB2 and WB3, and could occur in any network due to the loss of a large load. It is then again advantageous to increase $1-\cos(\Delta\theta)$, in this case so as to lose real power in the lines. When negative generation costs are introduced to the standard test problems most of them then have many local optima. In [29] it is observed that the situation of negative real power marginal price is one in which the SDP method can fail.

Finally in some networks the generator and line limits are so wide that they allow very large voltage angles across lines and bus voltages that spread over a wide area of the voltage diagram. The feasible region is then significantly nonconvex and local optima can occur. This is the situation in LMBM3 and in the modified 118 bus case (in which the generator limits were relaxed). In every local optima for these cases some line angle is greater than 145°. In contrast the line angles for all the optima in WB2 are less than 65°, in WB5 are less than 49° and in all other cases are less than 30°.

3.5 Performance of SDP method on test cases

The authors of [26] propose a semi-definite programming (SDP) relaxation of the OPF problem. They show that if a certain sufficient condition is satisfied, there is no duality gap between the original problem and the convex SDP dual, and that the globally optimal OPF solution can be recovered. The sufficient condition states that a certain matrix, A^{opt}, must have exactly two zero eigenvalues. The value of A^{opt} depends on the dual solution and it is not clear from the properties of the system alone whether or not the condition will hold, nor is it clear how often it holds in practice. We now investigate how well the method works on the examples in this chapter.

Consider the family of problems for the 2-bus network of Fig. 2.1 obtained by varying v_2^{UB}, the upper bound on v_2, over the range $[0.95, 1.06]$. When $v_2^{\text{UB}} \geq 1.035$ there are two solutions with the global one lying on the solid branch. (Tab. 3.1 and Fig. 3.1 show these solutions when $v_2^{\text{UB}} = 1.05$). When $v_2^{\text{UB}} < 1.035$ the S_1 solution is excluded and the global optimum now lies on the dotted branch. As v_2^{UB} decreases from 0.976 the optimal solution moves from S_2 to the right along the dotted curve. The optimal objective value is the primal curve in Fig. 3.8(a).

When the SDP dual method is applied to this problem with $v_2^{\text{UB}} \geq 1.035$ it correctly

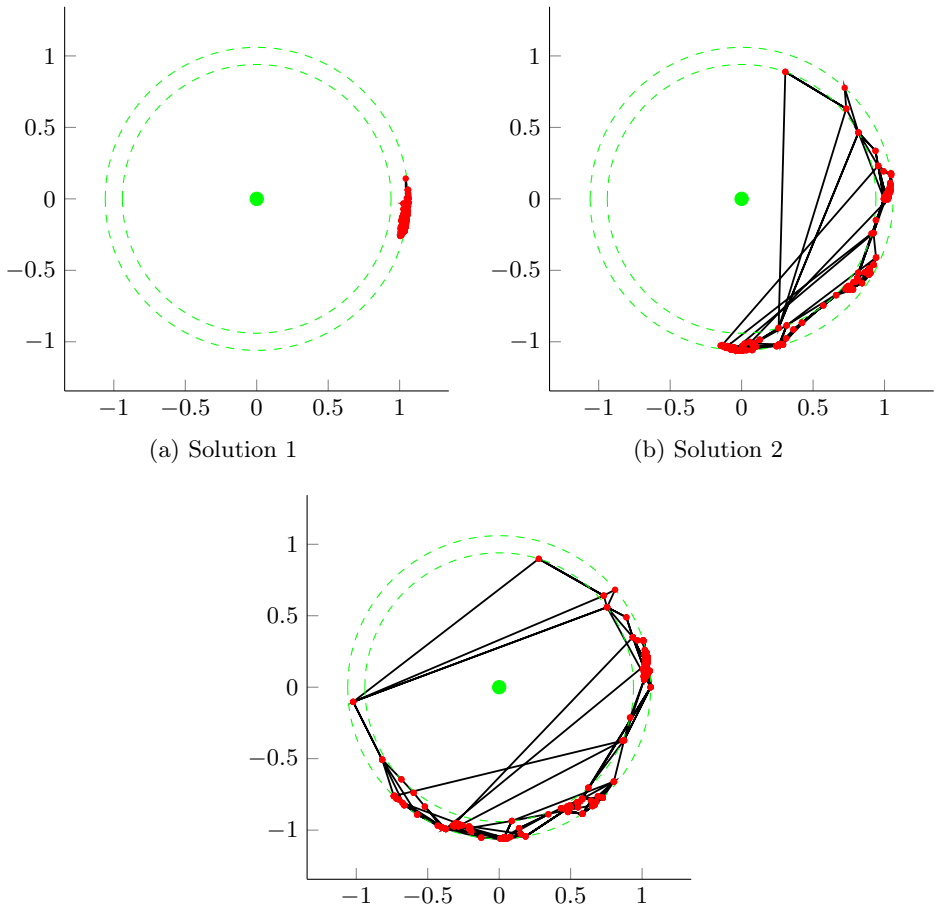

(a) Solution 1

(b) Solution 2

(c) Solution 3

Figure 3.7: Three Local Solutions of `case118mod`

identifies S_1 as the global solution, and for $v_2^{\mathrm{UB}} \leq 0.976$ it correctly identifies the global solution lying on the dotted branch. In both of these ranges exactly two of the four eigenvalues of A^{opt} are nonzero (which is the sufficient condition for the SDP dual method to give the global solution). However when $0.976 < v_2^{\mathrm{UB}} < 1.035$ the SDP method returns an objective value which is an average of the values at $v_2^{\mathrm{UB}} = 0.976$ and $v_2^{\mathrm{UB}} = 1.035$, all four eigenvalues are zero and the process of recovering a primal solution fails. The SDP dual objective value is the dotted curve in Fig. 3.8(a). The gap between the primal and dual curves is positive for the same range of v_2^{UB} values for which the SDP dual method fails to recover the optimal solution. Fig. 3.8(b) shows how the magnitude of the eigenvalues of A^{opt} depend on v_2^{UB}. Two of the eigenvalues are always zero and the other two are equal.

The number of local optima in LMBM3 depends on the value of $S_{32}^{\max}$, the apparent power limit on line 3–2. The objective values of the 5 solutions over the ranges where they are feasible are shown in Fig. 3.9. The $\times$ on the graphs show where (as it increases) the line limit becomes inactive. The maximum apparent power that can enter a line with the properties of line 3–2 occurs when the line angle is close to π. When the

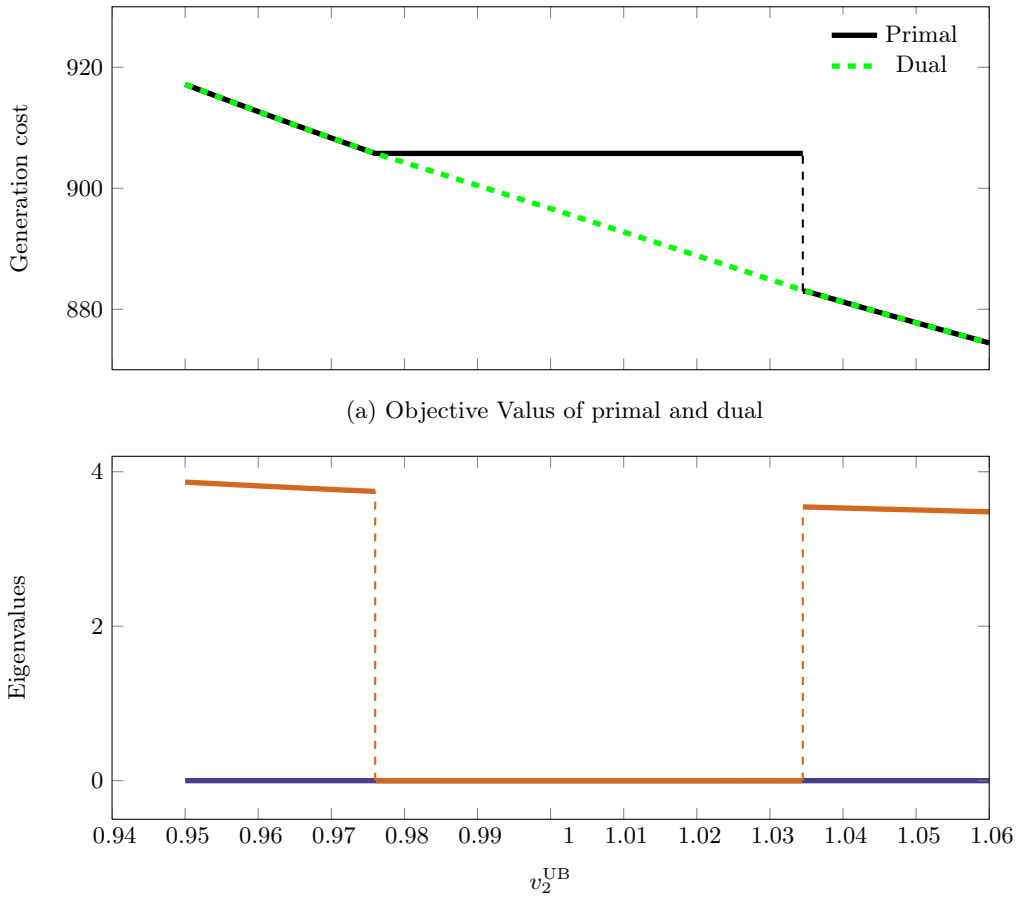

(a) Objective Valus of primal and dual

(b) Eigenvalues of the matrix $\mathrm{A}^{\mathrm{opt}}$

Figure 3.8: Performance of SDP optimization method on 2-bus problem.

voltages are 0.9, the minimum, the corresponding apparent power is 187.55 Mvar, so when $S_{32}^{\max}$ is larger than this it does not prevent the line angle passing through π. With this limit removed S_3 and S_4 stop being local optima so their graphs disappear. The minimum possible apparent power entering a line with the properties of line 3–2 is 28.33 Mvar and so if $S_{32}^{\max}$ is below this there are no feasible solutions. The reason for the lower limit of the ranges of S_2, S_3 and S_5 is that the curvature changes and the local optima disappears below the limit. Fig. 3.9 also shows the solution of the SDP dual. The method recovers the global solution for all value of $S_{32}^{\max}$ above 52.7, and fails for all lower values. This is consistent with [29] where it was shown to fail when $S_{32}^{\max} = 50$ and succeed when $S_{32}^{\max} = 60$.

In the 5 bus example given in Section 3.2.1 the lower bound on reactive power of the generator at bus 5, Q_2^{LB}, is -30 Mvar, and at this value the SDP method fails to recover solutions. Fig. 3.10 shows the primal and dual solutions as function of Q_2^{LB} and shows that for $Q_2^{\mathrm{LB}} \leq -30.8$ the duality gap is zero (so the SDP method works), but for greater values the duality gap is positive (so the SDP method fails). The random start procedure shows that local optima exist for $Q^{LB} \geq -40$. Hence there is a region

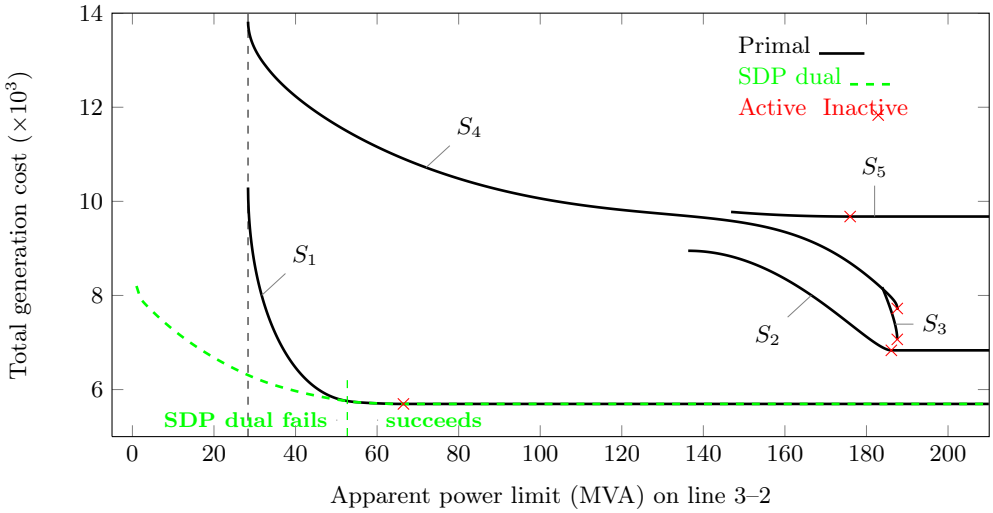

Figure 3.9: Primal and dual objectives of the LMBM3 3-bus problem.

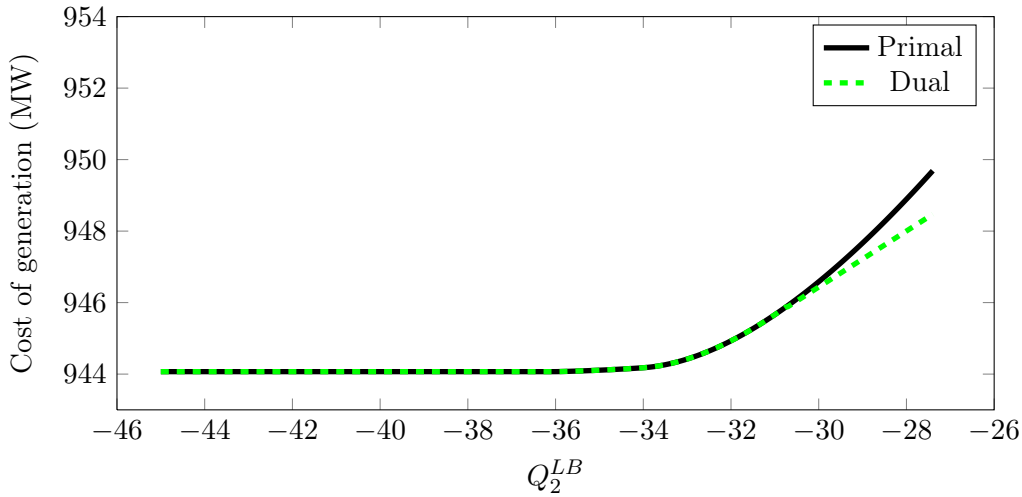

Figure 3.10: Primal and Dual Objectives of 5 Bus Problem

($-40 \leq Q_2^{LB} \leq -30.8$) where there are local optima and the SDP method works.

The SDP method successfully found the global minimum in all the standard test cases except for the 39-bus case. However these problems do not have local optima. When applied to the problems with local optima the SDP approach worked successfully or WB3 and the 22-bus loop case with default bounds and for some parameter values for WB2, WB5 and LMBM3, but it failed in all other cases. As suggested in [26] we have added a positive resistance to all transformer lines which have zero resistance. (We tested values from 10^{-5} to 10^{-3} per unit.) Without this modification the sufficient condition for zero duality gap cannot hold, however in the above failure cases it is not enough to ensure the sufficient condition holds. Tab. 3.7 gives a summary of the results when applied to the problems with local optima.

Case	$n^{\mathcal{B}}$	# of solutions	SDP Method
`WB2`	2	2	Succeeds/Fails
`WB3`	3	2	Succeeds
`WB5`	5	2	Succeeds/Fails
`LMBM3`	3	5	Succeeds/Fails
`case9mod`	9	4	Fails
`case22loop`	22	2	Succeeds
`case39mod1`	39	2	Fails
`case39mod2`	39	16	Fails
`case118mod`	118	3	Fails
`case300mod`	300	7	Fails

Table 3.7: Number of local solutions and outcome of SDP method.

Chapter 4

Relaxations of the Optimal Power Flow Problem

In this chapter we consider 3 relaxations of the OPF problem; a cos-relaxed relaxation which only relaxes the cos term in the power flow equations, the SDP relaxation already mentioned in chapter 3 and a new quadratically constrained relaxation. In chapter 3 and in [43] we have shown the existence of local solutions of the OPF. We proved that local solutions can exist because of the disconnected feasible region and/or because of the nonlinear constraints in the OPF problem.

OPF is an important optimization problem in power systems. The main issues involved in solving OPF problem are the existence of local solutions and convergence to infeasible point when the OPF problem is feasible. Given the nonlinear nature of OPF, it is very challenging to overcome these two issues. Also in some power systems optimization problems such as islanding or unit commitment it is important to get good bounds quickly for the NLP problem. These bounds can then be used to prune the branch and bound (B&B) tree which can save a lot of time and computational effort.

The authors of [26] recognized these difficulties and proposed a global optimization technique to solve OPF problem. We have already discussed the limitations of this approach on our test networks with local solutions. The approach was proposed in 2010 and since then there is a lot of interest in improving and modifying the approach for different power system optimization problems. One issue with the approach, which we have not yet touched upon, is the computational time it takes to solve the problem. In [44] authors propose a method to decompose the large matrix into smaller matrices which improves the computation time of the SDP approach. But still with the improved implementation of [44] solving large networks (*e.g.*,2736 bus Polish network) is not possible in one hour [45].

A quadratically constrained relaxation of the polar form of the OPF problem is proposed recently in [45]. The authors use convex quadratic and linear outer approx-

imations of the nonlinear power flow equations and they demonstrate the use of their relaxations on OPF, line switching and capacitor placement problems. Using the convex relaxations the OPF problem become quadratically constrained convex programming problem (QCP) and can be solved to the global optimality of the relaxed problem. One would imagine that the convex relaxation of OPF problem would yield good bounds, but it is not the case. In [45] the cases are reported where the optimality gap are up to 100%. Interestingly the bounds can be dramatically improved by introducing redundant constraints in the formulation. The authors report that the bounds can be improved by 96% in some cases and also compare their approach with the SDP approach of [26]. The bounds found by SDP method are better than the convex relaxation, but in terms of computational times the convex relaxation is much faster.

In this chapter we propose a new nonlinear relaxation of OPF problem. The salient features of this relaxation are that it is very likely to give global solutions than the original OPF formulation and is useful to get good bounds of the exact problem. We also present the convex relaxation of [45], and propose an improvement to that model. Finally we compare our relaxation with SDP approach and the convex relaxation of OPF problems and give the computational times.

4.1 cos-relaxed OPF formulation

The motivation of introducing this relaxation comes from the analysis of loss in a transmission line. The amount of real power lost, and the reactive power storage in a transmission line (b, b') are given as:

$$l^{\mathrm{P}}_{bb'} = g_{bb'}\left(\left(\frac{v_b}{\tau_{bb'}}\right)^2 + v_{b'}^2 - 2\left(\frac{v_b}{\tau_{bb'}}\right) v_{b'}\cos(\theta_b - \theta_{b'})\right), \tag{4.1a}$$

$$l^{\mathrm{Q}}_{bb'} = -b_{bb}\left(\left(\frac{v_b}{\tau_{bb'}}\right)^2 + v_{b'}^2 - 2\left(\frac{v_b}{\tau_{bb'}}\right) v_{b'}\cos(\theta_b - \theta_{b'})\right) - \left(\left(\frac{v_b}{\tau_{bb'}}^2\right) + v_{b'}^2\right)\frac{b^{\mathrm{C}}_{bb'}}{2}. \tag{4.1b}$$

The Eq. (4.1a-4.1b) are the real and reactive power loss respectively. From these two equations we can see that the real and reactive power losses in the line (b, b') are proportional to $1 - \cos(\theta_b - \theta_{b'})$ (assuming $v_b = v_{b'} = 1 = \tau_{bb'}$). The objective function of OPF problem is convex and increasing function of real power generation, thus the objective function naturally tries to minimize the losses provided this does not force more to be generated from more expensive generators. In other words the OPF problem tries to minimize $1 - \cos(\theta_b - \theta_{b'})$ or equivalently maximizes $\cos(\theta_b - \theta_{b'})$. Due to this reason we might expect the cos-relaxation always to be tight. However there

are cases where it is advantageous to increase the total loss of real power or increase the amount of reactive power stored because that allows more power to be delivered from cheaper generators. In these cases the relaxation will not be tight, but if solved to global optimality provide a good lower bound for the OPF problem.

The cos-relaxed OPF problem is given as:

$$\min \sum_{g \in \mathcal{G}} f(p^{\mathrm{G}}), \tag{4.2a}$$

subject to

$$\left.\begin{aligned} \sum_{g \in \mathcal{G}_b} p_g^{\mathrm{G}} &= \sum_{d \in \mathcal{D}_b} P_d^{\mathrm{D}} + \sum_{b' \in \mathcal{B}_b} p_{bb'}^{\mathrm{L}} + G_b^B v_b^2, \\ \sum_{g \in \mathcal{G}_b} q_g^{\mathrm{G}} &= \sum_{d \in \mathcal{D}_b} Q_d^{\mathrm{D}} + \sum_{b' \in \mathcal{B}_b} q_{bb'}^{\mathrm{L}} - B_b^B v_b^2, \end{aligned}\right\}, \ \forall\, b \in \mathcal{B}, \tag{4.2b}$$

$$\left.\begin{aligned} p_{bb'}^{\mathrm{L}} &= v_b^2 G_{bb} + v_b v_{b'}(G_{bb'} h_{bb'} + B_{bb'} \sin(\theta_b - \theta_{b'})), \\ q_{bb'}^{\mathrm{L}} &= -v_b^2 B_{bb} + v_b v_{b'}(G_{bb'} \sin(\theta_b - \theta_{b'}) - B_{bb'} h_{bb'}), \\ h_{bb'} &\leq \cos(\theta_b - \theta_{b'}), \end{aligned}\right\}, \ \forall\, (b, b') \in \mathcal{L}, \tag{4.2c}$$

$$\theta_{b_0} = 0, \tag{4.2d}$$

$$v_b^{\mathrm{LB}} \leq v_b \leq v_b^{\mathrm{UB}}, \ \forall b \in \mathcal{B}, \tag{4.2e}$$

$$\left.\begin{aligned} P_g^{\mathrm{LB}} \leq p_g \leq P_g^{\mathrm{UB}}, \\ Q_g^{\mathrm{LB}} \leq q_g \leq Q_g^{\mathrm{UB}}, \end{aligned}\right\}, \ \forall\, g \in \mathcal{G}, \tag{4.2f}$$

$${p_{bb'}^{\mathrm{L}}}^2 + {q_{bb'}^{\mathrm{L}}}^2 \leq (S_{bb'}^{\max})^2, \quad \forall (b, b') \in \mathcal{L}, \tag{4.2g}$$

where (4.2a) is the objective function, equations (4.2b) are Kirchhoff's Current Law (KCL) enforcing real and reactive power balance, (4.2c) are KVL and the nonlinear relaxation of cosine, (4.2d) removes the degeneracy in the bus voltage angles by fixing it to zero at the arbitrary reference bus, (4.2e)-(4.2f) are constraints on voltage and power generation, and (4.2g) are the line flow constraints.

The constraints (4.2d-4.2g) are convex, and in all the examples referred to in this chapter the generator costs are convex (linear or quadratic). However (4.2b) are nonlinear equality constraints and therefore nonconvex. Consequently the polar coordinate formulation of cos-relaxed OPF is nonconvex and so local optima cannot be ruled out even in this relaxed formulation.

Note that the cos-relaxed problem become the exact OPF problem when the inequality in (4.2c) is replaced by an equality.

4.1.1 Two Bus Example

Consider the OPF on two bus network as shown in Fig. 2.1. The feasible region of exact OPF problem is shown in Fig. 3.1. It consists of two disconnected sections. S_1 is the global solution and S_2 is the local solution of the exact OPF problem. If we move the lower bound on the variable v_1 to less than or equal to 0.948 then the feasible region becomes connected and there is only one solution to the OPF. Note that this relaxation of lower bound removes the local solution but does not affect the global solution. However for large networks it is not possible to know if the feasible region is disconnected and whether relaxing voltage bounds would make any difference.

The feasible region of the cos-relaxed OPF problem is the shaded gray area in Fig. 4.1. It is found by solving a series of problems for $h_{bb'} + \epsilon = \cos(\theta_b - \theta_{b'})$, by varying $0.950 \leq v_1 \leq 0.960$, and $0 \leq \epsilon \leq 0.02$. Note that the feasible region of the cos-relaxed problem is connected and again this relaxation allows the optimization to move to the global optimal solution on the downhill path which lies within the voltage bounds at all stages.

The feasible region of the cos-relaxed OPF problem is connected, and any local optimization technique starting from any point in the feasible region of the cos-relaxed problem will yield the global solution of the exact OPF problem

4.2 Numerical Results

4.2.1 The cos-relaxed OPF on Standard Test Cases

In Chapter 3 and in [43] we concluded that standard test networks do not have local solutions. This conclusion was drawn after solving the standard test cases with exact formulation and with large number of random initial points. The standard cases tested were the IEEE 14-, 24-, 30-, 57-, 118- and 300-bus cases as specified in the archive [41] and the 9 and 39 bus case from the MATPOWER test library [32]. We tested the cos-relaxed formulation on all these standard test cases and found that the gap between exact formulation and cos-relaxed formulation is less than 0.02%.

Tab. 4.1 gives the gap between exact formulation and the cos-relaxed formulation for very large networks (taken from [32]). For all the networks the gap is less than 0.4%.

4.2.2 cos-relaxed OPF on Test Cases With Local Solutions

In Chapter 3 and in [43] we gave test cases with local optima of the exact problem. If we solve all those examples with flat start and using cos-relaxed problem we always find global solution of the OPF problem. The solutions obtained by cos-relaxed OPF agree with the exact OPF solution in the test cases `WB2`, `WB3`, `case22loop`. For the test cases

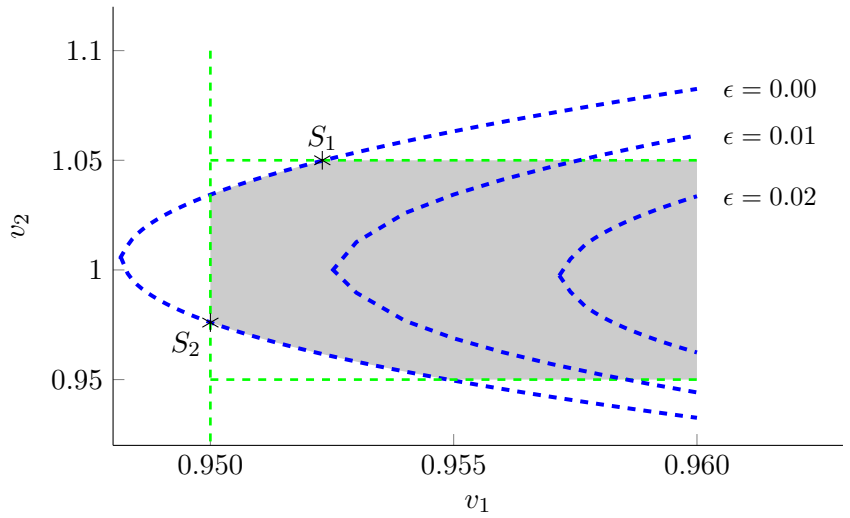

(a) Voltage

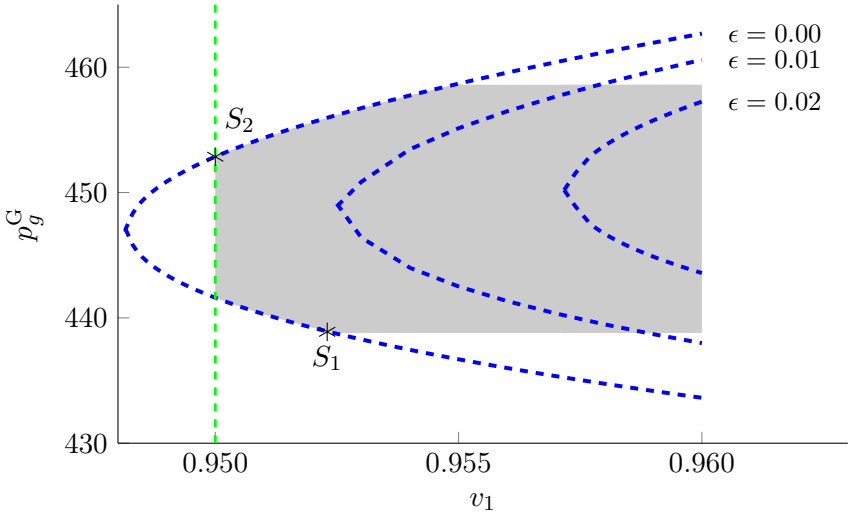

(b) Real Power Generated (Objective)

Figure 4.1: WB2 2 Bus System: Feasible region of cos-relaxed OPF is shown by gray area

`WB5`, `case39mod2`, `case118mod` and `case300mod` the gap between the objective values of cos-relaxed and exact OPF are within 1.0%, and in the test cases `case9mod` and `case39mod1`, the gaps are 10.8% and 3.7% respectively.

4.3 Comparison of cos-relaxed OPF with SDP approach

In this section we compare the quality of the bounds obtained by the SDP approach of [26] and the cos-relaxed OPF.

First, consider the three bus `LMBM3` test case. The OPF problem for this case is infeasible for $S_{23}^{\max} \leq 28.3$. Fig. 4.2 shows that the optimal objective for the cos-relaxed OPF is better than the bound obtained by SDP approach.

Case	n^{B}	Gap(%)
`case2383wp`	2383	0.39
`case2736sp`	2736	0.00
`case2737sop`	2737	0.00
`case2746wop`	2746	0.01
`case2746wp`	2746	0.00
`case3012wp`	3012	0.01
`case3120sp`	3012	0.00
`case3375wp`	3375	0.03

Table 4.1: Gap for cos-relaxed for large networks

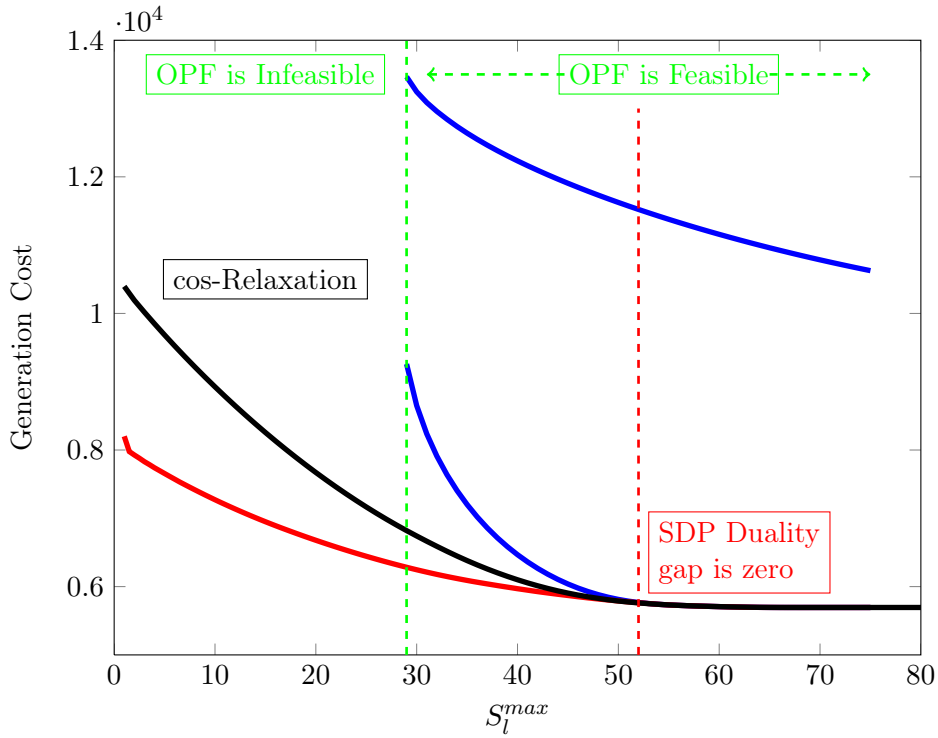

Figure 4.2: Line Limit vs Generation Cost

Tab. 4.2 gives the gaps of SDP approach and the cos-relaxed method on test cases with local optima. The cos-relaxed approached performs well in most of the cases and yields very good bounds. Note that in Tab. 4.2 SDP gaps for some of the cases are negative. This means that the objective value obtained by SDP approach is higher than the best known NLP objective. SDP method is a relaxation and should always yield a lower bound for the OPF problem. The negative values are due to the numerical issues of the solver. We have used the default tolerances for the solver `sedumi`. However if the tolerances are increased then the SDP approach gives a lower bound. The authors

Case	Gap (%)	
	cos-relaxed OPF	SDP Method
WB2	0.00	0.00
WB3	0.00	0.00
LMBM3	0.02	0.01
LMBM3-50	0.00	0.00
WB5	0.40	0.39
case9mod	10.80	35.44
case22loop	0.00	0.00
case39mod1	3.72	3.62
case39mod2	0.04	-0.01
case118mod	0.00	-0.07
case300mod	0.16	0.05

Table 4.2: Gap for cos-relaxed and SDP

in [45] also give negative values for SDP gap but no reason for the negative values were explained. This shows that SDP method to obtain lower bounds can give misleading results.

4.4 Robustness of the cos-relaxed OPF Formulation

The cos-relaxed formulation of OPF presented here is a nonconvex optimization problem. Therefore it is possible that local solutions may exist for this problem. In this section we discuss the robustness of this formulation to initial values and show that the cos-relaxed formulation is less likely than the non-relaxed formulation to get trapped in local optima using random and flat starts.

To check the robustness of the cos-relaxed formulation we generated large number of random initial points for the variables $(v_b, \theta_b, p_b^G, q_b^G)$ for bus b. The random points are generated uniformly within the bounds of the variables. There are no bounds for the phase angle in the default data, so we use different values within the range $[-\frac{\pi}{2}, \frac{\pi}{2}]$. We then tested exact formulation of OPF (`exact`), cos-relaxed formulation of OPF (`cosR`), and exact OPF started from cos-relaxed solution (`cosR+exact`), on the large number of random points. Note that we stop and do not solve `cosR+exact` when the result of `cosR` is infeasible. Also numerical experiments show that the choosing large values of phase angles for initial guess mostly results in IPOPT (or other local solvers) converging to an infeasible point. It is therefore sensible to use small values for angles for initial guess. Tab. 4.3 gives the summary of results for the test cases with local solutions.

Case	$n^{\mathcal{B}}$	Infeasible Cases (%)			Local Solutions (%)		
		exact	cosR	cosR+exact	exact	cosR	cosR+exact
`WB2`	2	2.5	0.0	0.0	6.0	0.0	0.0
`WB3`	3	2.0	0.0	0.0	1.0	0.0	0.0
`LMBM3`	3	0.5	0.3	0.0	7.0	0.0	0.0
`LMBM3-50`	3	1.8	0.0	0.0	3.0	0.0	0.0
`WB5`	5	0.8	0.5	0.2	21.0	0.0	0.0
`case9mod`	9	17.0	2.0	0.0	50.0	0.0	0.0
`case22loop`	22	1.0	0.0	0.0	2.0	5.0	5.0
`case39mod1`	39	37.1	3.5	0.0	1.5	0.3	0.3
`case39mod2`	39	21.8	4.0	0.0	4.0	0.0	0.0
`case118mod`	118	28.2	18.0	8.0	5.0	0.0	0.0
`case300mod`	300	44.6	21.0	6.5	29.0	0.5	0.5

Table 4.3: Summary of the results for randomly starting the exact formulation and the cos-relaxed formulation, and the exact formulation started from cos-relaxed solution.

The `cosR` formulation performs very well in overcoming the issue of infeasibility. On average over all cases `cosR` converged to a feasible solution for 95.5% of the random starts, and the solution found was the global solution of the relaxed problem in 99.5% of the cases. By contrast the `exact` formulation converged to a feasible solution in 85.5% of cases, and 88.0% of the solutions were global.

For all the cases in Tab. 4.3, the `exact` and `cosR` formulations converged to the global solution when started from the flat start. To investigate further we generated 200 cases from each of the cases given in Tab. 4.3 by randomly perturbing their costs. In all we found 1760 cases with local solutions. Then we found that from flat start, `cosR` always converged to the global solution of the relaxed problem, except for 0.3% of the cases where it converged to infeasible point. On the other hand with `exact` formulation, starting from flat start, IPOPT converged to local solution in 3.9% of the cases and to an infeasible point in 1.4% of the cases.

4.5 Convex relaxation of power flow equations

In this section we describe the convex relaxation given in [45]. This is a quadratically constrained problem. It is important to give the complete formulation here because of two reasons. First is that the method is new and not widely known/understood. Secondly later in this chapter we will propose a major improvement to the model of OPF proposed in [45] and show that the improvement can reduce the computational

times without compromising the quality of bounds.

Consider the power flow Eqs. (2.1c). Let us rewrite them in the following form:

$$p^{\mathrm{L}}_{bb'} = v_b^2 G_{bb} + G_{bb'}(v_b v_{b'} - v_b v_{b'}(1 - \cos(\theta_{bb'}))) + B_{bb'} v_b v_{b'} \sin(\theta_{bb'}), \tag{4.3a}$$

$$q^{\mathrm{L}}_{bb'} = -v_b^2 B_{bb} - B_{bb'}(v_b v_{b'} - v_b v_{b'}(1 - \cos(\theta_{bb'}))) - G_{bb'} v_b v_{b'} \sin(\theta_{bb'}), \tag{4.3b}$$

where $\theta_{bb'} = \theta_b - \theta_{b'}$. The advantage of writing power flow equations in this form is that the bilinear term $v_b v_{b'}$ is separated and can be modelled accurately by a set of inequalities. The nonlinear terms in Eq. (4.3a-4.3b) consists of a quadratic term, a bilinear term, and two terms involving product of a bilinear term with the trigonometric functions.

4.5.1 Convex relaxation of Nonlinearities

In this section we give the relaxations of the nonlinearities. Let "$a \sim b$" defines a to be the linear or convex quadratic relaxation of the nonlinear term b. We introduce new variables for the relaxation of nonlinearities in the equations (4.3a-4.3b) as:

$$t_b \sim v_b^2,$$

$$u_{bb'} \sim v_b v_{b'},$$

$$w_{bb'} \sim v_b v_{b'} \left(1 - \cos(\theta_{bb'})\right),$$

$$x_{bb'} \sim v_b v_{b'} \sin(\theta_{bb'}).$$

The power flow equations (4.3a-4.3b) become linear functions of the new variables, *i.e.*:

$$\tilde{p}^{\mathrm{L}}_{bb'} = t_b G_{bb} + G_{bb'}\left(u_{bb'} + w_{bb'}\right) + B_{bb'} x_{bb'}, \tag{4.4a}$$

$$\tilde{q}^{\mathrm{L}}_{bb'} = -t_b B_{bb} - B_{bb'}\left(u_{bb'} - w_{bb'}\right) - G_{bb'} x_{bb'}, \tag{4.4b}$$

where $\tilde{p}^{\mathrm{L}}_{bb'}$ and $\tilde{p}^{\mathrm{L}}_{bb'}$ are the relaxed values of $p^{\mathrm{L}}_{bb'}$ and $q^{\mathrm{L}}_{bb'}$ respectively. Now we give the convex/linear relaxations of the nonlinear terms.

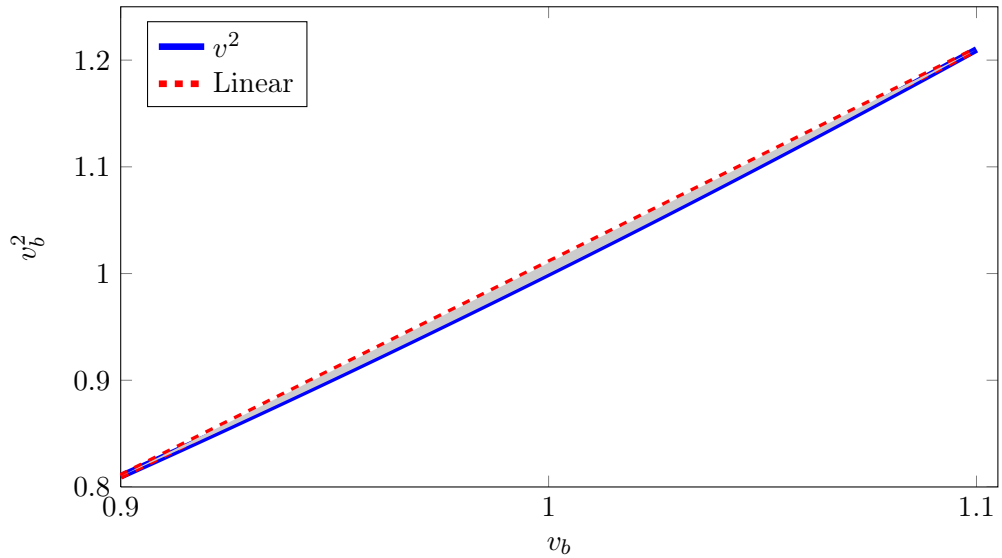

Figure 4.3: Convex envelopes of the voltage square term.

Convex Envelopes for quadratic terms: $t_b \sim v_b^2$

Let V_b^{LB}, V_b^{UB} be the lower and upper bound of the voltage at bus b. The relaxation of quadratic term is given by the following two inequalities:

$$v_b^2 \leq t_b, \tag{4.5a}$$

$$t_b \leq (V_b^{\text{LB}} + V_b^{\text{UB}})v_b - V_b^{\text{LB}}V_b^{\text{UB}}. \tag{4.5b}$$

The inequalities in (4.5a-4.5b) are convex and linear respectively. Usually in power networks the voltage bounds are less than $\pm 10\%$ off the nominal voltage (which is taken as 1 p.u.). The feasible region defined by the two inequalities for $\pm 10\%$ voltage bounds is shown in gray in Fig. 4.3. For this case the maximum error of 0.01p.u. in the approximation of (4.5) occurs at 1 p.u.

Relaxation of Bilinear Terms: $(u_{bb'} \sim v_b v_{b'})$

The bivariate functions can be approximated linearly by McCormick inequalities. These set of inequalities were first introduced in [46], and are given as:

$$u_{bb'} \geq V_b^{\text{LB}} v_{b'} + V_{b'}^{\text{LB}} v_b - V_b^{\text{LB}} V_{b'}^{\text{LB}}, \tag{4.6a}$$

$$u_{bb'} \geq V_b^{\text{UB}} v_{b'} + V_{b'}^{\text{UB}} v_b - V_b^{\text{UB}} V_{b'}^{\text{UB}}, \tag{4.6b}$$

$$u_{bb'} \leq V_b^{\text{LB}} v_{b'} + V_{b'}^{\text{UB}} v_b - V_b^{\text{LB}} V_{b'}^{\text{UB}}, \tag{4.6c}$$

$$u_{bb'} \leq V_b^{\text{UB}} v_{b'} + V_{b'}^{\text{LB}} v_b - V_b^{\text{UB}} V_{b'}^{\text{LB}}. \tag{4.6d}$$

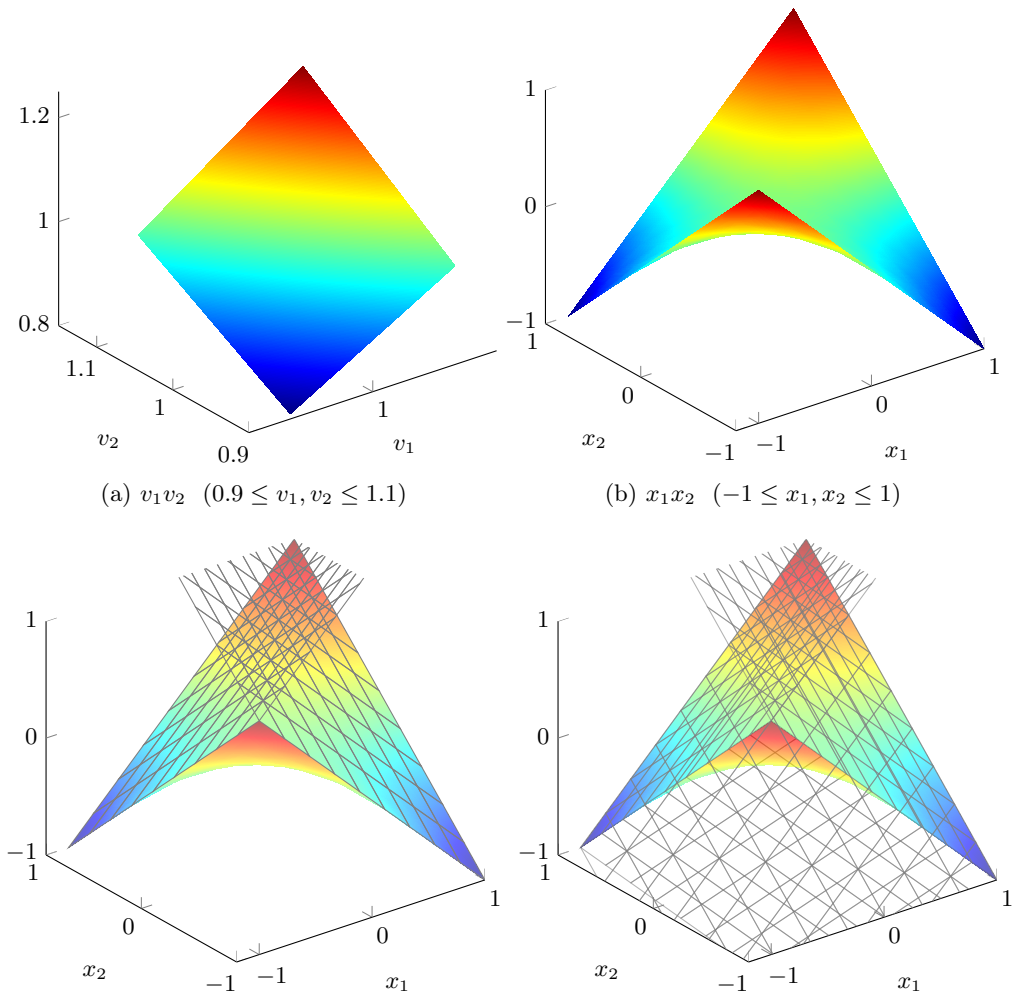

(a) $v_1 v_2$ $(0.9 \leq v_1, v_2 \leq 1.1)$

(b) $x_1 x_2$ $(-1 \leq x_1, x_2 \leq 1)$

(c) $x_1 x_2$, mesh shows two upper convex envelopes

(d) $x_1 x_2$, four convex envelopes forming a vertex polyhedral

Figure 4.4: McCormick Inequalities.

We are interested in approximating the bilinear function $v_1 v_2$. As mentioned before, the usual range for voltage bounds are $\pm 10\%$ of the 1 p.u., and the bilinear is very flat in this region (see Fig. 4.4a). To visualize the McCormick inequalities let us consider the bilinear function $x_1 x_2$, where $-1 \leq x_1, x_2 \leq 1$. The bounds include origin, so we can see the nice curvature of the the function in Fig. 4.4(b). The two upper envelopes of the bilinear function are shown in Fig. 4.4(c). These envelopes are obtained by the inequality constraints (4.6c-4.6d), where the lower and upper bounds are changed accordingly. Convex envelop of the bilinear function is bounded by four planes as shown in Fig. 4.4d.

If we consider the voltage bounds to be $\pm 10\%$ of 1 p.u., then the maximum error in the approximation of $v_1 v_2$ by McCormick inequalities is 0.01 p.u. and it occurs at 1 p.u.

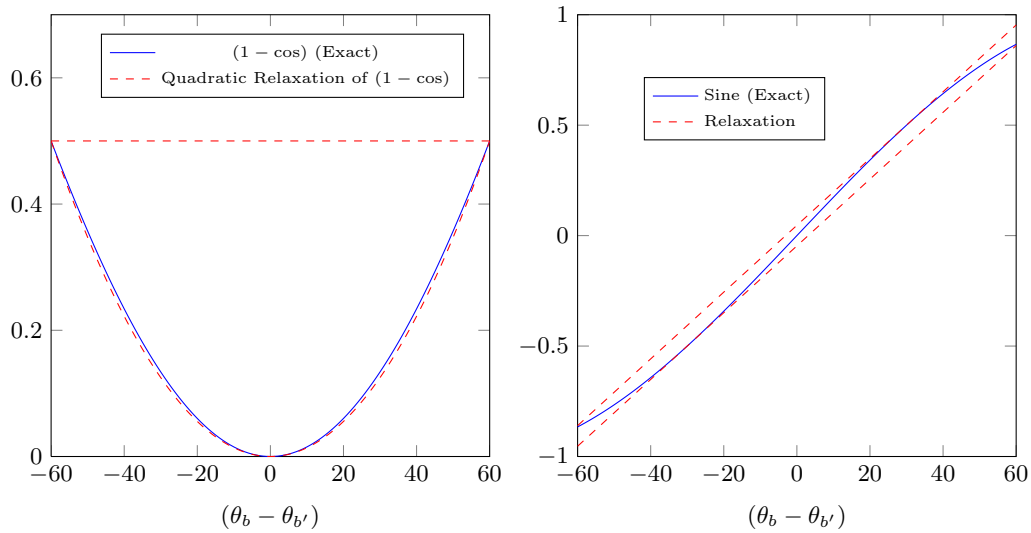

(a) Quadratic relaxation of 1-cosine function. (b) Linear relaxation of sine function.

Figure 4.5: Convex relaxation of trigonometric functions.

Quadratic Relaxation of $w_{bb'}$

Let us define $c_{bb'} \sim 1 - \cos(\theta_b - \theta_{b'})$. We can then write $w_{bb'}$ as:

$$w_{bb'} \sim u_{bb'} c_{bb'},$$

which is a bilinear function and we can tackle this by the McCormick inequalities. Note that the authors in [45] do not use McCormick inequalities to approximate this. We will give the formulation of [45] later in this section.

We first give the quadratic relaxation of the cosine function. Let the bounds on the phase angle difference given as follows:

$$-\Delta^+_{bb'} \leq \theta_b - \theta_{b'} \leq \Delta^+_{bb'}$$

A quadratic relaxation of $1 - \cos(\theta_b - \theta_{b'})$ is given as:

$$\frac{1 - \cos(\Delta^+_{bb'})}{(\Delta^+_{bb'})^2}(\theta_b - \theta_{b'})^2.$$

Fig. 4.5a shows this quadratic relaxation of $(1 - \cos)$ function over the interval $[-60°, 60°]$. The relaxation evaluates exactly on $0°$, and at the end points. This relaxation minimizes the maximum error. Let $\phi_{bb'} \sim (\theta_b - \theta_{b'})^2$, and the quadratic quantity can be approximated by Eqs. (4.5).

Now we give two approximations of $w_{bb'}$:

Approximation 1

Let $U_{bb'}^{\mathrm{LB}}$, $U_{bb'}^{\mathrm{UB}}$ be the lower and upper bound of $u_{bb'}$, respectively. Also let $C_{bb'}^{\mathrm{LB}}$, $C_{bb'}^{\mathrm{UB}}$ be the lower and upper bound of $c_{bb'}$. Following inequalities gives the approximation of $w_{bb'} \sim u_{bb'} c_{bb'}$:

$$w_{bb'} \geq U_{bb'}^{\mathrm{LB}} c_{bb'} + C_{bb'}^{\mathrm{LB}} u_{bb'} - U_{bb'}^{\mathrm{LB}} C_{bb'}^{\mathrm{LB}}, \tag{4.7a}$$

$$w_{bb'} \geq U_{bb'}^{\mathrm{UB}} c_{bb'} + C_{bb'}^{\mathrm{UB}} u_{bb'} - U_{bb'}^{\mathrm{UB}} C_{bb'}^{\mathrm{UB}}, \tag{4.7b}$$

$$w_{bb'} \leq U_{bb'}^{\mathrm{LB}} c_{bb'} + C_{b'}^{\mathrm{UB}} u_{bb} - U_{bb'}^{\mathrm{LB}} C_{bb'}^{\mathrm{UB}}, \tag{4.7c}$$

$$w_{bb'} \leq U_{bb'}^{\mathrm{UB}} c_{bb'} + C_{bb'}^{\mathrm{LB}} u_{bb'} - U_{bb'}^{\mathrm{UB}} C_{bb'}^{\mathrm{LB}}. \tag{4.7d}$$

Now we give approximation of $c_{bb'} \sim (1 - \cos(\delta_{bb'}))$:

$$c_{bb'} = \left(\frac{1 - \cos(\Delta_{bb'}^{+})}{(\Delta_{bb'}^{+})^2} \right) \phi_{bb'}, \tag{4.8a}$$

$$(\theta_b - \theta_{b'})^2 \leq \phi_{bb'}, \tag{4.8b}$$

$$\phi_{bb'} \leq (\Delta_{bb'}^{+})^2. \tag{4.8c}$$

Approximation 2

In [45], the approximation of $w_{bb'}$ is done by the following set of constraints:

$$w_{bb'} = \left(\frac{1 - \cos(\Delta_{bb'}^{+})}{(\Delta_{bb'}^{+})^2} \right) V_b^{\mathrm{LB}} V_{b'}^{\mathrm{LB}} \phi_{bb'}, \tag{4.9a}$$

$$(\theta_b - \theta_{b'})^2 \leq \phi_{bb'}, \tag{4.9b}$$

$$\phi_{bb'} \leq (\Delta_{bb'}^{+})^2. \tag{4.9c}$$

Note that in this approximation the nonlinear term $v_b v_{b'}$ is not approximated by the McCormick inequalities. Numerical tests shows that the objective function bound is up to 1% tighter when modelling the bilinear function using McCormick inequalities. However using McCormick inequalities for this results in bigger model.

Convex Relaxation of $x_{bb'}$

Let $s_{bb'} \sim \sin(\theta_b - \theta_{b'})$, and $S_{bb'}^{\mathrm{LB}}$, $S_{bb'}^{\mathrm{UB}}$ be the lower and upper bound, respectively of $s_{bb'}$. A polyhedral envelope of sine function used in [45] (see Fig. 4.5b) is given by the following two inequalities:

$$s_{bb'} \leq \cos\left(\frac{\Delta^+_{bb'}}{2}\right)\left(\theta_b - \theta_{b'} - \frac{\Delta^+_{bb'}}{2}\right) + \sin\left(\frac{\Delta^+_{bb'}}{2}\right), \tag{4.10a}$$

$$s_{bb'} \leq \cos\left(\frac{\Delta^+_{bb'}}{2}\right)\left(\theta_b - \theta_{b'} + \frac{\Delta^+_{bb'}}{2}\right) - \sin\left(\frac{\Delta^+_{bb'}}{2}\right). \tag{4.10b}$$

Now $x_{bb'} \sim u_{bb'}s_{bb'}$ can be approximated by the McCormick inequalities as:

$$x_{bb'} \geq S^{\mathrm{LB}}_{bb'}u_{bb'} + U^{\mathrm{LB}}_{bb'}s_{bb'} - S^{\mathrm{LB}}_{bb'}U^{\mathrm{LB}}_{bb'}, \tag{4.11a}$$

$$x_{bb'} \geq S^{\mathrm{UB}}_{bb'}u_{bb'} + U^{\mathrm{UB}}_{bb'}s_{bb'} - S^{\mathrm{UB}}_{bb'}U^{\mathrm{UB}}_{bb'}, \tag{4.11b}$$

$$x_{bb'} \leq S^{\mathrm{LB}}_{bb'}u_{bb'} + U^{\mathrm{UB}}_{bb'}s_{bb'} - S^{\mathrm{LB}}_{bb'}U^{\mathrm{UB}}_{bb'}, \tag{4.11c}$$

$$x_{bb'} \leq S^{\mathrm{UB}}_{bb'}u_{bb'} + U^{\mathrm{LB}}_{bb'}s_{bb'} - S^{\mathrm{UB}}_{bb'}U^{\mathrm{LB}}_{bb'}, \tag{4.11d}$$

where $S^{\mathrm{LB}}_{bb'} = -\sin(\Delta^+_{bb'})$, $S^{\mathrm{UB}}_{bb'} = \sin(\Delta^+_{bb'})$, $U^{\mathrm{LB}}_{bb'} = V^{\mathrm{LB}}_b V^{\mathrm{LB}}_{b'}$, $U^{\mathrm{UB}}_{bb'} = V^{\mathrm{UB}}_b V^{\mathrm{UB}}_{b'}$.

Note that the error in linear approximation of sine (and cosine) will increase with increasing the value of $\Delta^+_{bb'}$. In this chapter we always consider $\Delta^+_{bb'} \leq \frac{\pi}{2}$. This is a sensible assumption because of the dynamic stability considerations of power system. It is also important to note that taking very small values of $\Delta^+_{bb'}$ can lead to infeasible problems. It is not possible to come up with a good guess of the value of $\Delta^+_{bb'}$. In this chapter we use 15° for the standard test cases, 60° for the test cases with local solutions and 35° for the large networks. We choose these values after solving the NLP problem and taking the highest angle difference value among all the lines in these set of test cases and this choice insures that the QCP relaxation is always feasible on all test networks.

4.5.2 Convex Quadratic Relaxation of Power Flow Equations

The overall formulation for the convex relaxation of the power flow equations is given as:

$$\tilde{p}^{\mathrm{L}}_{bb'} = t_b G_{bb} + G_{bb'}\left(u_{bb'} + w_{bb'}\right) + B_{bb'} x_{bb'}, \tag{4.12a}$$

$$\tilde{q}^{\mathrm{L}}_{bb'} = -t_b B_{bb} - B_{bb'}\left(u_{bb'} - w_{bb'}\right) - G_{bb'} x_{bb'}, \tag{4.12b}$$

$$v_b^2 \leq t_b, \tag{4.12c}$$

$$t_b \leq (V_b^{\mathrm{LB}} + V_b^{\mathrm{UB}}) v_b - V_b^{\mathrm{LB}} V_b^{\mathrm{UB}}, \tag{4.12d}$$

$$u_{bb'} \geq V_b^{\mathrm{LB}} v_{b'} + V_{b'}^{\mathrm{LB}} v_b - V_b^{\mathrm{LB}} V_{b'}^{\mathrm{LB}}, \tag{4.12e}$$

$$u_{bb'} \geq V_b^{\mathrm{UB}} v_{b'} + V_{b'}^{\mathrm{UB}} v_b - V_b^{\mathrm{UB}} V_{b'}^{\mathrm{UB}}, \tag{4.12f}$$

$$u_{bb'} \leq V_b^{\mathrm{LB}} v_{b'} + V_{b'}^{\mathrm{UB}} v_b - V_b^{\mathrm{LB}} V_{b'}^{\mathrm{UB}}, \tag{4.12g}$$

$$u_{bb'} \leq V_b^{\mathrm{UB}} v_{b'} + V_{b'}^{\mathrm{LB}} v_b - V_b^{\mathrm{LB}} V_{b'}^{\mathrm{UB}}, \tag{4.12h}$$

$$w_{bb'} = \left(\frac{1 - \cos(\Delta^+_{bb'})}{(\Delta^+_{bb'})^2}\right) V_b^{\mathrm{LB}} V_{b'}^{\mathrm{LB}} \phi_{bb'}, \tag{4.12i}$$

$$(\theta_b - \theta_{b'})^2 \leq \phi_{bb'}, \tag{4.12j}$$

$$\phi_{bb'} \leq (\Delta^+_{bb'}), \tag{4.12k}$$

$$x_{bb'} \geq S_{bb'}^{\mathrm{LB}} u_{bb'} + U_{bb'}^{\mathrm{LB}} s_{bb'} - S_{bb'}^{\mathrm{LB}} U_{bb'}^{\mathrm{LB}}, \tag{4.12l}$$

$$x_{bb'} \geq S_{bb'}^{\mathrm{UB}} u_{bb'} + U_{bb'}^{\mathrm{UB}} s_{bb'} - S_{bb'}^{\mathrm{UB}} U_{bb'}^{\mathrm{UB}}, \tag{4.12m}$$

$$x_{bb'} \leq S_{bb'}^{\mathrm{LB}} u_{bb'} + U_{bb'}^{\mathrm{UB}} s_{bb'} - S_{bb'}^{\mathrm{LB}} U_{bb'}^{\mathrm{UB}}, \tag{4.12n}$$

$$x_{bb'} \leq S_{bb'}^{\mathrm{UB}} u_{bb'} + U_{bb'}^{\mathrm{LB}} s_{bb'} - S_{bb'}^{\mathrm{UB}} U_{bb'}^{\mathrm{LB}}, \tag{4.12o}$$

$$s_{bb'} \leq \cos\left(\frac{\Delta^+_{bb'}}{2}\right)\left(\theta_b - \theta_{b'} - \frac{\Delta^+_{bb'}}{2}\right) + \sin\left(\frac{\Delta^+_{bb'}}{2}\right), \tag{4.12p}$$

$$s_{bb'} \leq \cos\left(\frac{\Delta^+_{bb'}}{2}\right)\left(\theta_b - \theta_{b'} + \frac{\Delta^+_{bb'}}{2}\right) - \sin\left(\frac{\Delta^+_{bb'}}{2}\right). \tag{4.12q}$$

Note that in order to obtain the convex relaxation of Eqs. (2.1c), we have introduced 1 new bus variable and 5 new line variables. The new convex relaxation replaces the two nonlinear equations by a set of linear equality constraints, linear inequalities and convex inequalities.

4.5.3 Convexified Optimal Power Flow Problem

In this section we give the convex relaxation of the exact NLP OPF (2.1). In the original NLP formulation of OPF, the constraints (2.1b-2.1c) are nonconvex. We replace those constraints by their linear/convex quadratic relaxation to obtain a quadratically constrained convex programming problem (QCP). The overall formulation of the relaxation is:

$$\min \sum_{g \in \mathcal{G}} f(p_g^{\mathrm{G}}), \tag{4.13a}$$

subject to

$$\left.\begin{aligned} \sum_{g \in \mathcal{G}_b} p_g^{\mathrm{G}} &= \sum_{d \in \mathcal{D}_b} P_d^{\mathrm{D}} + \sum_{b' \in \mathcal{B}_b} \tilde{p}_{bb'}^{\mathrm{L}} + G_b^{\mathrm{B}} t_b, \\ \sum_{g \in \mathcal{G}_b} q_g^{\mathrm{G}} &= \sum_{d \in \mathcal{D}_b} Q_d^{\mathrm{D}} + \sum_{b' \in \mathcal{B}_b} \tilde{q}_{bb'}^{\mathrm{L}} - B_b^{\mathrm{B}} t_b, \end{aligned}\right\}, \forall\ (b, b') \in \mathcal{L} \tag{4.13b}$$

$$(4.12), \tag{4.13c}$$

$$(2.1d - 2.1g). \tag{4.13d}$$

Strengthening Convex relaxation of optimal power flow with redundant constraints

The real and reactive power lost in a line can be obtained from the Eqs. (2.1c) as:

$$p_{bb'}^{\mathrm{L}} + p_{b'b}^{\mathrm{L}} = v_b^2 G_{bb} + v_{b'}^2 G_{b'b'} + 2 v_b v_{b'} G_{bb'} \cos(\theta_b - \theta_{b'}), \tag{4.14a}$$

$$q_{bb'}^{\mathrm{L}} + q_{b'b}^{\mathrm{L}} = -v_b^2 B_{bb} - v_{b'}^2 B_{b'b'} - 2 v_b v_{b'} B_{bb'} \cos(\theta_b - \theta_{b'}). \tag{4.14b}$$

Using the convex relaxation of nonlinearities, we can write Eqs. (4.14) in the following form:

$$\tilde{p}_{bb'}^{\mathrm{L}} + \tilde{p}_{b'b}^{\mathrm{L}} = t_b G_{bb} + t_{b'} G_{b'b'} + 2 G_{bb'} (u_{bb'} - w_{bb'}), \tag{4.15a}$$

$$\tilde{q}_{bb'}^{\mathrm{L}} + \tilde{q}_{b'b}^{\mathrm{L}} = -t_b B_{bb} - t_{b'} B_{b'b'} - 2 B_{bb'} (u_{bb'} - w_{bb'}), \tag{4.15b}$$

but numerical tests show that including the Eqs. (4.15) in the formulation does not make any difference. Another way of writing the loss in a transmission line is:

$$\tilde{p}_{bb'}^{\mathrm{L}} + \tilde{p}_{b'b}^{\mathrm{L}} = g_{bb'} \left((\hat{v}_b - v_{b'})^2 + 2 w_{bb'} \right), \tag{4.16a}$$

$$\tilde{q}_{bb'}^{\mathrm{L}} + \tilde{q}_{b'b}^{\mathrm{L}} = -b_{bb'} \left((\hat{v}_b - v_{b'})^2 + 2 w_{bb'} \right), \tag{4.16b}$$

where $\hat{v}_b = \frac{v_b}{\tau_{bb'}}$. Let $d_{bb'} \sim (\hat{v}_b - v_{b'})^2$. The convex relaxation of (4.16) can be written as:

$$\tilde{p}^{\mathrm{L}}_{bb'} + \tilde{p}^{\mathrm{L}}_{b'b} = g_{bb'}\left(d_{bb'} + 2w_{bb'}\right), \tag{4.17a}$$

$$\tilde{q}^{\mathrm{L}}_{bb'} + \tilde{q}^{\mathrm{L}}_{b'b} = -b_{bb'}\left(d_{bb'} + 2w_{bb'}\right), \tag{4.17b}$$

$$\left(\hat{v}_b - v_{b'}\right)^2 \leq d_{bb'}, \tag{4.17c}$$

$$d_{bb'} \leq (D^{\mathrm{LB}} + D^{\mathrm{UB}})(\hat{v}_b - v_{b'}) - D^{\mathrm{LB}}D^{\mathrm{UB}}, \tag{4.17d}$$

where $D^{\mathrm{LB}} = \frac{V_b^{\mathrm{LB}}}{\tau_{bb'}} - V_{b'}^{\mathrm{UB}}$ and $D^{\mathrm{UB}} = \frac{V_b^{\mathrm{UB}}}{\tau_{bb'}} - V_{b'}^{\mathrm{LB}}$.

Authors in [45] reported that including constraints (4.17) in the convex relaxation of OPF the gap can be improved by 90% in some cases.

4.6 QCP model of OPF with one sided line flows

In the previous section we observed that including the relaxation of the redundant loss constraints can make a big difference to the lower bound of OPF problem. It is important to get an accurate model of loss and line storage as these are quantities that are conserved thoughout the network. In particular any error in line loss becomes an error in generation loss, and so affects the objective directly. However errors in how much flows into one side of lines are only important if they take lines over their thermal limit, and if that cannot be avoided by sending the power by a different route.

In this section we present a convex formulation of OPF problem with out including the redundant constraints, which gives the similar bounds. We model the line flows in a line from one side and model the loss in a line. Let us define a $n^{\mathrm{L}} \times 2$ line bus matrix $\mathcal{A}$ as $\mathcal{A}_{l,1} = b$ and $\mathcal{A}_{l,2} = b'$, where b and b' are the *to* and *from* ends of the line l, respectively. The formulation is given as:

$$\min \sum_{g \in \mathcal{G}} f(p_g^{\mathrm{G}}), \tag{4.18a}$$

subject to

$$\left.\begin{aligned} \sum_{g \in \mathcal{G}_b} p_g^{\mathrm{G}} &= \sum_{d \in \mathcal{D}_b} P_d^{\mathrm{D}} + \sum_{l \in \mathcal{L}: b = A_{l,1}} \tilde{p}_{bb'}^{\mathrm{L}} + \sum_{l \in \mathcal{L}: b = A_{l,2}} \left(l_{bb'}^{\mathrm{P}} - \tilde{p}_{bb'}^{\mathrm{L}}\right) + G_b^{\mathrm{B}} t_b, \\ \sum_{g \in \mathcal{G}_b} q_g^{\mathrm{G}} &= \sum_{d \in \mathcal{D}_b} Q_d^{\mathrm{D}} + \sum_{l \in \mathcal{L}: b = A_{l,1}} \tilde{q}_{bb'}^{\mathrm{L}} + \sum_{l \in \mathcal{L}: b = A_{l,2}} \left(l_{bb'}^{\mathrm{Q}} - \tilde{q}_{bb'}^{\mathrm{L}}\right) - B_b^{\mathrm{B}} t_b, \end{aligned}\right\}, \forall\ (b, b') \in \mathcal{L}, \tag{4.18b}$$

$$(4.12), \tag{4.18c}$$

$$\left.\begin{aligned} l_{bb'}^{\mathrm{P}} &= g_{bb'}\left(d_{bb'} + 2w_{bb'}\right), \\ l_{bb'}^{\mathrm{Q}} &= -b_{bb'}\left(d_{bb'} + 2w_{bb'}\right), \\ (\tilde{v}_b - v_{b'})^2 &\leq d_{bb'}, \\ d_{bb'} &\leq (D^{\mathrm{LB}} + D^{\mathrm{UB}})(\tilde{v}_b - v_{b'}) - D^{\mathrm{LB}} D^{\mathrm{UB}}, \end{aligned}\right\}, \forall\ (b, b') \in \mathcal{L}, \tag{4.18d}$$

$$(2.1d - 2.1g). \tag{4.18e}$$

Fig. 4.6 compares the three QCP formulations of OPF problem. The convex formulation with 2 sided voltage bounds and loss bounds must be atleast as tight as the relaxation with one sided bounds on the loss. However Fig. 4.6 shows that these two bounds are always identical. We can also observe that the two formulations are much better than just the convex relaxation of OPF problem.

4.7 Computational times to solve

In this section we give the computational times of the various models we have discussed. The problems are solved on Dell PowerEdge C6220 running Redhat Linux with Dual 8 Core Intel Xeon (Sandybridge) processors running in 64bit mode and with 128Gb RAM.

To start with we consider the cos relaxed model and compare it with the exact formulation of OPF problem. Both problems are NLP and are solved with the NLP solver `IPOPT`. Fig. 4.7 shows the run times of exact formulation and cos-relaxed formulation of OPF. The cos relaxed model takes more time to solve than the exact formulation.

Next we investigate the solution strategy to solve QCP problem. We solve our one sided QCP model of OPF on variety of solvers and compare their run times in Fig. 4.8. `KNITRO` is the most promising solver in all of them to solve QCP except for one case. `SNOPT` is not able to solve any of the large networks, and the performance of `CPLEX` is consistent over all the test cases.

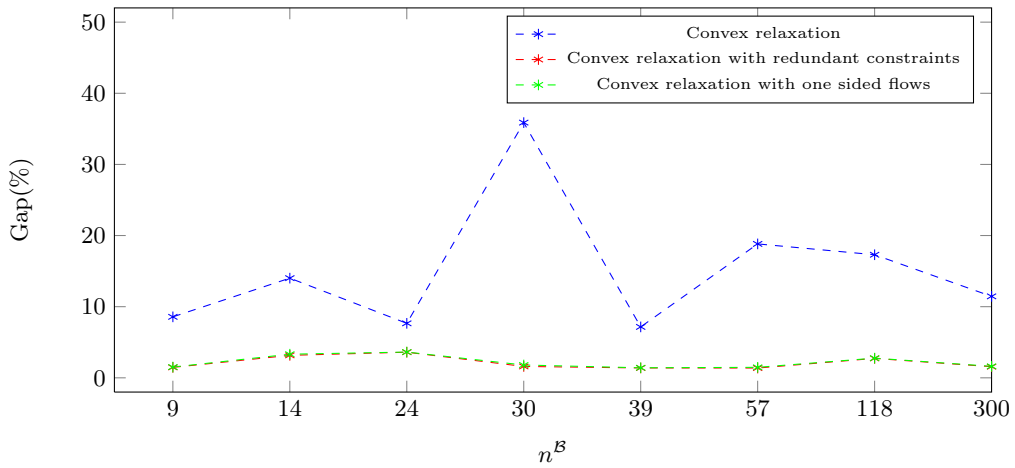

(a) Gap(%) in standard test cases.

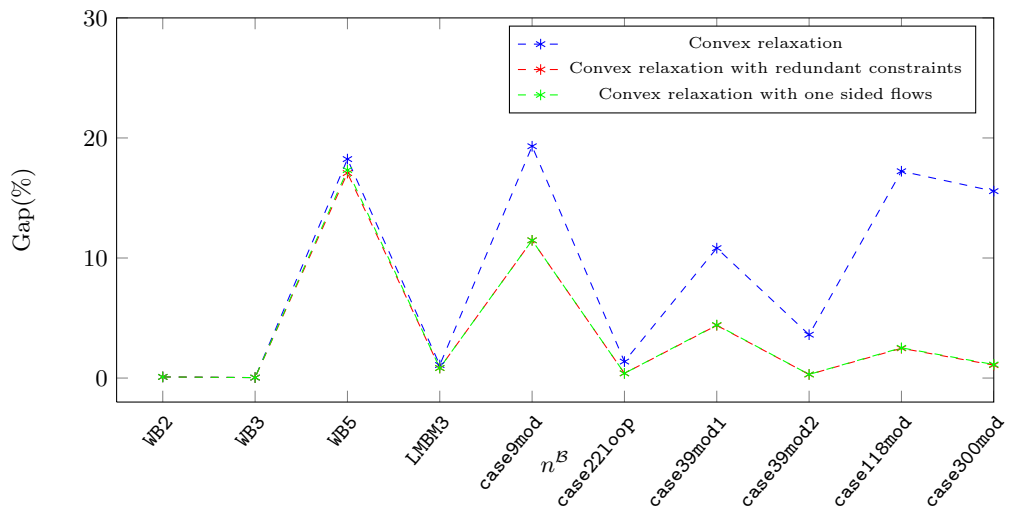

(b) Gap(%) in test cases with local solutions.

Figure 4.6: Gap in % using different models of convex relaxation.

Fig. 4.9 gives the comparison of the time for `CPLEX` to solve our one sided model and the two sided model of [45]. Our model does not include redundant constraints and hence it is smaller in size and therefore it is better in computational times.

In this chapter we presented a nonlinear relaxation of OPF problem. This relaxation does not come with a theoretical guarantee of lower bound of OPF but numerical test shows that is is more likely to give very good bounds to the global solution of OPF. Another salient feature of this relaxation is to converge to a feasible solution. Sometimes finding a feasible solution of OPF problem can be a challenge, especially when the network is new, or significant changes made to the existing network. `cosR` relaxation can be used to produce a good starting point for OPF problem. Also we proposed an improvement to the convex relaxation of [45] and showed that improved model is quicker to solve and the speed does not compromise the quality of solution.

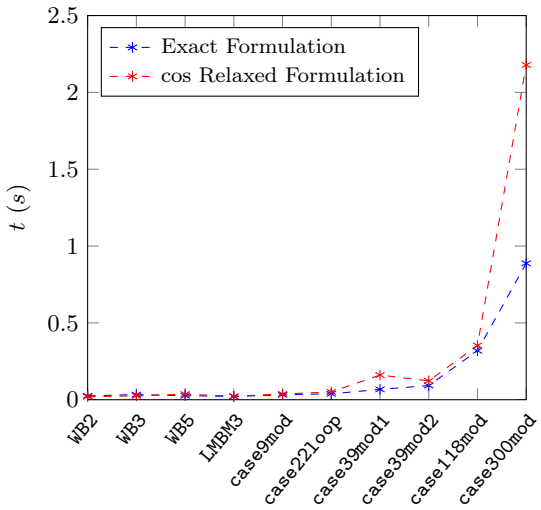

(a) Test cases with local solutions.

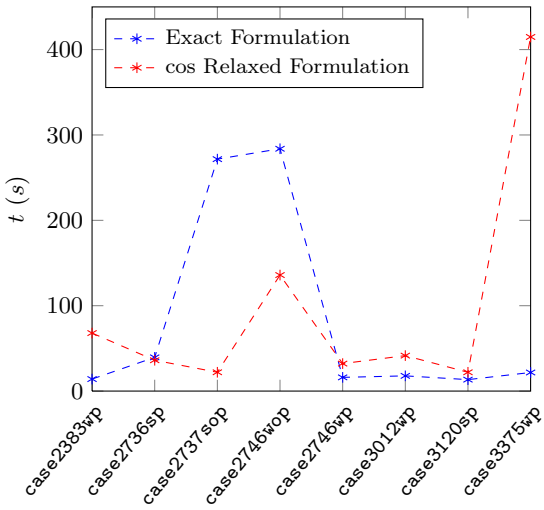

(b) Large Networks.

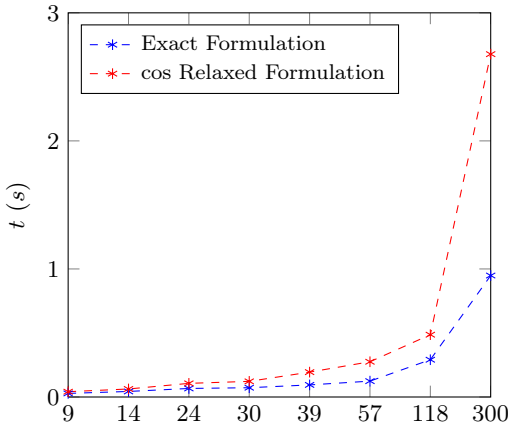

(c) Standard test cases.

Figure 4.7: Time in seconds for cos-relaxed OPF problems using `IPOPT` as a solver.

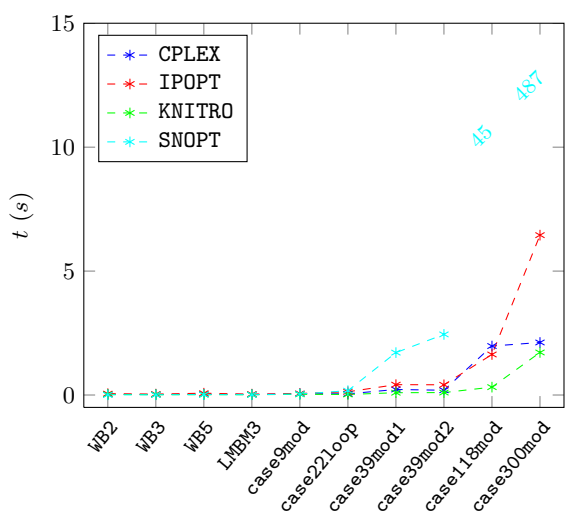

(a) Test cases with local solutions.

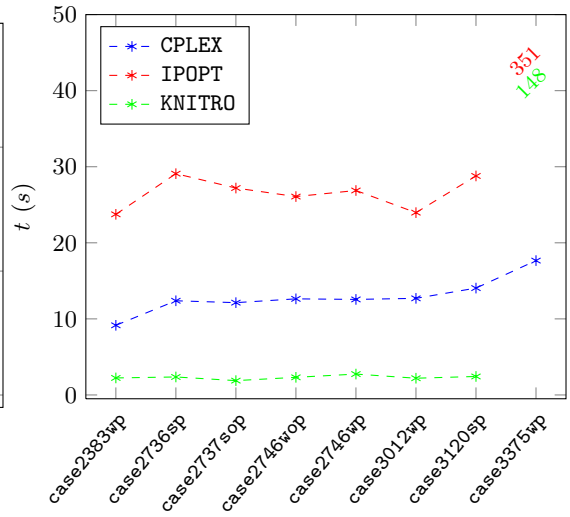

(b) Large Networks.

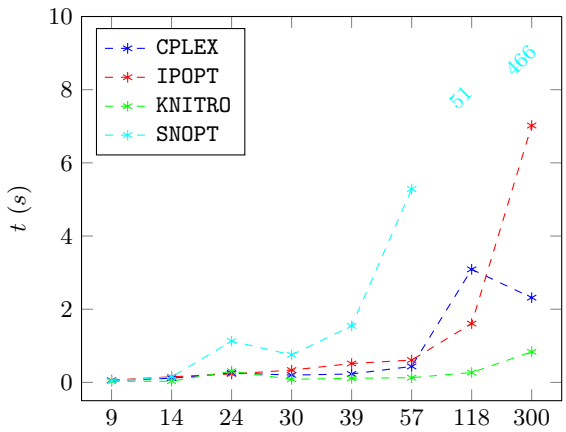

(c) Standard test cases.

Figure 4.8: Time in seconds for convex relaxation of OPF problem.

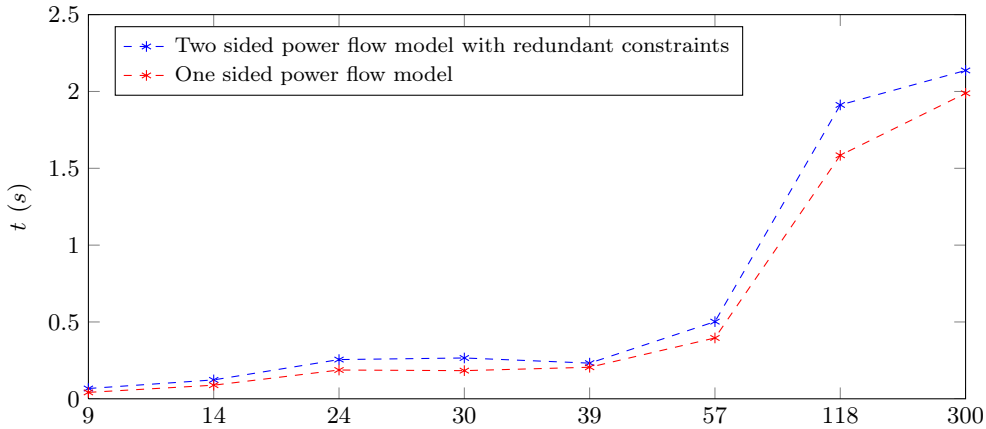

(a) Standard test cases.

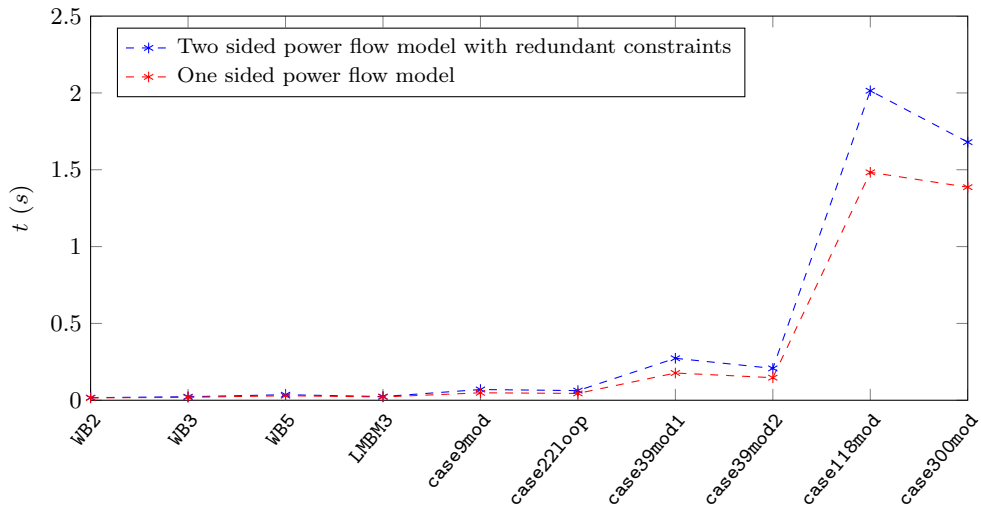

(b) Test cases with local solutions.

Figure 4.9: Comparision between one sided and two sided models.

Chapter 5

Steady state modelling of controls in power system

In this chapter we give the mathematical formulation of various control actions which are used in power systems. Depending on the application, these models can then be embedded in the optimization model. We will use these models in the islanding of power systems in subsequent chapters.

5.1 Load Model

Let us consider the real and reactive power load, P_d^{D} and Q^{D} respectively, at the demand bus $d \in \mathcal{D}$. During the operation of power system there may be situation where it is not possible to meet the load. It is important to shed some load to restore the load and generation balance in the system. We assume that the real and reactive load can be shed continuously in the equal proportions. This is modelled as:

$$p_d^{\mathrm{D}} = \alpha_d P_d^{\mathrm{D}}, \tag{5.1a}$$

$$q_d^{\mathrm{D}} = \alpha_d Q_d^{\mathrm{D}}, \tag{5.1b}$$

where $0 \leq \alpha_d \leq 1$ is a variable whose value determines the amount of load delivered at bus d, *i.e.*, $1 - \alpha_d$ is the proportion of real and reactive load which is shed.

Also our load model is constant power *i.e.*, independent of the voltage. This assumption helps to keep the load model linear. The other load models which are dependent on voltage (*e.g.*, see [47] for other voltage dependent load models) can be included but then the equations will become nonlinear; because of the product of voltage with α.

5.2 Optimal Load Shedding

In this section we give optimal load shedding (OLS) model of power system. The OLS model assumes the form of the OPF, but permits a proportion of the load at any bus to be shed. Note that this is *intentional* shedding and not automatic shedding as result of low voltages or frequency. To implement this in the real network there has to be central control over equipment. Now we will briefly give the formulations of AC and DC OLS and then test the models on 14 bus IEEE network.

5.2.1 AC Optimal Load Shedding

The OLS problem is closely related to the OPF problem of Sec. 2.2. The OLS problem is to maximize the amount of load delivered to the customers satisfying the bus voltage limits, the apparent power line limits and the real and reactive generator output power limits. It can be written as:

$$\max \sum_{d\in\mathcal{D}} M_d \alpha_d P_d^{\mathrm{D}}, \tag{5.2a}$$

subject to

$$\left.\begin{aligned} \sum_{g\in\mathcal{G}_b} p_g^{\mathrm{G}} &= \sum_{d\in\mathcal{D}_b} p_d^{\mathrm{D}} + \sum_{b'\in\mathcal{B}_b} p_{bb'}^{\mathrm{L}} + G_b^{\mathrm{B}} v_b^2, \\ \sum_{g\in\mathcal{G}_b} q_g^{\mathrm{G}} &= \sum_{d\in\mathcal{D}_b} q_d^{\mathrm{D}} + \sum_{b'\in\mathcal{B}_b} q_{bb'}^{\mathrm{L}} - B_b^{\mathrm{B}} v_b^2, \end{aligned}\right\}, \forall\, b\in\mathcal{B}, \tag{5.2b}$$

$$\left.\begin{aligned} p_{bb'}^{\mathrm{L}} &= v_b^2 G_{bb} + v_b v_{b'}(G_{bb'}\cos(\theta_b-\theta_{b'}) + B_{bb'}\sin(\theta_b-\theta_{b'})), \\ q_{bb'}^{\mathrm{L}} &= -v_b^2 B_{bb} + v_b v_{b'}(G_{bb'}\sin(\theta_b-\theta_{b'}) - B_{bb'}\cos(\theta_b-\theta_{b'})), \end{aligned}\right\}, \ \forall\, (b,b')\in\mathcal{L}, \tag{5.2c}$$

$$\left.\begin{aligned} p_d^{\mathrm{D}} &= \alpha_d P_d^{\mathrm{D}}, \\ q_d^{\mathrm{D}} &= \alpha_d Q_d^{\mathrm{D}}, \\ 0 &\le \alpha_d \le 1, \end{aligned}\right\}, \ \forall\, d\in\mathcal{D}, \tag{5.2d}$$

$$\theta_{b_0} = 0, \tag{5.2e}$$

$$V_b^{\mathrm{LB}} \le v_b \le V_b^{\mathrm{UB}}, \ \forall\, b\in\mathcal{B}, \tag{5.2f}$$

$$\left.\begin{aligned} P_g^{\mathrm{LB}} &\le p_g \le P_g^{\mathrm{UB}}, \\ Q_g^{\mathrm{LB}} &\le q_g \le Q_g^{\mathrm{UB}}, \end{aligned}\right\}, \ \forall\, g\in\mathcal{G}, \tag{5.2g}$$

$$p_{bb'}^{\mathrm{L}}{}^2 + q_{bb'}^{\mathrm{L}}{}^2 \le (S_{bb'}^{\max})^2, \ \forall\, (b,b')\in\mathcal{L}, \tag{5.2h}$$

where (5.2a) is the objective function, which is the maximization of the amount of load delivered at all buses. M_d is the reward of delivering load at the bus d. Equations (5.2b-5.2c) are the Kirchhoff's Current and Kirchhoff's Voltage laws, equations (5.2d) are the load model as given in the section (5.1). Equation (5.2e) removes the degeneracy

in the bus by fixing it to zero at arbitrary reference bus, (5.2f-5.2h) are the constraints on real power generation, reactive power generation and the apparent power flow in lines respectively.

The only difference in the problem 5.2 and the OPF model (given in section 2.2) is the objective function and the equations (5.2d). The objective function (5.2a) is linear and so are the equations (5.2d). The ACOLS problem is nonconvex but no new non convexity is introduced in this formulation. The AC-OLS is a nonlinear programming (NLP) problem and may be solved efficiently by interior point methods.

5.2.2 DC Optimal Load Shedding

DC OLS uses DC model of line flow equations (as discussed in section 2.5.2) and thus ignores voltages and the reactive power. There are no line loses in the DC model. The problem is as follows:

$$\max \sum_{d \in \mathcal{D}} M_d \alpha_d P_d^{\mathrm{D}}, \tag{5.3a}$$

subject to

$$\sum_{g \in \mathcal{G}_b} p_g^{\mathrm{G}} = \sum_{d \in \mathcal{D}_b} p_d^{\mathrm{D}} + \sum_{b' \in \mathcal{B}_b} p_{bb'}^{\mathrm{L}}, \quad \forall\, b \in \mathcal{B}, \tag{5.3b}$$

$$p_{bb'}^{\mathrm{L}} = B_{bb'}(\theta_b - \theta_{b'}), \quad \forall (b, b') \in \mathcal{L}, \tag{5.3c}$$

$$\left.\begin{aligned} p_d^{\mathrm{D}} &= \alpha_d P_d^{\mathrm{D}}, \\ 0 \le \alpha_d &\le 1, \end{aligned}\right\}, \forall\, d \in \mathcal{D}, \tag{5.3d}$$

$$\theta_{b_0} = 0, \tag{5.3e}$$

$$P_g^{\mathrm{LB}} \le p_g \le P_g^{\mathrm{UB}}, \quad \forall\, g \in \mathcal{G}, \tag{5.3f}$$

$$p_{bb'}^{\mathrm{L}} \le P_{bb'}^{\max}, \quad \forall\, (b, b') \in \mathcal{L}. \tag{5.3g}$$

The objective function and all the constraints are linear in 5.3, so DCOLS is an LP and can be solved easily.

5.2.3 Optimal Load Shedding on IEEE 14 bus test network

We use the IEEE 14 bus test system from [41] and test our ACOLS and DCOLS models on this test network. The network diagram of 14 bus network is shown in Fig 5.1. The network consists of 20 transmission lines, 2 generators and 3 synchronous generators. Synchronous generators are modelled with zero upper bound on real power generation. The bounds on two generators in this system are as follows:

$$0 \le p_1^{\mathrm{G}} \le 200 \text{ MW},$$

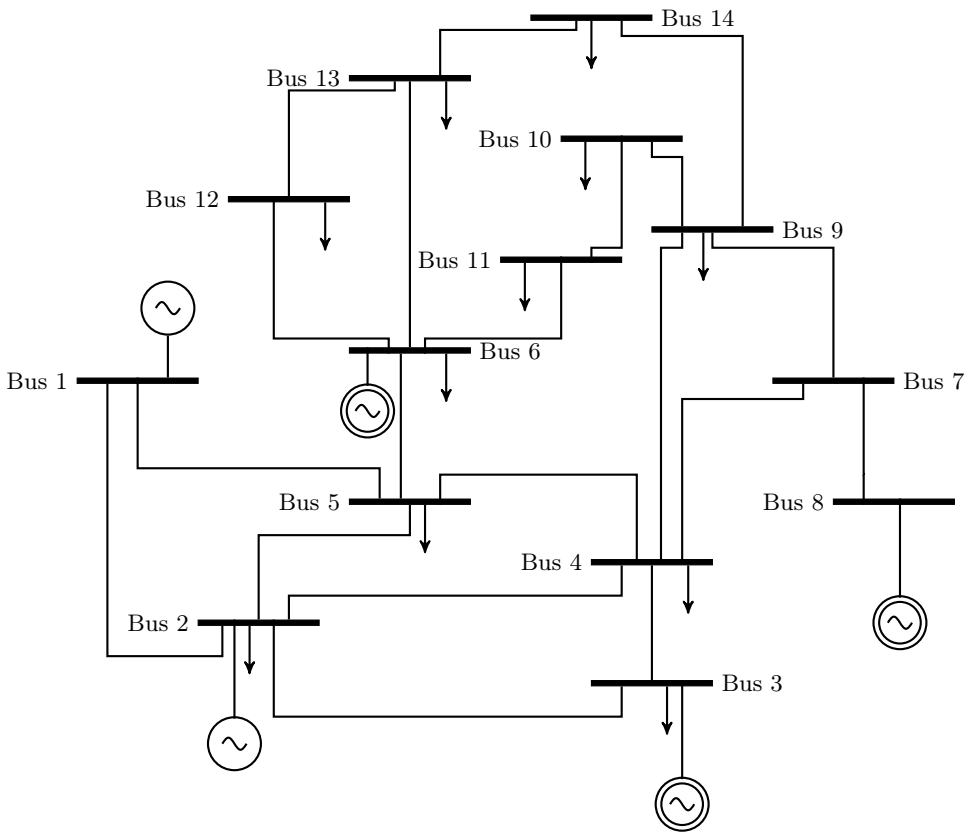

Figure 5.1: 14 Bus IEEE Network

$$0 \leq p_2^{\mathrm{G}} \leq 200 \text{ MW},$$
$$-150 \leq q_1^{\mathrm{G}} \leq 150 \text{ Mvar},$$
$$-150 \leq q_2^{\mathrm{G}} \leq 150 \text{ Mvar}.$$

The reactive power bounds on synchronous generators are in the interval $[0, 140]$ Mvar. Total demand in this network is 259 MW. Line limits are not specified in the data so we assume 100 MVA limits imposed on all lines. In normal operation all the loads are satisfied from the generators at buses 1 and 2.

To simulate the abnormal operating condition, we switch off the generator at bus 2. This is done by the following constraint:

$$0 \leq p_2^{\mathrm{G}} \leq 0 \text{ MW},$$

Now real power capacity in the system is 200 MW which is less that the demand (259 MW). We run our AC-OLS and DC-OLS model and analyse the results of both models.

Tab. A.1 and Tab. A.2 in the Appendix A give optimal solutions for the AC OLS and DC OLS respectively. The key points are summarized as follows:

- Total load supplied is 147.9 MW (AC) and 154.6 MW (DC).

- The load at bus 2 has been fully shed in both cases, while the AC OLS sheds 94.9% of the load at bus 3 compared with 87.8% for DC OLS.
- Total real power generation is 153.8 MW (AC) and 154.6 MW (DC). In neither case is the sole remaining generator operating at capacity (200 MW).
- Line (1,2) is operating at capacity. All others lines are within limits.
- Bus and line values for AC and DC match closely and the line flows determined by AC and DC models are in the same directions.
- The line losses are 5.9 MW in AC. DC model ignore these line losses.

5.2.4 Cutting lines to reduce load shed

We now use 14 bus example to illustrate the surprising result that switching off lines (and so reducing the capacity of that part of the network) can reduce the amount of load that has to be shed. Note that in our 14 bus example, the capacity of generator at bus 1 is 200 MW but in both models it is generating less than the capacity. It is not immediately obvious from the data as to why the single generator is unable to operate nearer to capacity, and so reduce the load shed. Sensitivity analysis shows that by far the highest shadow price is on the MVA limit constraint for line (1,2).

Fig. 5.2 shows the topology of network before and after line cuts, and in Appendix A Tab. A.3 and Tab. A.4 show the results from the ACOLS and DCOLS formulations when lines (2,3) and (2,5) are cut prior to solving the optimization problems. Having made these line cuts, the generator at bus 1 is now operating at or near to maximum capacity, providing 200 MW (DC) and 198.1 MW (AC) to the rest of the network. For AC, the same buses (2 and 3) as before have shed or part-shed their loads; bus 2 has fully shed but- as a consequence of the increased generation-bus 3 has shed only 56.2% compared with 94.9% previously. The situation for DC at first appears to be rather different: bus 2 has fully shed, while, of the rest, the only load that has not shed is at bus 3-all other buses have part shed between 3.6% (bus 5) and 99.6% (bus 2). However it should be noted that no losses are modelled, reactive power and voltage is neglected. This implies the limitation of DC model in capturing the real amount of load shed.

Disconnecting lines (2,3) and (2,5) has increased the real power carried over lines (1,5) and (2,4) to near capacity levels. Previously these lines carried 54.6 and 41.6 MW respectively. Meanwhile, line (1,2) remains at capacity. The net effect is a higher flow of real power from buses from 1 and 2 to the rest of the network. This better solution is not available without the line cuts in place; with the lines present, any phase angle differences between the bus 2 and buses 3 and 5 implies non zero flow of power. Viewed

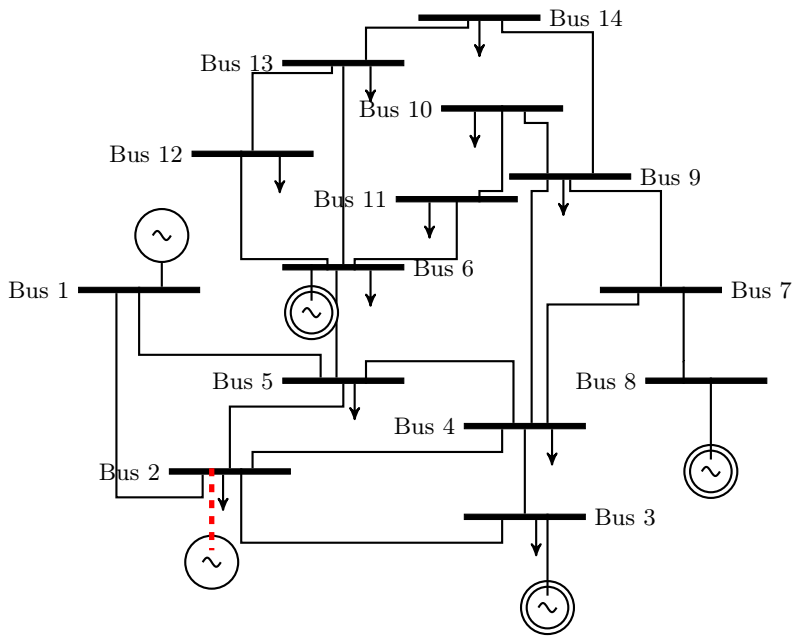

(a) No Line Cuts

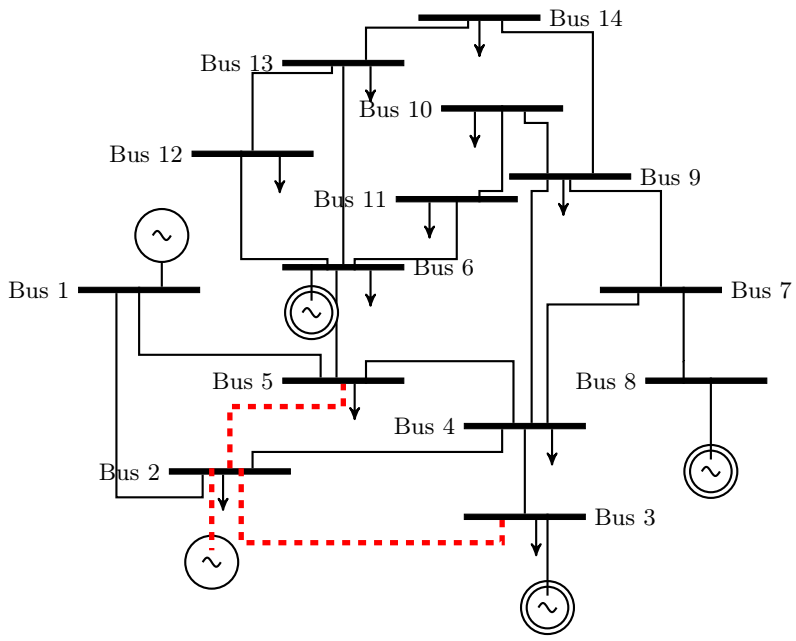

(b) Lines (2,3) and (2,5) cut

Figure 5.2: Network topologies of IEEE 14 bus system with no line cut, and with lines cut.

differently, with all lines intact the network is unable to establish the conditions required to "move" enough generated power from buses 1 and 2 to the rest of the buses.

The above example shows that by including more controls in the framework of optimization we can significantly improve the objective value. This is analogous to the result in OPF that on occasions the optimal generation cost can be reduced by switching off lines. Also this serves as a classical example to motivate line switching in

the context of OPF. In next sections we describe two such control models which can be incorporated in the optimization framework.

5.3 Line Switching

In section 5.2.3 we showed that the objective of DCOLS and ACOLS can be improved by changing the topology of the network. In this section we give the line switching model which can be incorporated in the optimization framework to decide the optimal topology of the network.

Let $\rho_{bb'}$ denotes the switch on the line (b, b'). When $\rho_{bb'} = 1$, the line is switched on, and when $\rho_{bb'} = 0$ the line is switched off and no power is flowing in the line. When a line is switched off we assume it is disconnected at both ends so that the line is no longer attached to a bus. The variables at the either end of the *off* line must be independent of the line properties. To model this, we introduce *line* variables—v_b^{L} and $v_{b'}^{\mathrm{L}}$ as end voltages and $\theta_{bb'}^{\mathrm{L}}$ as the angle difference—that are distinct from *bus* variables v_b, $v_{b'}$ and $\theta_{bb'}$. The following constraints control the relationship between line variables and bus variables. For a line $l \in \mathcal{L}$ with end buses b and b',

$$-\Theta_{bb'}\rho_{bb'} \leq \theta_l^{bb'} \leq \Theta_{bb'}\rho_{bb'}, \tag{5.4a}$$

$$-\Theta_{bb'}^{+}(1-\rho_{bb'}) \leq \theta_l^{bb'} - \theta_{bb'} \leq \Theta_{bb'}^{+}(1-\rho_{bb'}), \tag{5.4b}$$

$\forall i \in \mathcal{B}_{bb'}$:

$$0 \leq v_b - v_b^{\mathrm{L}} \leq (V_b^{\mathrm{UB}} - V_b^{\mathrm{LB}})(1-\rho_{bb'}), \tag{5.4c}$$

$$V_b^{\mathrm{LB}} \leq v_b^{\mathrm{L}} \leq V_b^{\mathrm{LB}} + (V_b^{\mathrm{UB}} - V_b^{\mathrm{LB}})\rho_{bb'}, \tag{5.4d}$$

and $\forall i \in \mathcal{B}$,

$$V_b^{\mathrm{LB}} \leq v_b \leq V_b^{\mathrm{UB}}, \tag{5.4e}$$

where $\Theta_{bb'}^{+} \geq \Theta_{bb'}$ is a "big-M" constant. Of these, (5.4a) and (5.4b) force equality of $\theta_l^{bb'}$ and $\theta_{bb'} = \delta_b - \delta_{bb'}$ for a connected line, but set $\theta_l^{bb'} = 0$ for a disconnected line while allowing the *bus* angles δ_b and $\delta_{b'}$ to vary independently. Likewise, if $\rho_{bb'} = 1$ then, by (5.4c), $v_l^b = v_b$ and $v_l^{b'} = v_{b'}$. However, if $\rho_{bb'} = 0$ then the line voltages are set to minimum values—$v_l^b = V_b^{\mathrm{LB}}$ and $v_l^{b'} = V_{b'}^{\mathrm{LB}}$—independent of the bus voltages v_b and $v_{b'}$.

5.4 Generator Switching

In real time operation of power system it is difficult to significantly change the mechanical input of generators. In small time scale either the generators can be switched off or can be changed slightly from there current operating point. We assume that a generator that is operating can either have its input mechanical power disconnected, in which case real output power drops to zero in steady state, or its output can be set to a new value within a small interval, $[P_g^{\mathrm{G}-}, P_g^{\mathrm{G}+}]$, say, for generator g, around the last known operating value. The limits will depend on the ramp and output limits of the generator, and the amount of immediate or short-term reserve capacity available to the generator.

For reactive power, it is assumed that a new output can be set in some range Q_g^{LB} to Q_g^{UB}. The set of possible real and reactive power outputs of a generator is usually convex.

In the more general case, since the range of values for the real power output is small, the feasible region for the problem is a narrow slice through a convex set, and—except when the real power output is close to its upper limit—it is a good approximation to treat the real and reactive power bounds as independent (see Fig. 5.3). If this is not the case, it is straightforward to add constraints that couple p_g^{G} and q_g^{G}.

The operating regime is modelled by the constraints

$$\zeta_g P_g^{\mathrm{G}-} \leq p_g^{\mathrm{G}} \leq \zeta_g P_g^{\mathrm{G}+}, \forall g \in \mathcal{G}, \tag{5.5a}$$

$$Q_g^{\mathrm{LB}} \leq q_g^{\mathrm{G}} \leq Q_g^{\mathrm{UB}}, \forall g \in \mathcal{G}, \tag{5.5b}$$

$$\zeta_g = 1, \forall g \in \{\mathcal{G} : P_g^{\mathrm{LB}} = 0\} \cup \mathcal{G}^1. \tag{5.5c}$$

Here, ζ_g is a binary variable and denotes the on/off setting of the real power output, and $\mathcal{G}^1$ is a subset of generators which are required to remain on.

5.5 Component switching

Similarly we can model on/off state of other components of power system using the binary variables. These components can be a bank of capacitors, shunts attached to the buses or other components. Such rules can easily be included in the formulation using standard techniques for deriving constraints from logical rules [48]. It is also possible to permit the switching of other network components directly as part of the decision problem. For example, the switching of a shunt component at a bus b can be modelled

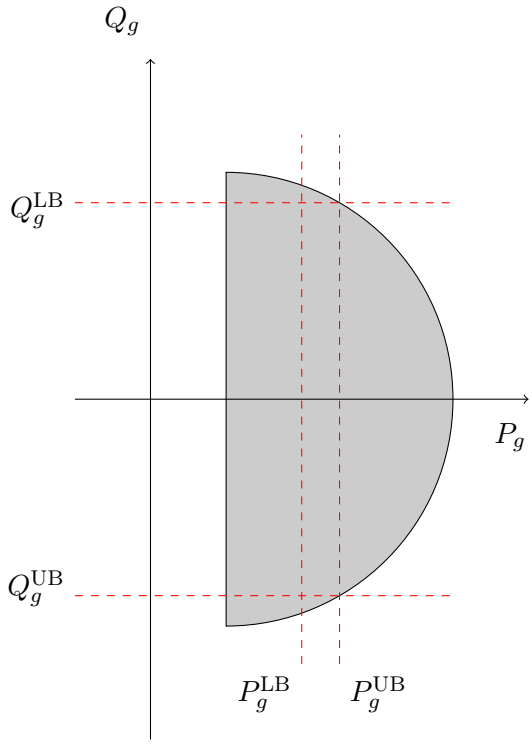

Figure 5.3: Generator limits for a generator

by introducing binary and continuous variables, ξ_b and u_b respectively, constraints

$$\xi_b(V_b^{\mathrm{LB}})^2 \leq u_b \leq \xi_b(V_b^{\mathrm{UB}})^2,$$
$$-(1-\xi_b)(V_b^{\mathrm{LB}})^2 \leq u_b - v_b^2 \leq (1-\xi_b)(V_b^{\mathrm{UB}})^2,$$

and replacing the $G_i^{\mathrm{B}} v_b^2$, $B_i^{\mathrm{B}} v_b^2$ terms in (5.2b) with $G_b^{\mathrm{B}} u_i$ and $B_b^{\mathrm{B}} u_i$, respectively.

Chapter 6

Islanding Model of Power Networks to avoid Large Area Blackouts

Power systems are designed to handle minor disturbances. But sometimes unpredictable events like wind storm or natural disasters happen and cause severe imbalance of generation and demand. Since power systems are not designed to handle such a situation, cascading outages occur and lead to large area blackout.

In recent years, there has been an increase in the occurrence of wide-area blackouts of power networks. In 2003, separate blackouts in Italy [49], Sweden/Denmark [50] and USA/Canada [51] affected millions of customers. The wide-area disturbance in 2006 to the European system caused the system to split in an uncontrollable way [52], forming three islands. More recently, the UK network experienced a system-wide disturbance caused by an unexpected loss of generation; blackout was avoided by local load shedding [53].

The biggest blackout of history recently happened in India (for detailed report see [54]). Approximately 670 million people were affected by this blackout and it took one week to restore the power. This blackout was caused by tripping of a 400 kV transmission line and a substation. Cascading tripping followed and 32GW of generating capacity was taken out of the system.

Fig. 6.1 (source: [55]) shows the average number of blackouts/outages around the world, and the average duration of it in hours. There is a lot of variation in this graph depending upon the countries. The power systems in the developed countries are very reliable but when the unpredictable events happen and blackouts strike, the economic costs are enormous and it takes a long time to mitigate its effects. To appreciate the scale of problems caused by blackouts, we give few examples here from the famous North eastern blackout of USA/Canada in 2003. Famous auto-mobile company Daimler Chrysler lost production at 14 of its 31 plants, and they had to scrap 10,000 vehicles which were going through the paint shop at the time of the blackout. New York city

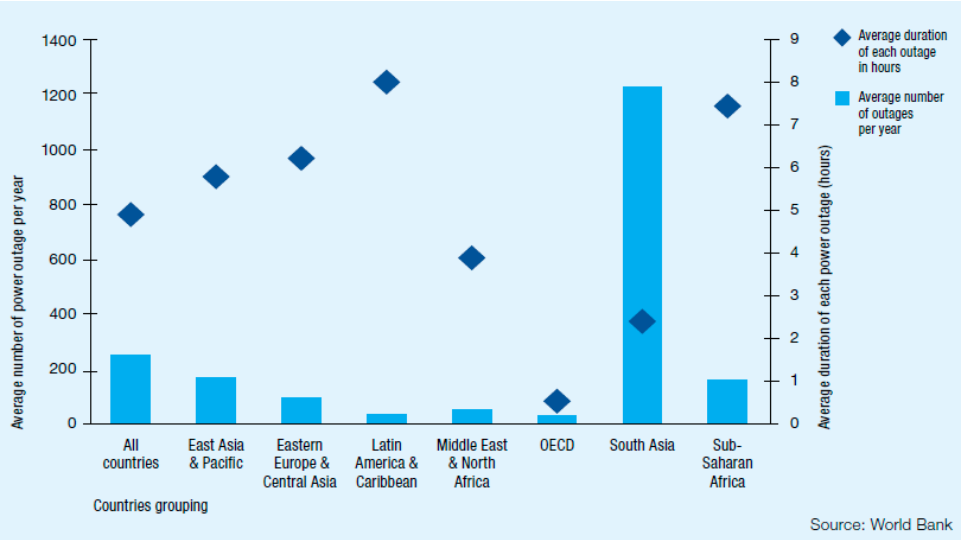

Figure 6.1: Blackouts around the world

mayor estimated USD 10 m to be given in overtime compensations, and approximately 1,000 flights were cancelled [55]. In nutshell, blackout cause a lot of problems in the developed world. Comparatively, blackouts are not that lethal for developing countries, as people's reliance on electricity is limited and alternate arrangements are handy if the outage occurs. Interesting thing to note in Fig. 6.1 is that the clearing time of blackouts is small in developing countries. This is because that most of the outages are planned, and happen because there is not enough generation to match the demand. People in these countries embrace for the planned load shedding accordingly.

6.1 Motivation of Controlled Islanding

While the exact causes of wide-area blackouts differ from case to case, some common driving factors emerge. Modern power systems are being operated closer to limits: liberalization of the markets, and the subsequent increased commercial pressures and change in expenditure priorities, has led to a reduction in security margins [56, 57, 58]. A more recently occurring factor is increased penetration of variable distributed generation, notably from wind power, which brings significant challenges to secure system operation [59].

The causes of blackouts can be categorized into following four general categories:

- Natural Causes
  - Lightening, rain, snow, wind storm
- Technical failures
  - Transformer faults, Short circuits

	% of events	Mean size in MW	Mean size in customers
Earthquake	0.8	1,408	375,900
Tornado	2.8	367	115,439
Hurricane/tropical storn	4.2	1,309	782,695
Ice storm	5.0	1,152	343,448
Lightening	11.3	270	70,944
Wind/rain	14.8	793	185,199
Other cold weather	5.5	542	150,255
Fire	5.2	431	111,244
Intentional attack	1.6	340	24,572
Supply storage	5.3	341	138,957
Other external cause	4.8	710	246,071
Equipment failure	29.7	379	57,140
Operator error	10.1	489	105,322
Voltage reduction	7.7	153	212,900
Volunteer reduction	5.9	190	134,543

Table 6.1: Statistics of causes of Large blackouts in USA during 1984-2006. (Source: [1])

- Human error
  - Error of judgement, communication errors between operators
- Terrorism
  - Bombing, cyber attacks, High Altitude Electromagnetic Pulse(HEMP) and Intentional Electromagnetic Interfernce(IEMI)

According to a study conducted in [1] on blackouts during 1984-2006, 44% of the power outages were caused by weather related issues. Equipment failure caused about 30% of the outages, and in 6% of the cases network operators shed the load to save the network from large blackout. Other statistics are reported in Tab. 6.1.

The risk of blackouts is increasing due to liberalization and integration of renewable sources of power. The recent liberalization of energy markets has reduced the security margin of operation. Also there is a lot of emphasizes on renewable resources. The downside of renewable energy is the volatile supply of power which is causing problems. Fig. 6.2 shows the increasing trend of blackouts.

When a large disturbance happens in some part of power system, it tends to propagate from its starting point, and if no control actions are taken in time, the disturbance

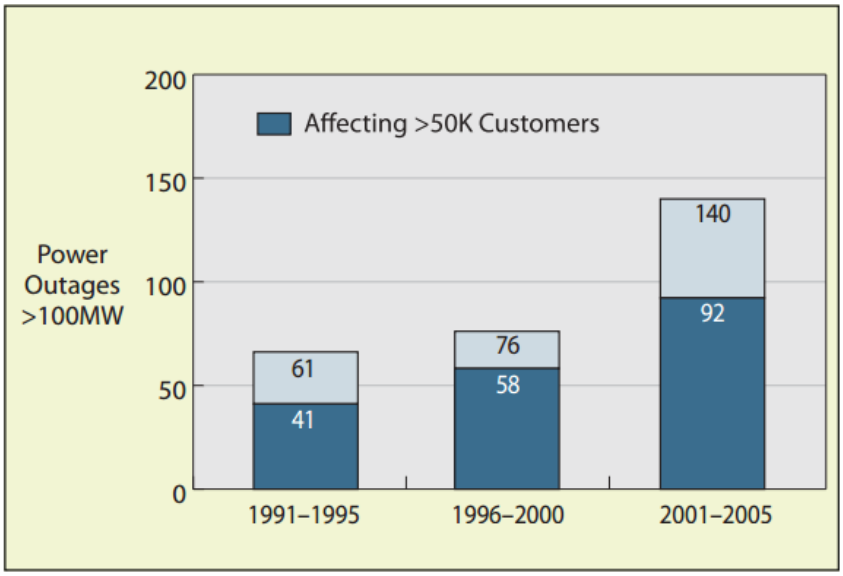

Figure 6.2: Increasing risk of blackouts (from: [2])

can affect large parts of the network. If the disturbance is big enough then it can start the cascade outages of components of power system and can potentially lead to wide area blackout. For several large disturbance events (*e.g.*, in [51]), studies have shown that a wide-area blackout could have been prevented by intentionally splitting the system into islands [60]. By isolating the faulty part of the network, the total load disconnected in the event of a cascading failure is reduced. *Controlled islanding* or *system splitting* is therefore attracting an increasing amount of attention. The problem is how to split the network into islands that are as closely balanced as possible in load and generation, have stable steady-state operating points within voltage and line limits, and so that the action of splitting does not cause dynamic instability.

6.2 Literature Review of Islanding Techniques

Islanding of power system is a combinatorial optimization problem because of the possible line switching decisions to island the network. The main focus of islanding is to find balanced islands. However islanding is a major operating decision and there are various other practical aspects to it as well *e.g.*, dynamic stability and operational requirements. Including all these aspects is a considerable challenge, since the search space of line cutsets grows exponentially with network size, and is exacerbated by the requirement for strategies that obey non-linear power flow equations and satisfy operating constraints.

It is not computationally practical to tackle all the aspects of the problem simultaneously within a single optimization, and approaches in the literature differ according to

which aspect is treated as the primary objective. Additionally different search methods have been proposed for defining the island boundaries. An example where the primary objective is to produce load balanced islands is [61]. This proposes a three-phase ordered binary decision diagram (OBDD) to generate a set of islanding strategies. The approach uses a reduced graph-theoretical model of the network to minimize the search space for islanding; power flow analyses are subsequently executed on islands to exclude strategies that violate operating constraints, *e.g.*, line limits.

In other approaches the primary objective is to split the network into electromechanically stable islands, commonly by splitting so that generators with coherent oscillatory modes are grouped. If the system can be split along boundaries of coherent generator groups while not causing excessive imbalance between load and generation, then the system is less likely to lose stability. Determining the required cutset of lines involves, as a secondary objective, considerations of load-generation balance and other constraints; algorithms include exhaustive search [62], minimal-flow minimal-cutset determination using breadth-/depth-first search [63], graph simplification and partitioning [64], and metaheuristics [65, 66]. The authors of [67] propose a framework that, iteratively, identifies the controlling group of machines and the contingencies that most severely impact system stability, and uses a heuristic method to search for a splitting strategy that maintains a desired stability margin. [68] employed a power flow tracing algorithm to first determine the domain of each generator, *i.e.*, the set of load buses that 'belong' to each generator. Subsequently, the network is coarsely split along domain intersections before refinement of boundaries to minimize imbalances. While it is known that the sensitivity of coherent machine groupings to fault location is low, it is true that splitting the network along the boundaries of *a-priori* determined coherent groups is not, in general, the only islanding solution that maintains stability. Moreover, such islands may be undesirable in terms of other criteria, such as the amount of load shed, the voltage profile or the possibility that the impacted region may be contained within a larger than necessary island. For example, in [69], the slow-coherence-based islanding of the 39-bus New England system isolates the network's largest generator in an island with no load. In [70], an optimization-based approach to islanding and load shedding was proposed. A key feature is that, unlike many other methods, it can take into account a part of the network that is desired to be isolated—*e.g.*, an impacted area—when determining islands, and isolate this while minimizing the expected amount of load shed or lost. The problem is formulated as a single mixed integer linear programming (MILP) problem, meaning that power balances, flows, and operating limits may be handled explicitly when designing islands, and satisfied in each island in a feasible solution.

The islanding MILP problem has similarities with the *transmission switching* prob-

lem [71], in that the decision variables include which lines to disconnect, while power flow constraints must be satisfied following any disconnection. Both approaches—islanding and transmission switching—may be seen as network topology optimization problems with added power flow constraints. In both cases, inclusion of AC power flow laws in the constraints results in a mixed integer nonlinear program (MINLP), which is difficult to solve. Hence, linear DC power flow has been used to date, resulting in a more computationally favourable MILP or MIQP problem.

Here we present an optimization framework for controlled islanding. The method's primary objective is to minimize the expected amount of load that has to be disconnected while leaving the islanded network in a balanced steady state. The post-islanding dynamics are not modelled explicitly in the optimization, as this greatly increases the computational difficulty of the problem. Instead penalties are used to discourage large changes to power flows, and it is shown by simulation in [70] that this results in the islanding solutions being dynamically stable.

6.3 Our Idea of Islanding

An application of islanding which has received little attention is islanding in response to particular contingencies so as to isolate vulnerable parts of the network. For example after some failure, part of the network may be vulnerable to further failure, or a suspected failure of monitoring equipment may have resulted in the exact state of part of the network being uncertain. In such a case an action that would prevent cascading failures throughout the network is to form an island surrounding the uncertain part of the network so isolating it from the rest. A method that does not take into account the location of the trouble when designing islands may leave the uncertain equipment within a large section of the network, all of which may become insecure as a result. Figure 6.3(a) illustrates the situation: uncertain lines and buses are indicated by a "?". Figure 6.3(b) shows a possible islanding solution for this network: all uncertain buses have been placed in Section 0 and all uncertain lines with at least one end in Section 1 are disconnected. The following distinction is made between *sections* and *islands*. The split network consists of two sections, an "unhealthy" Section 0 and a "healthy" Section 1 with no lines connecting the two sections, and all uncertain equipment in Section 0. However, neither section is required to be connected so may contain more than one island: in Figure 6.3(b), Section 1 comprises islands 1, 3 and 4, and Section 0 is a single island. The optimization will determine the boundaries of the sections, the number and boundaries of the islands, the generator adjustments, and the amount of each load that is planned to be shed.

A balance has to be found between the load that is planned to be shed and the

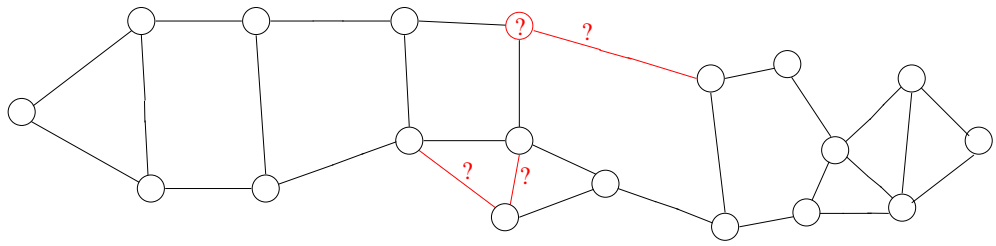

(a) Network prior to islanding

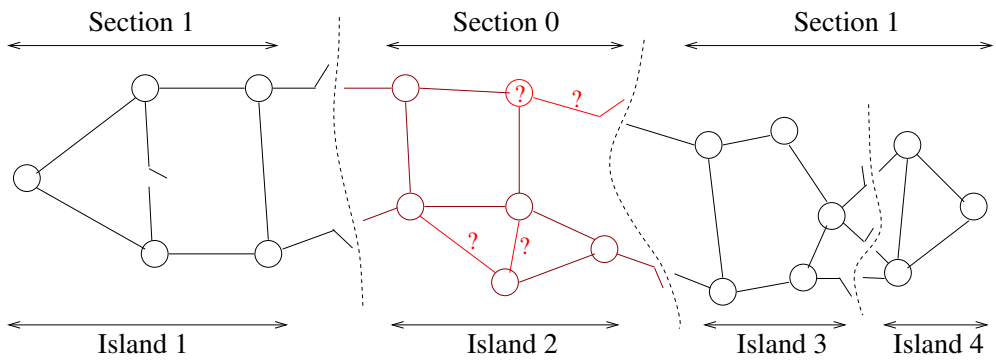

(b) Network post islanding

Figure 6.3: (a) Illustration of a network with uncertain buses and lines, and (b) the islanding of that network by disconnecting lines.

residual load that is left in Section 0, which may be lost because that section is vulnerable. This can be achieved by taking as objective the sum of the value of the loads remaining in both sections after the planned load shedding minus a proportion of the the value of the load remaining in Section 0 after the planned load is shed.

The proposed approach has two stages: first, a mixed-integer linear programming (MILP) islanding problem, which includes the linear DC flow equations and flow limits, is solved to determine a DC-feasible solution; secondly, an AC optimal load shedding optimization is solved to provide an AC-feasible steady-state post-islanding operating point. Integer programming has many applications in power systems, but its use in network splitting and blackout prevention is limited. [72] proposed an IP-based approach to the problem of designing networks that are robust to sets of cascading failures and thus avoid blackouts; whether to upgrade a line's capacity is a binary decision. [71, 73] propose methods for optimal transmission switching for the problem of minimizing the cost of generation dispatch by selecting a network topology to suit a particular load. In common with the formulation presented here, binary variables represent switches that open or close each line and the DC power flow model is used, resulting in a MILP problem. However, in our model sectioning constraints are present, and the problem is to design balanced islands while minimizing load shed.

6.4 MILP formulation of the Islanding problem

This section presents a MILP formulation for the problem of finding a steady state islanded solution in a stressed network, while minimizing the expected load lost.

Consider a network that comprises a set of buses $\mathcal{B} = \{1, 2, \ldots, n^{\mathrm{B}}\}$ and a set of lines $\mathcal{L}$. There exists a set of generators $\mathcal{G}$ and a set of loads $\mathcal{D}$. A subset $\mathcal{G}_b$ of generators is attached to bus $b \in \mathcal{B}$; similarly, $\mathcal{D}_b$ contains the subset of loads present at bus $b \in \mathcal{B}$.

6.4.1 Sectioning constraints

Motivated by the previous section, the intention is to partition the buses and lines between Sections 0 and 1. It is suspected that some subset $\mathcal{B}^0 \subseteq \mathcal{B}$ of buses and some subset $\mathcal{L}^0 \subseteq \mathcal{L}$ of lines are faulty or at risk. No uncertain components are allowed in Section 1.

A binary variable γ_b is defined for each bus $b \in \mathcal{B}$; γ_b is set equal to 0 if b is placed in section 0 and $\gamma_b = 1$ otherwise. A binary variable $\rho_{bb'}$ is defined for each $(b, b') \in \mathcal{L}$; $\rho_{bb'} = 0$ if line (b, b') is disconnected and $\rho_{bb'} = 1$ otherwise.

Constraints (6.1a) and (6.1b) apply to lines in $\mathcal{L} \backslash \mathcal{L}^0$. A line is cut if its two end buses are in different sections (*i.e.* $\gamma_b = 0$ and $\gamma_{b'} = 1$, or $\gamma_b = 1$ and $\gamma_{b'} = 0$). Otherwise, if the two end buses are in the same section then $\rho_{bb'} \leq 1$, and the line may or may not be disconnected. Thus, these constraints enforce the requirement that any certain line between sections 0 and 1 shall be disconnected.

$$\rho_{bb'} \leq 1 + \gamma_b - \gamma_{b'}, \forall (b, b') \in \mathcal{L} \setminus \mathcal{L}^0, \tag{6.1a}$$

$$\rho_{bb'} \leq 1 - \gamma_b + \gamma_{b'}, \forall (b, b') \in \mathcal{L} \setminus \mathcal{L}^0. \tag{6.1b}$$

Constraints (6.1c) and (6.1d) apply to lines assigned to $\mathcal{L}^0$. A line $(b, b') \in \mathcal{L}^0$ is disconnected if at least one of the ends is in Section 1. Thus, an uncertain line either (i) shall be disconnected if entirely in Section 1, (ii) shall be disconnected if between sections 0 and 1, or (iii) may remain connected if entirely in Section 0.

$$\rho_{bb'} \leq 1 - \gamma_b, \forall (b, b') \in \mathcal{L}^0, \tag{6.1c}$$

$$\rho_{bb'} \leq 1 - \gamma_{b'}, \forall (b, b') \in \mathcal{L}^0, \tag{6.1d}$$

Constraints (6.1e) and (6.1f) set the value of γ_b for a bus b depending on what section that bus was assigned to. $\mathcal{B}^1$ is defined as the set of buses that are required to remain in Section 1. It may be desirable to exclude buses from the "unhealthy" section,

and such an assignment will usually reduce computation time.

$$\gamma_b = 0, \forall\ b \in \mathcal{B}^0, \tag{6.1e}$$

$$\gamma_b = 1, \forall\ b \in \mathcal{B}^1. \tag{6.1f}$$

Given some assignments to $\mathcal{B}^0, \mathcal{B}^1$ and $\mathcal{L}^0$, the optimization will disconnect lines and place buses in Sections 0 or 1, hence partitioning the network into Sections 0 and 1. What else is placed in Section 0, what other lines are cut, and which loads and generators are adjusted, are degrees of freedom for the optimization, and will depend on the objective function.

Note that if $\mathcal{B}^1 = \{\}$, then it is up to the optimization to decide wheather to island or not. In this case the islanding decision would depend on the objective function. If $\mathcal{B}^1 \neq \{\}$, then the sectioning constraints (6.1a)-(6.1f) force the network to island.

6.4.2 DC power flow model with line losses

The power flow model employed is a variant of the "DC" model. As in the standard DC model it assumes unit voltage at each bus and uses a linearization of Kirchhoff's voltage law, but unlike the standard DC model the variant also accounts for line losses. We model the line flows in a line from one side and model the loss in a line. Let us consider a $n^{\mathrm{L}} \times 2$ line bus matrix $\mathcal{A}$. The matrix is defined as $\mathcal{A}_{l,1} = b$ and $\mathcal{A}_{l,2} = b'$ where b and b' are the *to* and *from* ends of the line l. Kirchhoff's current law is applied at each bus $b \in \mathcal{B}$:

$$\sum_{g \in \mathcal{G}_b} p_g^{\mathrm{G}} = \sum_{d \in \mathcal{D}_b} p_d^{\mathrm{D}} + \sum_{b' \in \mathcal{B}_b : b = \mathcal{A}_{l,1}} p_{bb'}^{\mathrm{L}} - \left(\sum_{b' \in \mathcal{B}_b : b = \mathcal{A}_{l,2}} (p_{b'b}^{\mathrm{L}} - \bar{h}_{bb'}^{\mathrm{L}}) \right), \tag{6.2}$$

where p_g^{G} is the real power output of generator $g \in \mathcal{G}_b$ at bus b, p_d^{D} is the real power demand from load $d \in \mathcal{D}_b$. The variable $p_{bb'}^{\mathrm{L}}$ is the real power flow from bus b . The variable $p_{bb'}^{\mathrm{L}}$ is the real power flow from bus b into the first end of line (b, b'), and $p_{b'b}^{\mathrm{L}} - \bar{h}_{bb'}^{\mathrm{L}}$ is the flow out of the second end of line (b, b') into bus b', the difference in the flows being the loss $\bar{h}_{bb'}^{\mathrm{L}}$.

The standard DC model has no line loss, *i.e.*, $\bar{h}_{bb'}^{\mathrm{L}} = 0$, but this model results in the load loss being underestimated. Actual line losses are non-linear functions of voltages and phase angle differences, and these can be approximated in the DC model by a piecewise linear function. However investigations have shown that this offers little or no improvement in the objective over a simple constant-loss approximation, but adversely affects computation [74]. Therefore, a constant loss model is employed. The loss for line (b, b') is given by

$$\bar{h}_{bb'}^{\mathrm{L}} = \rho_{bb'} h_{bb'}^{\mathrm{L0}}, \tag{6.3}$$

where $h^{\mathrm{L0}}_{bb'}$ is the loss immediately before islanding. The inclusion of $\rho_{bb'}$ drives the loss to zero if the islanding optimization cuts the line.

The linearized version of Kirchhoff's voltage law has the form

$$\hat{p}^{\mathrm{L}}_{bb'} = B^{\mathrm{L}}_{bb'}\Big(\delta_b - \delta_{b'}\Big), \tag{6.4}$$

where $\hat{p}^{\mathrm{L}}_{bb'}$ an auxiliary variable for the real power flow. When the line (b, b') is connected then it is required that $p^{\mathrm{L}}_{bb'} = \hat{p}^{\mathrm{L}}_{bb'}$, but when it is disconnected then $p^{\mathrm{L}}_{bb'} = 0$ and $\hat{p}^{\mathrm{L}}_{bb'}$ is free. This is modelled as follows.

$$-\rho_{bb'} P^{\mathrm{UB}}_{bb'} \leq p^{\mathrm{L}}_{bb'} \leq P^{\mathrm{UB}}_{bb'} \rho_{bb'}, \tag{6.5a}$$

$$-(1 - \rho_{bb'})\hat{P}^{\mathrm{UB}}_{bb'} \leq \hat{p}^{\mathrm{L}}_{bb'} - p^{\mathrm{L}}_{bb'} \leq \hat{P}^{\mathrm{UB}}_{bb'}(1 - \rho_{bb'}), \tag{6.5b}$$

where $P^{\mathrm{UB}}_{bb'}$ is the maximum possible magnitude of real power flow through a line l, and $\hat{P}^{\mathrm{UB}}_{bb'}$ should be large enough to allow two buses across a disconnected line to maintain sufficiently different phase angles. (Note that at the very minimum $\hat{P}^{\mathrm{UB}}_{bb'} \geq P^{\mathrm{UB}}_{bb'}$.) If $\rho_{bb'} = 0$, then $p^{\mathrm{L}}_{bb'} = 0$ but $\hat{p}^{\mathrm{L}}_{bb'}$ may take whatever value is necessary to satisfy the KVL constraint (6.4), while if $\rho_{bb'} = 1$ then $p^{\mathrm{L}}_{bb'} = \hat{p}^{\mathrm{L}}_{bb'}$.

Line limits $P^{\mathrm{UB}}_{bb'}$ may be expressed either directly as MW ratings on real power for each line, or as a limit on the phase angle difference across a line. Since in the model the real power through a line is just a simple scaling of the phase difference across it, then any phase angle limit may be expressed as a corresponding MW limit.

6.4.3 Generation constraints

In the short time available when islanding in response to a contingency it is not possible to start up generators. Generators that are operating can either have their input power disconnected, in which case their real output power drops to zero, or their output can be changed to a value within a small interval, $\left[P^{\mathrm{G}-}_g, P^{\mathrm{G}+}_g\right]$ say for generator g, around their pre-islanded value. The limits will depend on the ramp and output limits of the generator, and the amount of immediate or short-term reserve capacity available to the generator. This alternative operating regime is modelled by the constraints (5.5) given in section 5.4.

6.4.4 Load shedding

Because of the limits on generator power outputs and network constraints it may not be possible after islanding to fully supply all loads. It is therefore necessary to permit some shedding of loads. The load shedding is implemented using the model given by Eq. (5.1) in Section 5.1.

6.4.5 Objective function

The overall goal in islanding is to split the network and leave it in a secure steady state while maximizing the expected value of the load supplied. Suppose a reward M_d per unit is associated with the supply of load d. However if this load is part of Section 0, then because this section is vulnerable, it is assumed there is a risk of not being able to supply power to that load. Accordingly, a load loss penalty $0 \leq \beta_d < 1$ is defined, which may be interpreted as the probability of being able to supply a load d if placed in section 0. If d is placed in Section 1, a reward M_d is realized per unit supply, but if d is placed in Section 0 a lower reward of $\beta_d M_d < M_d$ is realized. The expected value of the load supplied is J_{DC}:

$$J_{\mathrm{DC}} = \sum_{d \in \mathcal{D}} M_d P_d \Big(\beta_d \alpha_{0d} + \alpha_{1d} \Big),$$

where,

$$\alpha_d = \alpha_{0d} + \alpha_{1d}, \forall d \in \mathcal{D}, \tag{6.6a}$$

$$0 \leq \alpha_{0d} \leq 1, \forall d \in \mathcal{D}, \tag{6.6b}$$

$$0 \leq \alpha_{1d} \leq \gamma_b, \forall b \in \mathcal{B}, d \in \mathcal{D}_b. \tag{6.6c}$$

Here a new variable α_{sd} is introduced for the load d delivered in Section $s \in \{0, 1\}$. If $\gamma_b = 0$, (and so the load at bus b is in Section 0), then $\alpha_{1d} = 0, \alpha_{0d} = \alpha_d$ and the reward is $\beta_d M_d P_d \alpha_d$. On the other hand, if $\gamma_b = 1$ then $\alpha_{1d} = \alpha_d$ and $\alpha_{0d} = 0$, giving a higher reward $M_d P_d \alpha_d$. Thus maximizing J_{DC} gives a preference for $\gamma_b = 1$ and a smaller section 0.

The DC optimal islanding problem with objective of maximizing J_{DC} usually has multiple feasible solutions with objectives close to the optimal value. This flexibility is exploited by introducing two penalty terms to the objective which are small enough not to affect significantly the primary objective, but improve the computational performance and provide the flexibility to guide the search towards solutions with good dynamic behaviour. The modified objective is to maximize

$$J_{\mathrm{DC}} - \epsilon_1 \sum_{l \in \mathcal{L} \setminus \mathcal{L}^0} W_{bb'}(1 - \rho_{bb'}) - \epsilon_2 \sum_{g \in \mathcal{G}} W_g (1 - \zeta_g) \tag{6.7}$$

where the $W_{bb'}$, ϵ_1, W_g and ϵ_2 are non-negative weights. The value of J_{DC} in the optimal is denoted by J^*_{DC}. The penalties discourage the disconnection of healthy lines and generators, *i.e.* they encourage the binary variables $\rho_{bb'}$ and ζ_g to take the integer values 1 in the LP relaxations. This improves computational efficiency by reducing the size of the branch and bound tree.

A uniform weight, *e.g.*, $W_{bb'} = 1, \forall (b, b')$, will discourage equally all line cuts, while cuts to high-flow lines may be more heavily discouraged with $W_{bb'} = s^{\mathrm{L0}}_{bb'}$, where $s^{\mathrm{L0}}_{bb'}$ is the pre-islanding apparent power flow through the line. Generation disconnection is uniformly penalized by setting W_g equal to the generator's capacity P^{UB}_g.

6.4.6 Overall formulation

The overall formulation for islanding model is an MILP and is given as follows:

$$\max \quad \left(J_{\mathrm{DC}} - \epsilon_1 \sum_{l \in \mathcal{L} \setminus \mathcal{L}^0} W_{bb'}(1 - \rho_{bb'}) - \epsilon_2 \sum_{g \in \mathcal{G}} W_g (1 - \zeta_g), \right) \tag{6.8a}$$

subject to

$$\sum_{g \in \mathcal{G}_b} p^{\mathrm{G}}_g = \sum_{d \in \mathcal{D}_b} p^{\mathrm{D}}_d + \sum_{b' \in \mathcal{B}_b} p^{\mathrm{L}}_{bb'} - \left(\sum_{b' \in \mathcal{B}_b} p^{\mathrm{L}}_{b'b} - \bar{h}^{\mathrm{L}}_{bb'} \right), \ \forall\, b \in \mathcal{B}, \tag{6.8b}$$

$$\left.\begin{aligned} \hat{p}^{\mathrm{L}}_{bb'} &= B^{\mathrm{L}}_{bb'} \Big(\delta_b - \delta_{b'} \Big), \\ \bar{h}^{\mathrm{L}}_{bb'} &= \rho_{bb'} h^{\mathrm{L0}}_{bb'}, \\ -\rho_{bb'} P^{\mathrm{UB}}_{bb'} &\le p^{\mathrm{L}}_{bb'} \le P^{\mathrm{UB}}_{bb'} \rho_{bb'}, \\ -(1 - \rho_{bb'}) \hat{P}^{\mathrm{UB}}_{bb'} &\le \hat{p}^{\mathrm{L}}_{bb'} - p^{\mathrm{L}}_{bb'} \le \hat{P}^{\mathrm{UB}}_{bb'} (1 - \rho_{bb'}), \end{aligned}\right\}, \ \forall\, (b, b') \in \mathcal{L}, \tag{6.8c}$$

$$\left.\begin{aligned} p^{\mathrm{D}}_d &= \alpha_d P^{\mathrm{D}}_d, \\ \alpha_d &= \alpha_{0d} + \alpha_{1d}, \\ 0 &\le \alpha_{0d} \le 1, \end{aligned}\right\}, \ \forall\, d \in \mathcal{D}, \tag{6.8d}$$

$$0 \le \alpha_{1d} \le \gamma_b, \forall\, b \in \mathcal{B}, d \in \mathcal{D}_b, \tag{6.8e}$$

$$\rho_{bb'} \le 1 + \gamma_b - \gamma_{b'}, \forall\, (b, b') \in \mathcal{L} \setminus \mathcal{L}^0, \tag{6.8f}$$

$$\rho_{bb'} \le 1 - \gamma_b + \gamma_{b'}, \forall\, (b, b') \in \mathcal{L} \setminus \mathcal{L}^0, \tag{6.8g}$$

$$\rho_{bb'} \le 1 - \gamma_b, \forall\, (b, b') \in \mathcal{L}^0, \tag{6.8h}$$

$$\rho_{bb'} \le 1 - \gamma_{b'}, \forall\, (b, b') \in \mathcal{L}^0, \tag{6.8i}$$

$$\gamma_b = 0, \forall\, b \in \mathcal{B}^0, \tag{6.8j}$$

$$\gamma_b = 1, \forall\, b \in \mathcal{B}^1, \tag{6.8k}$$

$$\zeta_g P^{\mathrm{LB}}_g \le p^{\mathrm{G}}_g \le \zeta_g P^{\mathrm{UB}}_g, \forall\, g \in \mathcal{G}. \tag{6.8l}$$

6.5 Post-islanding AC optimal load shedding

The solution of the DC islanding optimization includes values for loads shed and generator real outputs. In general, however, because these values come from a linearized model that ignores voltage and reactive power, these values will not be exactly optimal

or feasible for the true AC problem. Therefore, to determine a good feasible AC solution for the islanded network, an AC optimal load shedding (OLS) problem is solved after the islanding optimization using the islands and generator disconnections determined by the DC islanding.

The use the AC-OLS optimization problem as discussed in section 5.2.1. The AC-OLS is solved for the network in its islanded state. That is, the set $\mathcal{L}$ is modified by removing lines for which $\rho_{bb'} = 0$. Furthermore, any generator for which $\zeta_g = 0$ has its upper and lower bounds on real power set to zero; others are free to vary real power output within a restricted region, as described previously.

We consider the real and reactive power bounds in ACOLS as: $(p_g^{\mathrm{G}}, q_g^{\mathrm{G}}) \in \mathcal{O}_g$, $\forall g \in \mathcal{G}$. The set $\mathcal{O}_g$ is the post-islanding region of operation for generator g, and depends on the solution of the islanding optimization and pre-islanded outputs of the generator. If $\zeta_d = 1$ the unit remains fully operational, and its output may vary within some region around the pre-islanded operating point; most generally $(p_g^{\mathrm{G}}, q_g^{\mathrm{G}}) \in \mathcal{O}_g\left(p_g^{\mathrm{G0}}, q_g^{\mathrm{G0}}\right)$, where $\left(p_g^{\mathrm{G0}}, q_g^{\mathrm{G0}}\right)$ is the pre-islanding operating point and $\mathcal{O}_g$ is defined by the output capabilities of the generating unit. If real and reactive power are independent, $p_g^{\mathrm{G}} \in \left[P_g^{\mathrm{LB}}, P_g^{\mathrm{UB}}\right]$ and $q_g^{\mathrm{G}} \in \left[Q_g^{\mathrm{LB}}, Q_g^{\mathrm{UB}}\right]$. If, conversely, $\zeta_g = 0$, then real power output is set to zero: $p_g^{\mathrm{G}} = 0$. In that case, the unit may remain electrically connected to the network, with reactive power output free to vary within some specified interval $\left[Q_g^{\mathrm{LB}}, Q_g^{\mathrm{UB}}\right]$. Each load is assumed to be homogeneous, *i.e.* real and reactive components are shed in equal proportions.

6.6 Computational results

This section presents computational results using the above islanding formulation. First, a demonstration is given of the islanding approach on a 24-bus network. Following that, the construction of the further test problems is described, then computation times for different convergence criteria for the MILP islanding calculation is given, and finally the accuracy of the DC solutions are assessed by comparing them with the AC solutions.

6.6.1 24-bus network case study

The IEEE Reliability Test System [75] network comprises 38 lines and 24 buses, 17 of which have loads attached. Total generation capacity is 3405 MW from 33 generators. The total load demand is 2850 MW.

The islanding scenario is described as follows. With the network operating initially at a state determined from an AC OPF, it is suspected that bus 9 has a fault, and it is decided to island this bus to avoid further failures; hence, bus 9 is assigned to $\mathcal{B}^0$. It is assumed that $\beta_d = 0.75, \forall d \in \mathcal{D}$. In obtaining a new steady-state solution for the

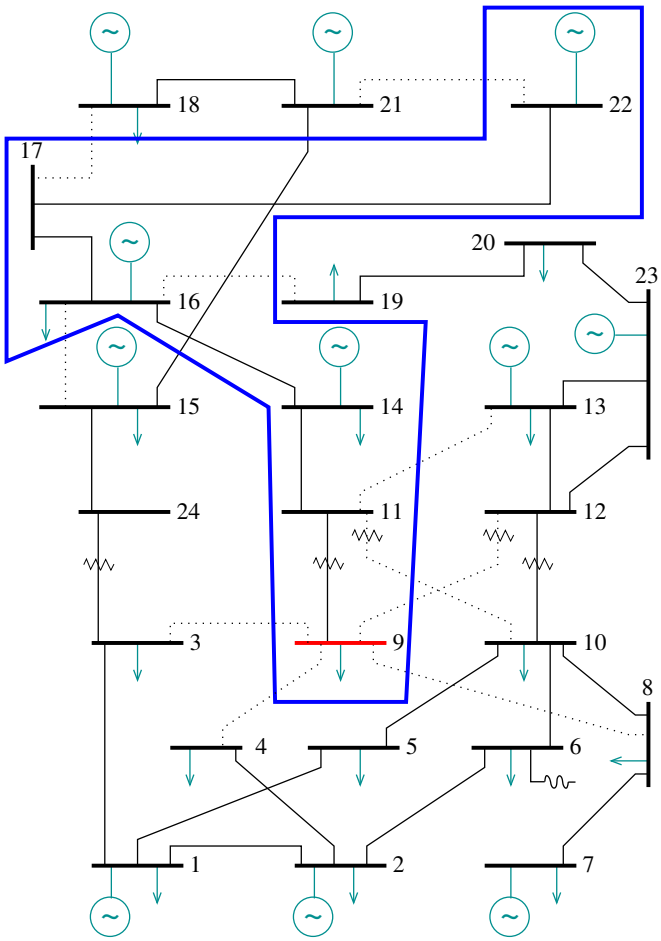

Figure 6.4: Islanding of the 24-bus network.

islanded network, each generator is permitted to varying real power output by up to 5% of its pre-islanding value, or switch off. In the objective, a unity reward, $R_d = 1$, is assumed for each load, and small penalties are placed on line cuts and generator disconnections ($\epsilon_1 = 0.001$, $W_{bb'} = 1$, $\epsilon_2 = 0.01$, $W_g = P_g^{\text{Gmax}}$ in (6.7)).

Figure 6.4 shows the optimal islanding solution, obtained by solving the DC MILP islanding problem. Table 6.2 shows the real and reactive power outputs at each generator bus, both prior to, and after, islanding. All individual unit outputs are within limits. Table 6.3 shows the objective value—the expected load supply—and total values of generation and load for the DC islanding solution, and compares these values with those obtained from the post-islanding AC OLS. Buses 9, 11, 14, 16, 17 and 22 have been placed in section 0. No generators have been switched off. Of the original 2850 MW demand, 469 MW has been placed in the "risky" section 0, and 34.58 MW of load has been shed (as determined by the AC OLS). The returned AC OLS solution is feasible with respect to system line flow limits and all voltages are between 0.95 and 1.05 p.u.

Note that islanding bus 9 alone would have resulting in the loss of the entire 175 MW

Bus		1	2	7	13	14	15	16	18	21	22	23
p^{G} (MW)	Pre	184	184	211	236	0	167	155	400	400	300	660
	Post	184	184	216	224	0	164	155	400	400	300	660
q^{G} (Mvar)	Pre	7	4	49	98	115	110	80	73	−8	−39	46
	Post	71	19	66	100	137	110	76	53	96	1	38

Table 6.2: Pre- and post-islanding generator outputs for the 24-bus test example.

	DC MILP	AC OLS
Objective (6.7)	2712.29	2706.81
Penalties	0.01	0.00
Exp. load supply, J^*_{DC} or J^*_{AC} (MW)	2712.30	2706.81
Generation (MW)	2863.57	2886.54
Load supplied (MW)	2822.73	2815.42
Load shed (MW)	27.27	34.58

Table 6.3: Comparison of DC islanding and post-islanding AC OLS solutions for the 24-bus network.

load at that bus, plus further possible losses in section 1 in order to balance the system. The optimized solution places more buses and loads in section 0, but allows balanced, feasible islands to be obtained with minimum expected load shed.

6.6.2 Effect of the parameter β on the Islanding Solutions

A salient feature of our islanding model is the dependence of islanding solution on the parameter β. The parameter β in the objective function (6.8a) allows us to assign the importance to the area of disturbance. To illustrate this, consider IEEE 14 bus network. This network consists of 20 transmission lines, and 11 load buses with total load of 259 MW. There are five generators in this system. We suspect that bus 4 has some fault in it, so we assign it to the set $\mathcal{B}^0$. The demand at bus 4 is 18% of the total load. No buses are assigned to the set $\mathcal{B}^1$. Fig. 6.5 shows the three islanding solutions obtained by varying the value of β. Fig. 6.6 shows the objective function value, load supplied and the real power generated as the value of β tends to one.

6.6.3 Further islanding test cases

A set of islanding test cases was built based on test networks with between 9 and 300 buses. For a network with n^{B} buses, n^{B} scenarios were generated by assigning in turn each single bus to $\mathcal{B}^0$. No assignments were made to $\mathcal{B}^1$.

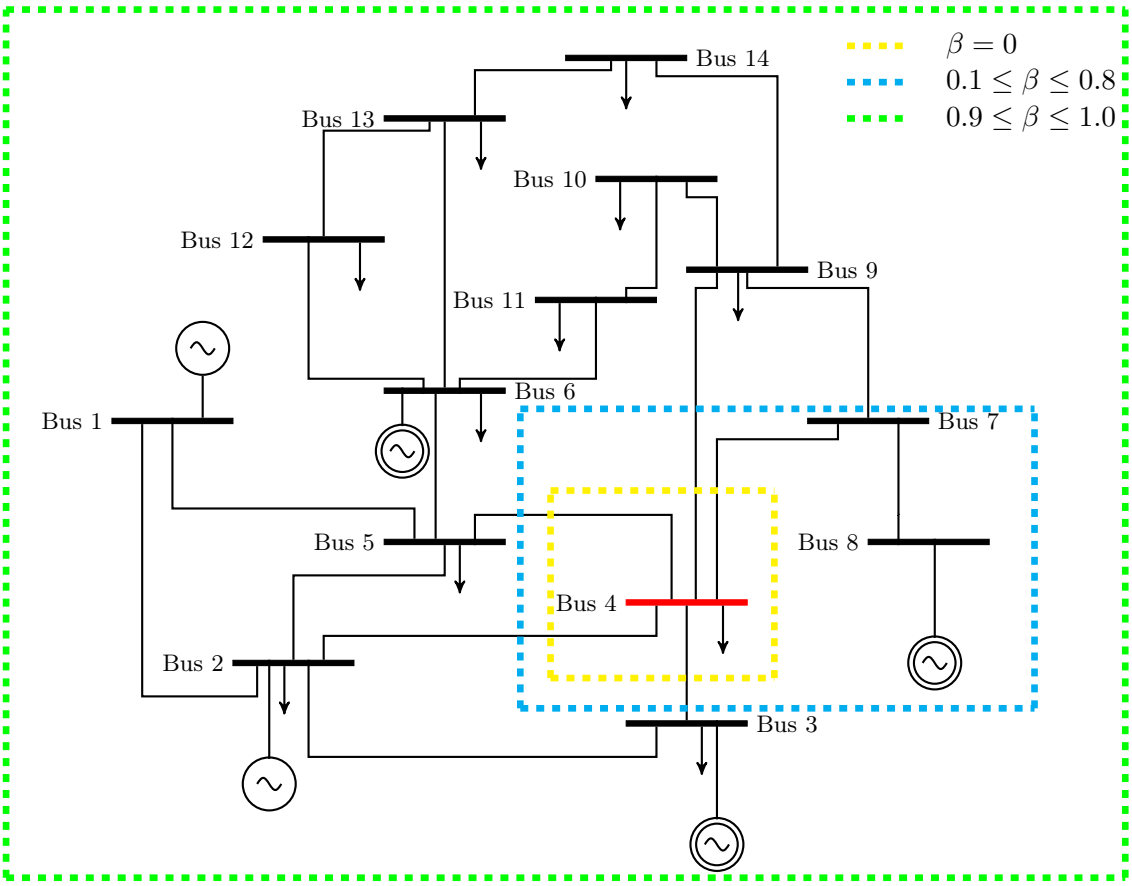

Figure 6.5: Effect of β on islanding solutions of IEEE 14 bus system.

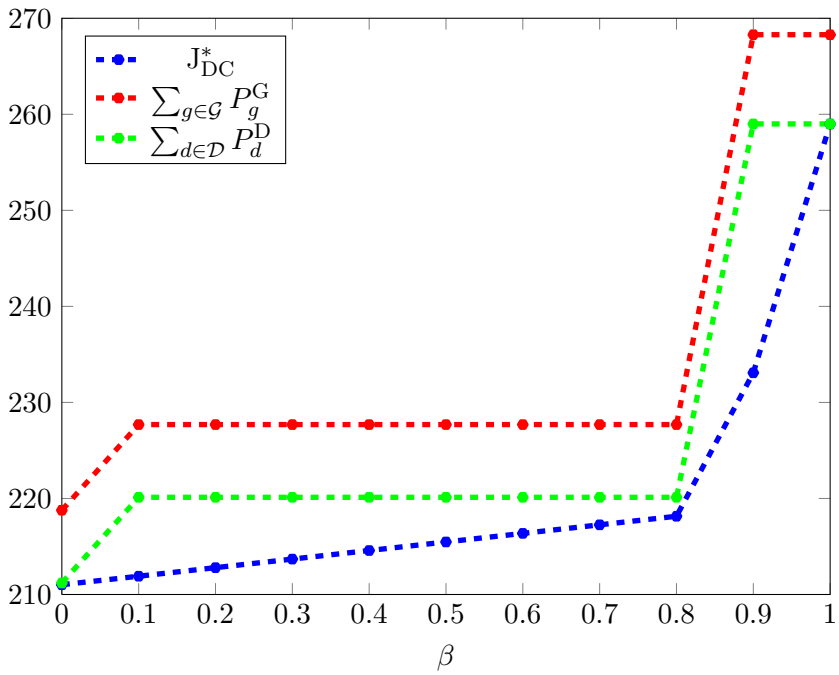

Figure 6.6: Effect of β on objective value, load supplied and power generated.

The possible post-islanding range of outputs for generator g when it is generating were defined as

$$\left[P_g^{\mathrm{LB}}, P_g^{\mathrm{UB}}\right] = \left[P_g^{\min}, P_g^{\max}\right] \cap \left[p_g^{\mathrm{G0}} - R_g^{\mathrm{G}}, p_g^{\mathrm{G0}} + R_g^{\mathrm{G}}\right],$$

where $P_g^{\min}$ and $P_g^{\max}$ are the minimum and maximum steady-state limits when generating, p_g^{G0} is the pre-islanding generation and R_g^{G} is the limit on change of output owing to ramp rate limits and/or generator reserve. For the 24-bus network, for which ramp rates are given, R_g^{G} is set to the maximum change over 2 minutes. For all other networks R_g^{G} is set to equal to 5% of p_g^{G0}. The pre-islanding generation levels are those obtained by solving an AC OPF.

Where no line limits are present for a network, a maximum phase angle difference of 0.4 rad is imposed for each line. In the objective function, a value of 0.75 is used for the load loss penalty β_d, while the values of ϵ_1 and ϵ_2 in (6.7)—the penalties on line cuts and generator disconnection respectively—are 0.1 and 0.0001, with $W_{bb'} = 1$ and $W_g = P_g^{\mathrm{UB}}$.

6.6.4 Computation times and optimality

The speed with which islanding decisions have to be made depends on whether the decision is being made *before* a fault has occurred, as part of contingency planning within secure OPF, or *after*, in which case the time scale depends on the cause of the contingency. Especially in the second case it is important to be able to produce feasible solutions within short time periods even if these are not necessarily optimal. Results are therefore presented for a range of optimality tolerances: 'feasible' *i.e.* first integer feasible solution found, and relative MIP gaps of 5%, 1% and 0%.

Problems were solved on a dual quad-core 64-bit Linux machine with 8 GiB RAM, using AMPL 11.0 with parallel CPLEX 12.3 to solve MILP problems. Computation times quoted include only the time taken to solve the islanding optimization to the required level of optimality, and not the AC-OLS, and are obtained as the elapsed (wall) time used by CPLEX during the `solve` command. A time limit of 5000 seconds is imposed.

Figure 6.7 shows the times required to find obtain feasible islanding solutions to varying proven levels of optimality. Minimum, mean and maximum times are obtained for each network by solving each of the n^{B} scenarios once.

The first set of times show that all problems are solved to feasibility well within 1 s. In all cases, a feasible solution was found at the root node, without requiring branching.

For a MILP problem solved by branch and bound, the optimal integer solution is bounded from below (for maximization) by the highest integer objective value found

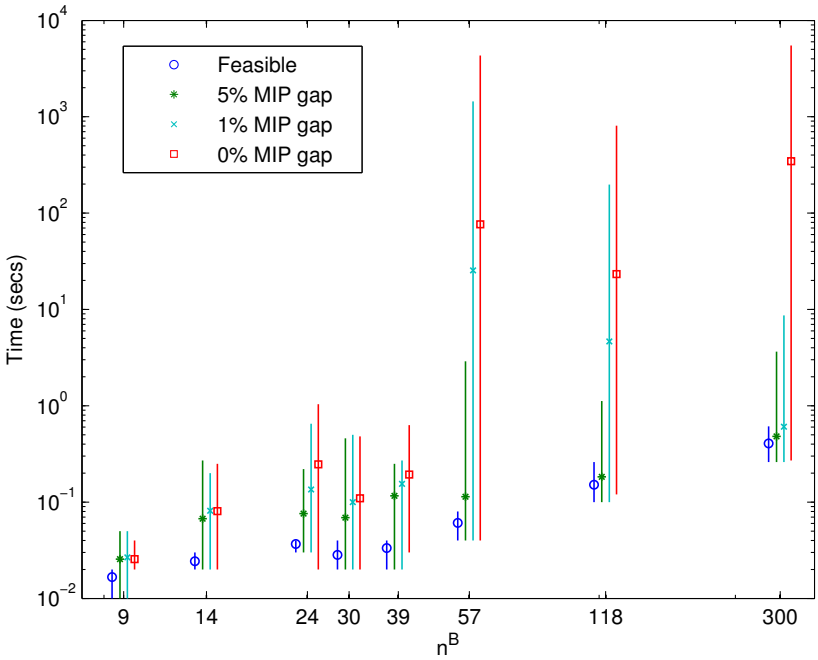

Figure 6.7: Mean, max and min times for finding, to different levels of optimality, islanding solutions for different test networks.

so far during the solution process, and from above by the maximum objective of the relaxed solution among all leaf nodes of the tree. The relative MIP gap is the relative error between these two bounds. Figure 6.7 indicates the progress made by the CPLEX solver, in terms of the times required to reach relative MIP gaps of 5%, 1% and 0% (*i.e.*, optimality) respectively. Performance is very promising for solving to 5%, with all problems solved to this tolerance within five seconds. Times to 1% and 0% gaps are of the same order for the smaller networks (up to 39 buses), but the 57-, 118- and 300-bus networks can taken significantly longer to solve to these tolerances.

Table 6.4 shows the means of the relative errors between the solution value returned at termination of the solver and the actual optimum, where this has been obtained by solving the problem to full optimality (0%). The actual gaps between early termination solutions and the true optima are nearer zero than the 5% or 1% bounds. Therefore, good islanding solutions with respect to the DC model can be provided even when the solver is terminated early and moreover these solutions can be found quickly. Moreover, because the DC model is an approximation of the AC model, there is little advantage in solving it to proven optimality.

	Feasible	5% gap	1% gap
Min	0.00	0.00	0.00
Mean	8.57	0.42	0.04
Max	25.00	3.86	0.80

Table 6.4: Relative errors (%) between optimal and returned solutions.

n^{B}	9	14	24	30	39	57	118	300
MIP gap > 0%	0	0	0	0	0	1	1	17
Voltage infeasible	0	2	7	7	9	6	17	72

Table 6.5: Number of nonzero gap cases and voltage infeasible cases.

6.6.5 Feasibility and accuracy of DC islanding solution

The post-islanding AC-OLS showed that some of the islanding solutions were AC infeasible, *i.e.*, there was no solution to the AC-OLS lying within normal voltage bounds. Relaxing the normal voltage bounds by an extra 0.06 p.u. gave a solution in all cases; however, this is not always possible for practical networks.

It was noted that in many of these AC-infeasible cases, there was sufficient global reactive power capacity in each island. However, reactive power and voltage is a local problem, and hence achieving a global reactive power balance is not sufficient to ensure a normal voltage profile. This is an issue that is overlooked by most controlled islanding schemes, and instead it is assumed that reactive power can be compensated locally. This is not always a justifiable assumption.

Table 6.5 gives the number of these AC-infeasible cases as well as the number that did not solve to 0% optimality gap within 5000 seconds. For all the remaining cases the differences between the objectives as predicted by the DC islanding optimization and the actual value from post-islanding AC-OLS was calculated as is shown in Figure 6.8. The adopted islanding solution in each case is that from solving the problem to full optimality.

The comparison in Figure 6.8 shows how well the DC model predicts the AC objective. There are a few cases where the DC objective is a significant over-estimate, however on average the objective values are within 0.3%.

Solving the MILP islanding problem and, subsequently, the AC-OLS provides a feasible steady-state operating point for the network in its post-islanding configuration. Since the objective minimizes the load shed and the constraints limit the changes to generator outputs, the proposed solution will naturally limit, to some extent, the disruption to the system power flows. Nevertheless, since neither the transient response

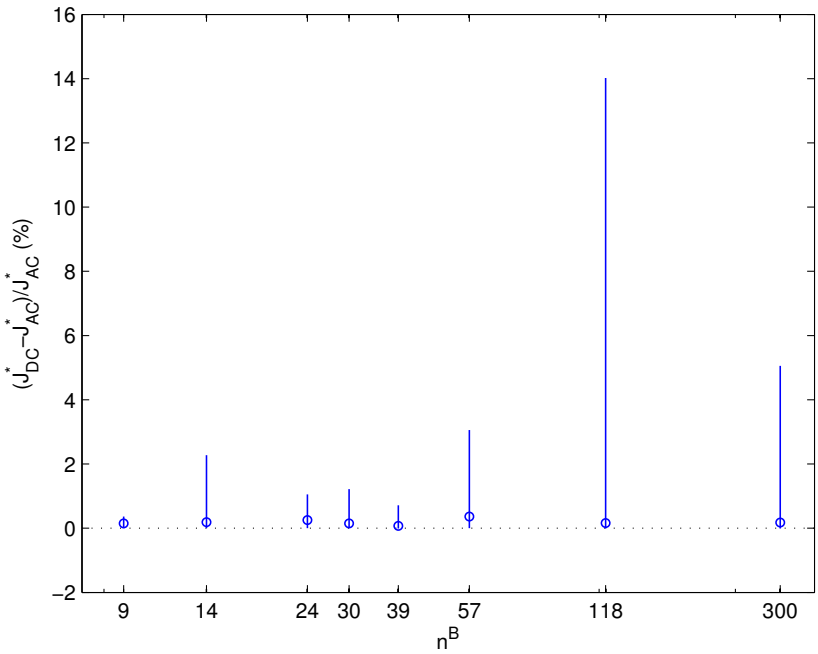

Figure 6.8: Mean, max and min relative errors between DC and AC objective values.

n^{B}	9	14	24	30	39	57	118	300
Min	0.00	0.00	0.00	0.00	0.00	0.00	0.00	0.00
Mean	0.16	0.78	0.59	0.03	0.34	0.06	0.20	0.46
Max	0.48	10.85	2.87	0.68	5.09	1.00	2.70	7.03

Table 6.6: Decrease in objective J^*_{DC} (%) for line-cut and generator penalties increased versus previous penalties.

is modelled when designing islands nor the generators are necessarily grouped according to coherent modes, it is possible that the islanding actions may lead to dynamic instability.

In total, 14 out of 452 islanding solutions were found to lead to instability. Investigation of the individual cases found that, in all cases, severe transients were caused by cuts to high-flow lines. However, re-solving the islanding optimizations with increased penalties on high-flow lines ($W_l = s_l^{\mathrm{L0}}$ and $\epsilon_1 = 10^{-4}\sum_d P_d^{\mathrm{D}}$) and switching-off of generators ($W_g = P_g^{\mathrm{G+}}$ and $\epsilon_2 = 1$) resulted in all cases being feasible.

As expected these larger penalty coefficients caused a drop in the primary DC objective value, J^*_{DC}. However Table 6.6 shows that this degradation is small, and is an acceptable trade-off for removing all of the unstable cases. As an added advantage, as Figure 6.9 shows, solve times for the larger networks are shorter with the heavier penalties.

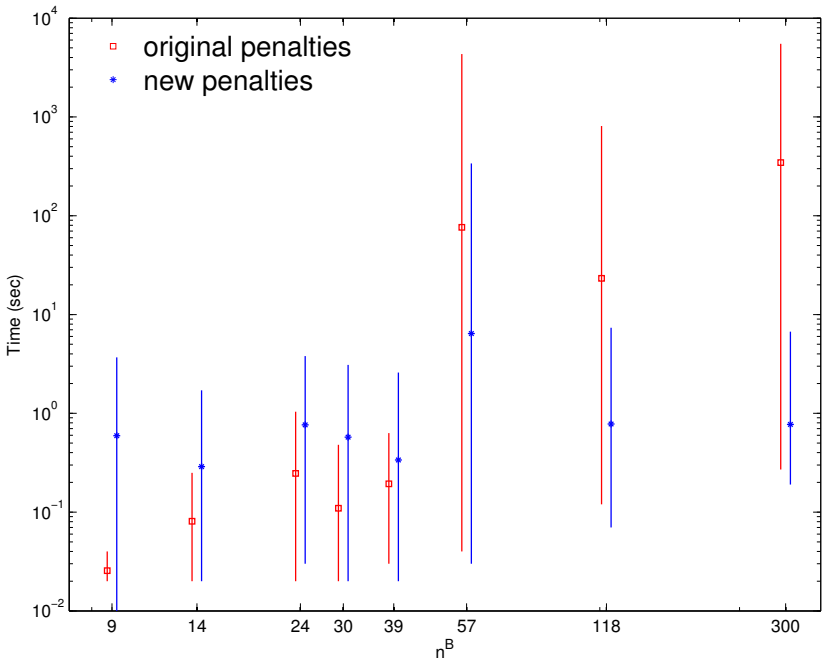

Figure 6.9: Mean, max and min solve times to optimality with original penalties ($\epsilon_1 = 0.1$, $W_l = 1$, $\epsilon_2 = 10^{-4}$, $W_g = P_g^{\mathrm{G+}}$) and new penalties ($\epsilon_1 = 10^{-4} \sum_d P_d^{\mathrm{D}}$, $W_l = s_l^{\mathrm{L0}}$, $\epsilon_2 = 1$, $W_g = P_g^{\mathrm{G+}}$).

Chapter 7

Improvement to the Islanding Model by using Piecewise Linear Approximation to Power Flow Equations

7.1 Introduction

A disadvantage of the DC power flow model is that the effect of line disconnections on network voltages is not considered. This is not exclusive to MILP-based islanding and transmission switching; a number of islanding approaches consider real power only, and assume that reactive power may be compensated locally after splitting. In Tab. 6.5, however, cases are reported where a solution could not be found to satisfy AC power flow and voltage constraints when the islands were designed considering DC power flow, *even when sufficient reactive power generation capacity was present in each island.* Investigation found that local shortages or surpluses of reactive power led to abnormal voltages in certain areas of the network.

In this chapter we present a flexible approach to the problem of designing system islands while considering voltage and reactive power. Firstly, a piecewise linear approximation to AC power flow is developed for use in power system optimization problems. This model is used in a MILP-based approach to islanding, where the decisions to make are which lines to disconnect, loads to shed and how to adjust generators in order to isolate a part of the network. Results obtained for test networks demonstrate the advantage of considering voltage and reactive power when deciding how to island, since instances of AC-infeasible islands are eliminated. Additionally we also demonstrate the flexibility of the method in dealing with different islanding situations. For example,

the aim may be to minimize the load shed while splitting the network so that coherent synchronous machines remain in the same island. Alternatively, it may be to split the network in two so as to ensure that the majority of it is left in a known-safe state, isolated from a troubled region that has been identified as a possible source of cascading failures. The objective would be to minimize the load that is planned to be shed, plus the expected extra load that might be lost due to failures in the small island surrounding the troubled region. There can be many reasons for suspecting trouble from a region—*e.g.*, incomplete or inconsistent measurements, estimates of system stress such closeness to instability or equipment operating limits, or indications of component failures—but the precise definition of what evidence would lead to islanding being initiated is complex and is beyond the scope of this chapter.

The second improvement, when compared to the last chapter, is flexibility in the definition of the primary motivation and aims for islanding. For example, the aim may be split the network such that coherent synchronous machines remain in the same section. An alternative aim is to isolate an impacted area while minimizing the expected load shed or lost. The identification of such areas is a complex issue, beyond the scope of this work; however, we demonstrate the method's flexibility by showing its use in isolating impacted areas while minimizing expected load shed and considering generator coherency.

7.2 Piecewise Linear AC Power Flow

7.2.1 A linear-plus-cosine model of AC power flow

The linear "DC" model is a widely accepted approximation to AC power flow, whose benefits (linearity, simplicity) often outweigh its shortcomings. Recently, however, there has been renewed research interest in the DC model itself [76] and more accurate alternative linearizations [77]. In chapter 6 we found that a DC-based approach to controlled islanding sometimes led to infeasible islands being created, mainly owing to out-of-bound voltages and local shortages or surpluses of reactive power. Motivated by this, this section presents a piecewise linear approximation to AC power flow, in which voltage and reactive power are modelled. The formulation models as piecewise linear, thus to arbitrary levels of accuracy, the cosine term that is the dominant source of error in a standard linear formulation.

The AC power flow equations are described by the equations (2.1b-2.1c). To simplify the notation, let us define two new variables as: $y_{bb'} = \cos\theta_{bb'}$, and $z_{bb'} = \sin\theta_{bb'}$, where $\theta_{bb'} = \delta_b - \delta_{b'}$. The standard "DC" approximation to AC power flow, as discussed in Chapter 1, linearizes these equations by using the approximations $v_i = v_j = 1$, $z_{ij} = \theta_{ij}$, $y_{ij} = 1$, and $b_l \gg g_l \approx 0$ yielding $p^{\mathrm{L}}_{bb'} = B_{bb'}\theta_{bb'}$. The reactive power variables

and equations are dropped. In the model in this chapter, voltage and reactive power are retained. Expanding the line flows about $v_b = 1$, $v_{b'} = 1$ and $\theta_{bb'} = 0$ (hence $y_{bb'} = 1, z_{bb'} = 0$):

$$p^{\mathrm{L}}_{bb'} \approx G_{bb}(2v_b - 1) + G_{bb'}(v_b + v_{b'} + y_{bb'} - 2) + B_{bb'} z_{bb'}, \tag{7.1a}$$

$$q^{\mathrm{L}}_{bb'} \approx B_{bb}(1 - 2v_b) - B_{bb'}(v_b + v_{b'} + y_{bb'} - 2) + G_{bb'} z_{bb'}. \tag{7.1b}$$

In a standard linearization, the small-angle approximations would then be used: $y_{bb'} = \cos\theta_{bb'} \approx 1$ and $z_{bb'} = \sin\theta_{bb'} \approx \theta_{bb'}$. Tab. 7.1 gives the maximum absolute errors for each of the constituent terms in the linearized flows, over a typical range of operating voltages and angles, *i.e.*, $0.95 \leq v_b \leq 1.05$ at each end of the line, and $|\theta_{bb'}| \leq 40°$. The cosine approximation incurs the largest error. Fig. 7.1 shows maximum and minimum power flows and errors over this range of voltages and angles for a line with $g_{bb'} = 1, b_{bb'} = -5, b^{\mathrm{C}}_{bb'} = 1$. Approximation errors are obtained for when the $y_{bb'} = \cos\theta_{bb'}$ term is approximated as 1 (a linear model) and modelled exactly (linear plus cosine). In both cases, $z_{bb'} = \theta_{bb'} \approx \sin\theta_{bb'}$ is used. Although little reduction in errors is apparent in the real flows, the importance of modelling the cosine term is clear for reactive flows.

A similar analysis shows that including the sine term (instead of its linearization) in addition to the cosine term reduces the error in the real flows slightly, but makes no significant difference to the reactive power. Since the infeasibilities that occur using the DC approach to islanding are mainly owing to the reactive power and voltage limits [70], the appropriate approximation to use is the linear-plus-cosine one. And although cosine terms cannot be used directly in an MILP model, they can be modelled to arbitrary levels of accuracy by piecewise linear functions. The next section demonstrates the use of the model in an OPF formulation.

7.2.2 Piecewise linear AC OPF

The piecewise linear (PWL) AC OPF problem is defined as

Term	Approximation	Max abs error
v_b^2	$2v_b - 1$	0.0025
$v_b v_j y_{bb'}$	$v_b + v_b + y_{bb'} - 2$	0.0253
$v_b v_j z_{bb'}$	$z_{bb'}$	0.0659
$y_{bb'}$	1	0.2340
$z_{bb'}$	$\theta_{bb'}$	0.0553

Table 7.1: Approximation errors in line flow terms

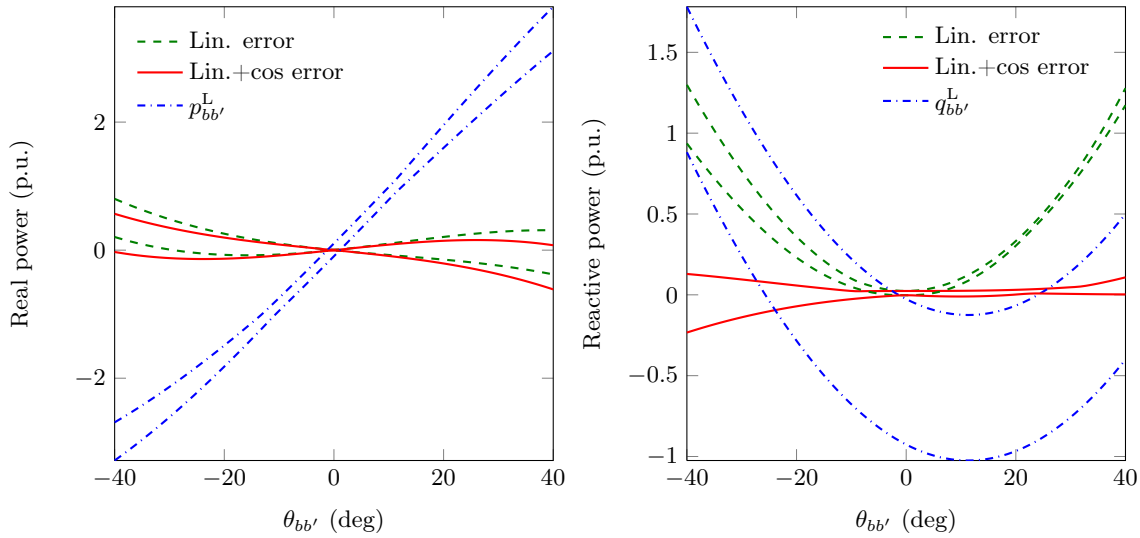

Figure 7.1: Maxima and minima of power flows, and of approximation errors, as a function of phase angle difference.

$$\min \sum_{g \in \mathcal{G}} f(p_g^{\mathrm{G}}), \tag{7.2a}$$

subject to

$$\left.\begin{aligned} \sum_{g \in \mathcal{G}_b} p_g^{\mathrm{G}} &= \sum_{d \in \mathcal{D}_b} P_d^{\mathrm{D}} + \sum_{b' \in \mathcal{B}_b} p_{bb'}^{\mathrm{L}} + G_i^{\mathrm{B}}(2v_i - 1), \\ \sum_{g \in \mathcal{G}_b} q_g^{\mathrm{G}} &= \sum_{d \in \mathcal{D}_b} Q_d^{\mathrm{D}} + \sum_{b' \in \mathcal{B}_b} q_{bb'}^{\mathrm{L}} - B_i^{\mathrm{B}}(2v_i - 1), \end{aligned}\right\}, \ \forall\, b \in \mathcal{B}, \tag{7.2b}$$

$$\left.\begin{aligned} p_{bb'}^{\mathrm{L}} &= G_{bb}(2v_b - 1) + G_{bb'}(v_b + v_{b'} + y_{bb'} - 2) + B_{bb'}\theta_{bb'}, \\ q_{bb'}^{\mathrm{L}} &= B_{bb}(1 - 2v_b) - B_{bb'}(v_b + v_{b'} + y_{bb'} - 2) + G_{bb'}\theta_{bb'}, \\ y_{bb'} &= h_{bb',k}\theta_{bb'} + d_{bb',k}, \forall \theta_{bb'} \in [x_{bb',k}, x_{bb',k+1}], k = 0 \ldots N-1, \end{aligned}\right\}, \ \forall\, (b, b') \in \mathcal{L}, \tag{7.2c}$$

$$V_b^{\mathrm{LB}} \le v_b \le V_b^{\mathrm{UB}}, \ \forall\, b \in \mathcal{B}, \tag{7.2d}$$

$$\left.\begin{aligned} P_g^{\mathrm{LB}} \le p_g^{\mathrm{G}} \le P_g^{\mathrm{UB}}, \\ Q_g^{\mathrm{LB}} \le q_g^{\mathrm{G}} \le Q_g^{\mathrm{UB}}, \end{aligned}\right\}, \forall\, g \in \mathcal{G}, \tag{7.2e}$$

$$p_{bb'}^{\mathrm{L}} + p_{b'b}^{\mathrm{L}} \le P_l^{\mathrm{UB}}, \ \forall\, (b, b') \in \mathcal{L}, \tag{7.2f}$$

where equation (7.12a) is the objective function, equations (7.2b-7.2c) are the Kirchhoff's laws and are linear equations of voltage and angle difference. $y_{bb'}$ gives the N-piece PWL approximation to $\cos\theta_{bb'}$, where $h_{bb',k}$ and $d_{bb',k}$ are chosen so that the approximation coincides with $\cos x$ at breakpoints $\{x_{bb',0}, \ldots, x_{bb',N}\}$. Equations (7.2d-7.2f) are the system limits.

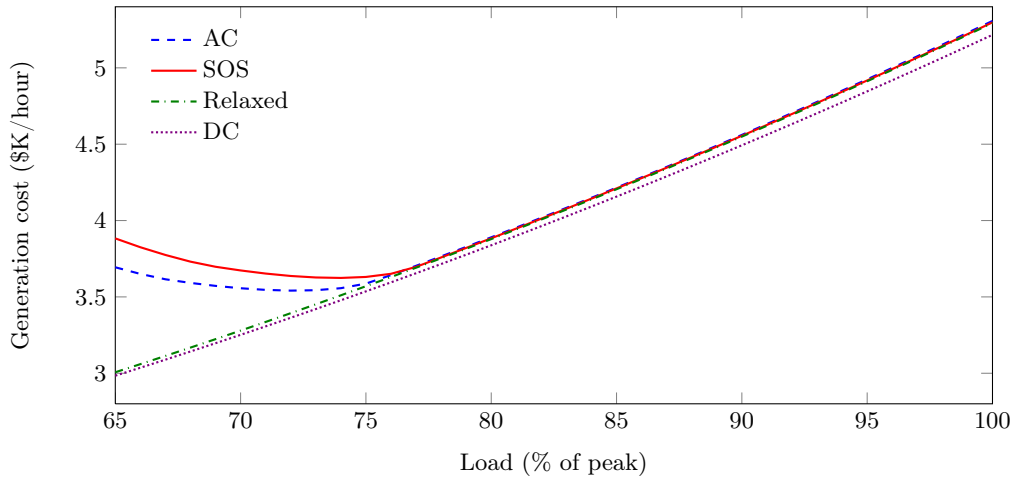

Figure 7.2: Generation costs as a function of load for the 9-bus network.

Note that line flow limits in (7.2f) are limits on real power (I^2R) loss. If an Mva limit S_l^{UB} is given, this may be converted by assuming nominal voltage, *i.e.*, $P_{bb'}^{\mathrm{UB}} = \frac{g_{bb'}}{g_{bb'}^2+b_{bb'}^2}(S_{bb'}^{\mathrm{UB}})^2$.

The implementation of the PWL model of $\cos\theta_{bb'}$ requires either binary variables or special ordered sets of type 2 (SOS-2) [78]. The overall problem is then, depending on c_g, a mixed integer linear or quadratic program (MILP or MIQP). If the equation of $y_{bb'}$ is replaced by its relaxation $y_{bb'} \leq h_{bb',k}\theta_{bb'} + d_{bb',k}$, then the problem becomes a convex optimization problem and no binary variables or SOS sets are needed. Since real and reactive line losses decrease as $y_{bb'}$ increases, it is tempting to assume that equality will hold for one of the PWL sections, and this relaxation will yield a tight result. However, as Fig. 7.2 shows, situations exist where the SOS formulation is necessary. This shows, for the WSCC 9-bus network, optimal generation costs against load level, as obtained by OPFs using AC, PWL with SOS, relaxed PWL, and DC power flow models. The network is modified to set voltage limits to $\pm 5\%$ and the lower reactive power limit for each generator is raised from -300 to -5 Mvar. This means that at low load levels the generators find it increasingly difficult to balance the reactive power, as more lines become sources rather than sinks of reactive power, and the generation cost rises with falling load. While the SOS PWL is able to capture this effect, the relaxed PWL and DC-based models are not; the former "cheats" by having some lines continue to store reactive power irrespective of their end voltages and angles—allowed because $y_{bb'} < h_{bb',k}\theta_{bb'} + d_{bb',k}$ is permitted—and this allows more of the real power to be generated by the cheaper generators.

7.3 A formulation for system islanding using piecewise linear AC power flow

In the last chapter, we have discussed the problem of determining how to split a transmission network into islands. The aim is to limit the effects of possible cascading failures and prevent the onset of wide-area blackouts by re-configuring the network—*via* line switching—so that problem areas are isolated. The MILP-based method defines two *sections* of the network. All of the buses that must be isolated are pre-assigned to section 0, and the optimization determines which other buses and lines to place in section 0. All the remaining components are in section 1. This creates at least two islands. The optimization will also determine the best strategy to adjust generation and shed load so as to establish a load-generation balance in each island while respecting all network equations and operating constraints after the split.

7.3.1 Motivation: effect of topology changes on voltage profile

Solution of the MILP islanding problem provides a set of lines to switch, loads to shed and generators to adjust. However, if only the DC power flow equations are included in the constraints, the effects of changing the network topology on voltages and reactive power flows is not considered. Thus, in chapter 6, an AC optimal load shedding (OLS) problem is solved *after* the MILP islanding problem, using the islanded network topology. If a solution to this can be found, the islanded network is feasible with respect to AC power flow and operating constraints. The solution provides the correct generator output and load adjustments to make, now having considered voltage and reactive power.

However, in chapter 6 a number of islanding solutions were found to be AC infeasible. Investigation found the primary cause of infeasibility to be the voltage bounds; a solution can be recovered, albeit with abnormally high or low voltages, by relaxing the normal limits. One such example, for the 24-bus IEEE Reliability Test System (RTS) [75], is described as follows. Given the problem of isolating bus 6 while minimizing the expected load shed or lost, the optimal solution islands buses 1, 2 and 6, as indicated in Fig. 7.3. There remains sufficient real power capacity in both islands to meet demand, and no load is shed. Moreover, but not by design, there is sufficient reactive power capacity in each island to meet the total reactive power demand. Despite this, a feasible solution to the AC-OLS can not be found. Softening the voltage constraints recovers a solution, but with an abnormally low voltage of 0.6443 p.u. at bus 6 and an over-limit flow on line $(2, 6)$. Further inspection reveals that this situation has arisen because of the disconnection of line $(6, 10)$, a cable with high shunt capacitance. The passive shunt reactor at bus 6 would, in normal circumstances, balance locally the excess reactive

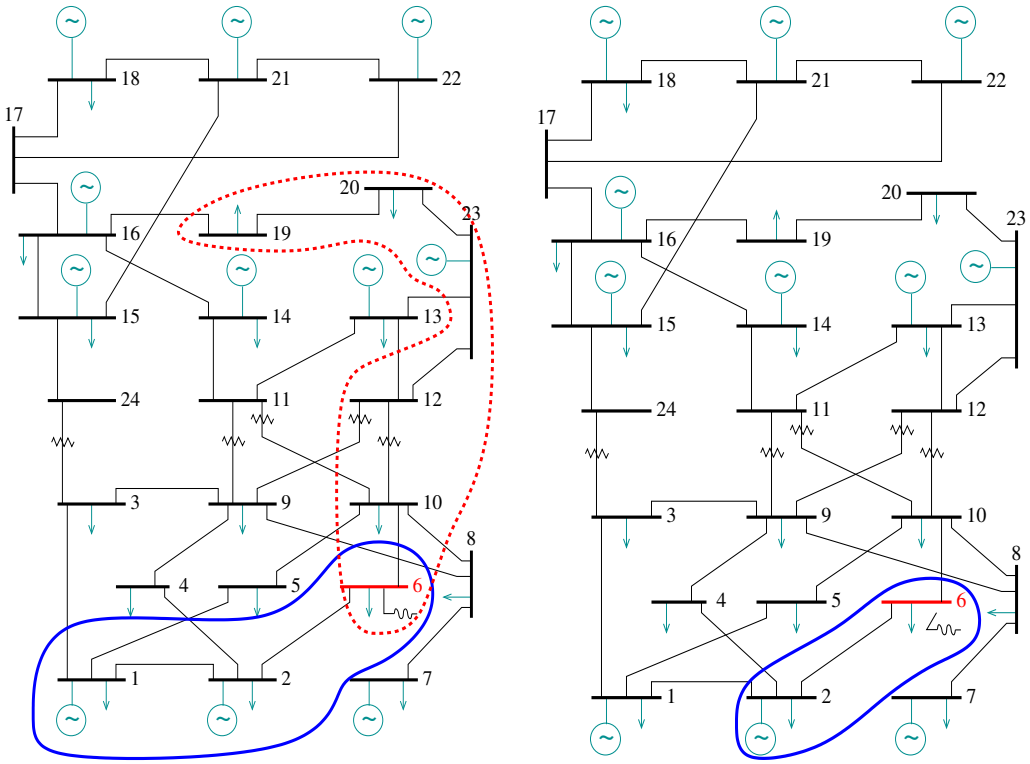

Figure 7.3: IEEE 24-bus RTS with bus 6 isolated. On the left, DC method (solid) and PWL method without shunt switching (dashed). On the right, PWL method with shunt switching.

power and maintain a satisfactory voltage profile. This problem could be avoided by linking together the disconnection of line $(6, 10)$ and the shunt reactor at 6. The optimal solution when these actions are linked is shown in the right-hand diagram of Fig. 7.3, and it yields a better feasible solution than when the reactor is not disconnected. Rules like this are easy to incorporate in the model; however, it is difficult *a-priori* to define all possible rules. A better solution is to allow the model to decide the combination of equipment to disconnect, and when this is done the optimal solution disconnects both line $(6, 10)$ and the reactor at bus 6. The models and result for this example are given in later in this Section and in Section 7.4.

This is just one example of where an islanding solution formed by considering only real power—even if network constraints are included—is unsatisfactory. It also shows that even if reactive power balance is achieved within each island, local shortages or surpluses can lead to an abnormal voltage profile. Many test networks are prone to this problem [70]. Moreover, it is not just system islanding that is susceptible; DC-based transmission switching also does not consider the consequences on voltage of disconnecting lines. Thus, there is a need for network topology optimization methods that can determine AC-feasible solutions, but without having to resort to solving the full MINLP problem. The focus of this chapter is topology optimization for the purpose of

islanding, and in the next section, a formulation is presented that uses the PWL model of AC power flow.

7.3.2 Formulation of constraints for islanding

The problem is to decide which lines to switch in order to isolate a part of the network. Separation of sections is enforced by sectioning constraints. The islanded network must satisfy power balance and flow equations and operating limits, and so these are included as constraints in the problem.

Sectioning constraints

Define $\mathcal{B}^0$ and $\mathcal{B}^1$, where $\mathcal{B}^0 \cap \mathcal{B}^1 = \emptyset$, as the subsets of buses that are desired to be separated. For now, the motivation for this separation is left open, but it may be that these buses in, say, $\mathcal{B}^0$ represent a failing area of the network, or are associated with a coherent group of synchronous machines that will be separated from other groups. As discussed in Chap. 6, the proposed approach will split the network into two *sections*: section 0 will contain all buses in $\mathcal{B}^0$ and section 1 all buses in $\mathcal{B}^1$. For a bus $i \in \mathcal{B}$, γ_i denotes the section (0 or 1) to which that bus is assigned. That is, if b is to be placed in section 0, then $\gamma_b = 0$. Separation between sections is achieved by switching lines: $\rho_{bb'}$ denotes the connection status of a line (b, b'), and the convention followed is for $\rho_{bb'} = 0$ when (b, b') is disconnected. The exact boundaries of each section will depend on the objective, defined later, and the optimization will determine how to assign to sections those buses not in $\mathcal{B}^0$ or $\mathcal{B}^1$, in order achieve balance and optimize the objective. However, the following constraints enforce the separation of sections 0 and 1, without defining precisely their boundaries.

$$\rho_{bb'} \leq 1 + \gamma_b - \gamma_{b'}, \forall bb' \in \mathcal{L}, b, b' \in \mathcal{B}_{bb'} : b \neq b', \tag{7.3a}$$

$$\gamma_b = s, \forall b \in \mathcal{B}^s, s \in \{0, 1\}. \tag{7.3b}$$

Power flow

The remainder of the constraints are concerned with achieving a balanced, steady state for the islanded network. It is assumed that generators are permitted to make only small-scale changes to output or be switched off, and loads may be fully or partly shed in order to maintain a balance. As a consequence of these changes and the topological changes, bus voltages, angles and line flows will change, and so must be modelled to ensure satisfaction of network constraints and operating limits.

First, the power balances, (7.2b), are included without modification. Next, the line flow equations are modified so that when a line is disconnected, power flows across it are zero irrespective of its end bus voltages and angles. To assist this, we use the line switching model as given in Sec. 5.3

This switching between line and bus variables is made use of in modified line flow equations. For a line $(b, b') \in \mathcal{L}$,

$$\begin{aligned} p^{\mathrm{L}}_{bb'} &= G^{bb}_{l}(2v^{\mathrm{L}}_{b} - 1) + G_{bb'}(v^{\mathrm{L}}_{b} + v^{\mathrm{L}}_{b'} + y_{bb'} - 2) + B_{bb'}\theta_{bb'} \\ &\quad -(G_{bb}(2V^{LB}_{b} - 1) + G_{bb'}(V^{\mathrm{LB}}_{b} + V^{\mathrm{LB}}_{b'} - 1))(1 - \rho_{bb'}), \qquad (7.4a) \\ q^{\mathrm{L}}_{bb'} &= B_{bb}(1 - 2v^{\mathrm{L}}_{b}) - B_{bb'}(v^{\mathrm{L}}_{b} + v^{\mathrm{L}}_{b'} + y_{bb'} - 2) + G^{bb'}\theta_{bb'} \\ &\quad -(B^{bb}_{l}(1 - 2V^{\mathrm{LB}}_{b}) - B_{bb'}(V^{\mathrm{LB}}_{b} + V^{\mathrm{LB}}_{b'} - 1))(1 - \rho_{bb'}), \qquad (7.4b) \end{aligned}$$

and $y_{bb'}$ is given by (7.2b), using $\theta_{bb'}$. Note that since $\theta_{bb'} = 0$ if $\rho_{bb'} = 0$, then $y_{bb'} = 1$ for a disconnected line. Hence, if $\rho_{bb'} = 0$ then $p^{\mathrm{L}}_{bb'} = 0$, irrespective of v_b, $v_{b'}$ and $\theta_{bb'} = \delta_b - \delta_{b'}$. If $\rho_{bb'} = 1$, the normal power flow equations are recovered.

Operating constraints

In the short time available when islanding in response to a contingency, any extra generation that is needed will be achieved by a combination of the ramping-up of on-line units and the commitment of fast-start units. For simplicity, fast-start units are not considered in the examples in this chapter. We can use of the generator switching model as given in Sec. 5.4.

For loads, because of the limits on generator outputs and network constraints, it may not be possible after islanding to fully supply all loads. It is therefore assumed that some shedding of loads is permissible. Because of the limits on generator power outputs and network constraints it may not be possible after islanding to fully supply all loads. It is therefore necessary to permit some shedding of loads. The load shedding is implemented using the model given in Section 5.1. Finally, line limits are applied via constraint (7.2f).

Rules and other component switching

As motivated by Section 7.3.1, sometimes it is necessary to have rules for switching components or adjusting controls in different situations. Such rules can easily be included in the formulation using standard techniques for deriving constraints from logical rules [48]. It is also possible to permit the switching of other network components directly as part of the decision problem. For example, the switching of a shunt component at a bus b can be modelled by the set of constraints given in Sec. 5.5 of Chap. 5.

7.3.3 Objective functions for islanding

The general aim is to split the network, separating the two sections 0 and 1, yet leaving it in a feasible state of operation. The specific motivations and objectives for islanding are discussed in this section. Clearly, if a network can be partitioned with minimal disruption to load, and with minimal disturbances to generators, then its chances of viable operation until future restoration are increased.

Isolating uncertain components and maximizing expected load supply

We assume that there is an identifiable localized area of the network that is believed could be a trigger for cascading failure. Similar to the approach in [70], the goal is to include this area of potential trouble in an island, leaving the rest of the network in a known, secure steady state. The sets $\mathcal{B}^0$ and $\mathcal{L}^0$ consist of all buses and lines in the troubled area and, additionally, any buses and lines whose status is uncertain. To ensure section 1 contains no uncertain components, all lines $(b, b') \in \mathcal{L}^0$ remaining in this section are disconnected by replacing (7.3a) for all $(b, b') \in \mathcal{L}^0$

$$\rho_{bb'} \leq 1 - \gamma_b, \forall b \in \mathcal{B}_{bb'}. \tag{7.5}$$

Because section 0 is vulnerable, containing the uncertain or failing components, it is assumed there is a risk of not being able to supply any load placed in that section. Accordingly, a load loss penalty $0 \leq \beta_d < 1$ is defined for a load d, which may be interpreted as the probability of being able to supply a load if placed in section 0. Suppose a reward R_d is obtained per unit supply of load d. If d is placed in section 1 a reward R_d is realized per unit supply; however, if d is placed in section 0, a lower reward of $\beta_d R_d < R_d$ is realized.

The objective is then to maximize the expected total value of load supplied:

$$J^{\text{exp load}} = \sum_{d \in \mathcal{D}} R_d P_d^{\text{D}} (\beta_d \alpha_{0d} + \alpha_{1d}), \tag{7.6}$$

where $\alpha_d = \alpha_{0d} + \alpha_{1d}$, and $0 \leq \alpha_{1d} \leq \gamma_b, \forall b \in \mathcal{B}, d \in \mathcal{D}_b$. Here a new variable α_{sd} is introduced for the load d delivered in section $s \in \{0, 1\}$. If $\gamma_b = 0$ (and so the load at bus b is in section 0), then $\alpha_{1d} = 0$, $\alpha_{0d} = \alpha_d$, and the reward is $\beta_d R_d P_d^{\text{D}} \alpha_d$. Conversely, if $\gamma_b = 1$ then $\alpha_{1d} = \alpha_d$ and $\alpha_{0d} = 0$, giving a larger reward $R_d P_d^{\text{D}} \alpha_d$. Thus, maximizing (7.6) gives a preference for $\gamma_b = 1$ and a smaller section 0, so that the impacted area is limited.

Promoting generator coherency

Another aim is to ensure the synchronicity of generators within islands. Large disturbances in the network cause electro-mechanical oscillations, which can lead to a loss of synchronism. A popular approach is to split the system along boundaries of near-coherent generator groups, as determined by slow-coherency analysis [79]. Thus, weak connections between machines—which give rise to slow, lightly-damped oscillations—are cut, leaving separate networks of tightly-coupled, coherent machines.

Consider those buses in the network with generators attached, the set of which is defined as $\mathcal{B}^{\mathrm{G}}$, and define $\mathcal{B}^{\mathrm{GG}} \triangleq \{(b, b') \in \mathcal{B}^{\mathrm{G}} \times \mathcal{B}^{\mathrm{G}} : b' > b\}$ as the set of all pairs of such buses. For what follows, it may be assumed that multiple units at a bus are tightly coupled and are aggregated to a single unit. The dynamic coupling, $W_{bb'}$, between a pair of machines at buses $(b, b') \in \mathcal{B}^{\mathrm{GG}}$ may be determined from slow-coherency analysis. For example, assuming as in [69] the undamped second order swing equation,

$$W_{bb'} = \frac{\partial(\dot{\omega}_b - \dot{\omega}_{b'})}{\partial(\delta_b - \delta_{b'})} = (\frac{1}{M_b} + \frac{1}{M_{b'}})\frac{\partial P_{bb'}}{\partial \delta_{bb'}},$$

where M_b, ω_b, δ_b are the inertia constant, angular frequency and rotor angle of the machine at bus b, and $\frac{\partial P_{bb'}}{\partial \delta_{bb'}}$ is the synchronizing power coefficient or "stiffness" between machines at b and b'. To favour, in the objective, separating loosely-coupled generators, introduce a new variable $0 \leq \eta_{bb'} \leq 1$ for all $(b, b') \in \mathcal{B}^{\mathrm{GG}}$. Then the constraint

$$-\eta_{bb'} \leq \gamma_b - \gamma'_b \leq \eta_{bb'}, \tag{7.7}$$

sets $\eta_{bb'}$ to 1 if generator buses b and b' are in different sections of the network (and hence electrically isolated), but otherwise may be zero. Minimizing the function

$$J^{\mathrm{coh}} = \sum_{(b,b') \in \mathcal{B}^{\mathrm{GG}}} W_{bb'}\eta_{bb'} \tag{7.8}$$

gives a preference for machines in different sections having small $W_{bb'}$, *i.e.*, being weakly coupled, and those within the same section have stronger coupling. This may be used in conjunction with (7.6), *i.e.*, $\max J^{\text{exp load}} - kJ^{\mathrm{coh}}$, with weighting $k > 0$, so that section 0 is the "unhealthy" section, and the expected load supply is maximized while keeping together strongly-coupled machines.

Minimizing (7.8) alone will favour keeping all machines in the same section, and to force the machines apart additional constraints may be needed. Alternatively, the following implementation splits the network directly into coherent groups, making different use of the sets $\mathcal{B}^0$ and $\mathcal{B}^1$.

Splitting into coherent groups

Suppose that coherent groups of generators have been determined, and that assigned to $\mathcal{B}^0$ and $\mathcal{B}^1$ are those buses in $\mathcal{B}^{\mathrm{G}}$ corresponding to machines in different groups. For example, $\mathcal{B}^0$ may contain the critical coherent group of machines, and $\mathcal{B}^1$ all others. The sectioning constraints will ensure that the machines are separated, but which other buses are assigned to each section is determined by the optimization. The solution that minimizes the amount of load shed can be found by maximizing the function

$$J^{\mathrm{load}} = \sum_{d \in \mathcal{D}} \alpha_d P_d^{\mathrm{D}}. \tag{7.9}$$

Alternatively, to seek a solution that changes the generator outputs the minimally from their initial values P_g^{G0}, minimize

$$J^{\mathrm{gen}} = \sum_{g \in \mathcal{G}} t_g \tag{7.10}$$

where $t_g \geq 0$, $t_g \geq p_g^{\mathrm{G}} - P_g^{\mathrm{G0}}$, and $t_g \geq -p_g^{\mathrm{G}} + P_g^{\mathrm{G0}}, \forall g \in \mathcal{G}$. The sectioning constraints ensure that the machines are split into two sections. If further separation is required, the optimization can be re-run on each island of the network.

Penalties

Often there may be multiple feasible solutions with objective values close to the optimum. Including additional penalty terms in the objective—small enough to not significantly affect the primary objective—improves computation by encouraging binary variables to take integral values in the relaxations, and also guides the solution process towards particular solutions. For example, consider the penalty terms (for a minimization problem)

$$\sum_{bb' \in \mathcal{L}} W^y (1 - y_{bb'}) + \sum_{bb' \in \mathcal{L}} W_{bb'}^{\mathrm{L}} (1 - \rho_{bb'}) + \sum_{g \in \mathcal{G}} W_g^{\mathrm{G}} (1 - \zeta_{bb'}) \tag{7.11}$$

where W^y, $W_{bb'}^{\mathrm{L}}$, W_g^{G} are weights to be chosen appropriately. The first term penalizes $1 - \cos\theta_{bb'}$, and hence the total line loss. The second penalizes cuts to lines. For example, setting $W_{bb'}^{\mathrm{L}}$ equal to the some small multiple of the pre-islanding power flow through the line will penalize most heavily disconnections of high-flow lines; in [70] it was shown that this leads more often to solutions that retain dynamic stability. The third term penalizes the switching-off of generators. If $W_g^{\mathrm{G}} = \epsilon P_g^{\mathrm{G+}}$ then units are given uniform weighting. If, say, $W_g^{\mathrm{G}} = \epsilon (P_g^{\mathrm{G+}})^2$, then the disconnection of large units is discouraged.

7.3.4 Overall formulation

The overall formulation of the islanding problem is given as:

$$\max\ W_1 J^{\text{exp load}} + W_2 J^{\text{coh}} + W_3 J^{\text{load}} + W_4 J^{\text{gen}}, \tag{7.12a}$$

subject to

$$\left.\begin{aligned} \sum_{g\in\mathcal{G}_b} p_g^{\text{G}} &= \sum_{d\in\mathcal{D}_b} P_d^{\text{D}} + \sum_{b'\in\mathcal{B}_b} p_{bb'}^{\text{L}} + G_i^{\text{B}}(2v_i - 1), \\ \sum_{g\in\mathcal{G}_b} q_g^{\text{G}} &= \sum_{d\in\mathcal{D}_b} Q_d^{\text{D}} + \sum_{b'\in\mathcal{B}_b} q_{bb'}^{\text{L}} - B_i^{\text{B}}(2v_i - 1), \end{aligned}\right\},\ \forall\ b \in \mathcal{B} \tag{7.12b}$$

$$\left.\begin{aligned} p_{bb'}^{\text{L}} &= G_l^{bb}(2v_b^{\text{L}} - 1) + G_{bb'}(v_b^{\text{L}} + v_{b'}^{\text{L}} + y_{bb'} - 2) + B_{bb'}\theta_{bb'}, \\ &\quad -(G_{bb}(2V_b^{LB} - 1) + G_{bb'}(V_b^{\text{LB}} + V_{b'}^{\text{LB}} - 1))(1 - \rho_{bb'}), \\ q_{bb'}^{\text{L}} &= B_{bb}(1 - 2v_b^{\text{L}}) - B_{bb'}(v_b^{\text{L}} + v_{b'}^{\text{L}} + y_{bb'} - 2) + G^{bb'}\theta_{bb'} \\ &\quad -(B_l^{bb}(1 - 2V_b^{\text{LB}}) - B_{bb'}(V_b^{\text{LB}} + V_{b'}^{\text{LB}} - 1))(1 - \rho_{bb'}), \\ y_{bb'} &= h_{bb',k}\theta_{bb'} + d_{bb',k}, \forall\theta_{bb'} \in [x_{bb',k}, x_{bb',k+1}], k = 0\ldots N-1, \\ \rho_{bb'} &\le 1 + \gamma_b - \gamma_{b'}, \\ p_{bb'}^{\text{L}} + p_{b'b}^{\text{L}} &\le P_l^{\text{L+}}, \end{aligned}\right\},\ \forall\ (b, b') \in \mathcal{L}$$

$$\gamma_b = s, \forall b \in \mathcal{B}^s, s \in \{0, 1\}, \tag{7.12c}$$

$$\left.\begin{aligned} \zeta_g P_g^{\text{Gmin}} \le p_g^{\text{G}} &\le \zeta_g P_g^{\text{Gmax}}, \forall g \in \mathcal{G}, \\ Q_g^{\text{Gmin}} \le q_g^{\text{G}} &\le Q_g^{\text{Gmax}}, \forall g \in \mathcal{G}, \\ \zeta_g = 1, \forall g \in \{\mathcal{G} : P_g^{\text{Gmin}} = 0\} &\cup \mathcal{G}^1, \end{aligned}\right\},\ \forall\ g \in \mathcal{G} \tag{7.12d}$$

$$V_b^{\text{LB}} \le v_b \le V_b^{\text{UB}}, \forall b \in \mathcal{B}, \tag{7.12e}$$

$$\left.\begin{aligned} P_g^{\text{LB}} \le p_g^{\text{G}} &\le P_g^{\text{UB}}, \forall g \in \mathcal{G}, \\ Q_g^{\text{LB}} \le q_g^{\text{G}} &\le Q_g^{\text{UB}}, \forall g \in \mathcal{G}, \end{aligned}\right\},\ \forall\ g \in \mathcal{G} \tag{7.12f}$$

$$\left.\begin{aligned} p_d^{\text{D}} &= \alpha_d P_d^{\text{D}}, \\ q_d^{\text{D}} &= \alpha_d Q_d^{\text{D}}. \\ 0 \le \alpha_d &\le 1, \end{aligned}\right\},\ \forall\ d \in \mathcal{D} \tag{7.12g}$$

$$\tag{7.12h}$$

where (7.12a) is the objective function, $W_i, 1 \le i \le 4$ are the weights and can be assigned either binary values of 0 and 1 or continuous values depending on the objective of islanding. Over all depending on the objective function this optimization problem is MILP or MIQP and can be solved with CPLEX.

7.4 Computational results

7.4.1 Islanding to minimize expected load loss

A set of scenarios was built based on test systems with between 9 and 300 buses. For a network with n^{B} buses, n^{B} scenarios were generated by assigning in turn each single bus to $\mathcal{B}^0$. No buses were included in $\mathcal{B}^1$ and no lines in $\mathcal{L}^0$. For each scenario, the islanding solution was obtained by solving the previously described MILP problem. The feasibility of an islanding solution was checked by solving an AC optimal load shedding (OLS) problem on the islanded network, which includes all AC power balance, flow and operating constraints, but permits load shedding as per (5.1a) and (5.1b).

Data for the islanding problems are described as follows. In the objective function, $J^{\text{exp load}}$, a value of 0.75 is used for the load loss penalty β_d. The generator coherency objective, J^{coh}, was not included initially. The penalties are $W_g^{\mathrm{G}} = 0.01 P_g^{\mathrm{G+}}$, $W^y = 0.1$ and $W_{bb'}^{\mathrm{L}} = 0.0025 \sum_d P_d^{\mathrm{D}}$, so that the line-cut penalty is scaled by the total load in the system. Our investigations show that these penalties have a negligible effect (0.2%) on the quality of the solutions, but reduce computation time by an order of magnitude. For the PWL approximation for a line l, first the angle difference prior to islanding, θ_l^*, is determined from the base-case AC OPF solution, and then 12 pieces are used over $\pm(|\theta_l^*| + 10°)$.

Operating limits, including voltage and line limits, were obtained from each network's data file [32]. Generator real power output limits (P_g^{LB} and P_g^{UB}) were set, as explained in Section 7.3.2, to allow a 2-minute ramp change from the current output P_g^{G0}, where ramp rates were available in the network data, or a 5% change where they were not. In either case, the output limits were limited by capacity limits. P_g^{G0} was obtained by solving an AC OPF on the intact network prior to islanding. Then in the islanding problem, the lower limit was raised by 5% of $(P_g^{\mathrm{LB}} - P_g^{\mathrm{UB}})$. The post-islanding AC OLS, however, was permitted to use the full range, $[P_g^{\mathrm{LB}}, P_g^{\mathrm{UB}}]$. This avoids those solutions where an island is infeasible because of too much generated real power.

AC-feasible islanding of 24-bus network

Returning to the example of Section 7.3.1, the PWL AC islanding approach is applied to the problem of islanding bus 6. The islanding problem was solved both with and without the option (as part of the optimization) of switching the shunt reactor at bus 6. The optimal solutions are shown in Fig. 7.3. Without shunt switching (PWL-AC-1), the cable $(6, 10)$ is left intact and the final network topology is significantly different from before. With shunt switching permitted (PWL-AC-2), the cable is again switched, but fewer buses are islanded than for the DC solution. The feasibility of each solution was checked by solving the AC OLS problem on the islanded network, and both PWL

AC solutions satisfied all AC constraints. Tab. 7.2 compares the DC, PWL-AC-1 and PWL-AC-2 solutions, using values obtained from both the MILP solutions and the post-islanding AC solutions. The PWL AC islanding solutions are close to the final AC OLS solutions. Note that the PWL AC solutions achieve AC feasibility at the cost of a lower expected load supply (hence higher expected load shed).

Solution	DC	PWL-AC-1	PWL-AC-2
MILP islanding solution			
$J^{\text{exp load}}$ (MW)	2764.8	2679.2	2753.8
Generation (MW)	2850.0	2892.7	2844.1
Exp. load shed (MW)	85.3	170.8	96.2
Post-islanding AC-OLS			
$J^{\text{exp load}}$ (MW)	$\star$	2671.2	2753.2
Generation (MW)	$\star$	2884.4	2847.8
Exp. load shed (MW)	$\star$	178.9	96.8

Table 7.2: 24-bus system: Comparison of solutions.

Computation time

The speed with which islanding decisions have to be made depends on whether the decision is being made before a fault has occurred, as part of contingency planning within secure OPF, or after, in which case the time scale depends on the cause of the contingency. Finding solutions that are optimal, or to within a pre-specified percentage of optimality, can take an unpredictable amount of time. Hence, especially in the latter case of reacting after a fault has occurred, it is important to be able to produce good feasible solutions within short time periods even if these are not necessarily optimal. To illustrate how the quality of the solution depends on the solution time, tests were run for a set of fixed times of between 5 and 60 seconds, returning the best found integer feasible solution. Tab. 7.3 summarizes these results for the 57−, 118- and 300-bus scenarios, quoting the average relative MIP gap of returned solutions. The 9- to 57-bus cases were solved to negligible % gaps within the time available, and are not shown. Also shown are the average gaps between the returned and best-known AC solutions for each scenario, where an AC solution was obtained from a returned PWL islanding solution by solving the AC-OLS on the islanded network. The mean error between the objectives of the returned PWL-AC and AC solutions was 0.04%. For each network and scenario, the best-known AC solution was the best from those found from the different termination times, plus a longer 1000-second run. The platform was a 64-bit desktop

machine with Intel i7-2600 processor and 8 GiB RAM, using CPLEX 12.5 as the solver, and permitting up to 4 cores for parallel computation.

Time (s)	5	10	15	30	45	60
Percentage with no islanding solution found within time						
57-bus	7.0	5.0	0.0	0.0	0.0	0.0
118-bus	1.7	5.0	0.0	0.0	0.0	0.0
300-bus	20.3	13.7	8.7	2.3	0.7	0.0
Mean % between best MIP solution and the MIP bound						
57-bus	2.11	1.50	1.04	0.40	0.33	0.28
118-bus	0.50	0.50	0.46	0.28	0.14	0.09
300-bus	0.09	0.06	0.09	0.17	0.19	0.22
Mean % between best AC solution found in time and best known						
57-bus	0.89	0.76	0.58	0.12	0.08	0.05
118-bus	0.17	0.22	0.21	0.11	0.02	0.02
300-bus	0.01	0.00	0.02	0.06	0.06	0.08

Table 7.3: Solutions to islanding problems for different time limits.

The results show that good islanding solutions can be found within 1 minute—and usually sooner—for all networks. Moreover, the islanding topology changes little, and usually not at all, between the solutions returned at 5sec and 60 second.

AC feasibility

Using the DC model 20% of cases led to AC-infeasible islands [70], whereas none of the islands found using the PWL AC model were infeasible.

Promoting generator coherency

The generator coherency objective, J^{coh}, may be included for the 24-bus network example by taking second-order dynamic data taken from [80]. For example, when $\mathcal{B}^0 = 3$, maximizing just $J^{\text{exp load}}$ leads to an optimal solution that places bus 1 in section 0 along with bus 3, and an expected load supply of 2699 MW. In doing this, the line between buses 1 and 2 is switched, separating the large generator sets at these buses (which would incur a cost of $J^{\text{coh}} = 2.26$). However, when maximizing the joint objective with $k = 100$, the optimal solution does not include bus 1 in section 0, opting instead to leave the line $(1, 2)$ intact and placing just buses 3 and 9 in section 0. With $k = 100$, the expected load supply is slightly smaller (2670 MW), but the strongly-coupled generators

	Section 0	Section 1
Buses	1–3, 5–9, 30, 31, 39	4, 10–29, 32–38
Generation (MW)	2007.18	3992.29
Load supplied (MW)	1997.89	3945.37
Load shed (MW)	297.21	13.76

Table 7.4: Coherency-based islanding of 39-bus network.

at buses 1 and 2 remain connected ($J^{\text{coh}} = 0.00$).

7.4.2 Coherency-based islanding

The coherency-based splitting approach was applied to the 10-machine, 39-bus New England test network. Slow coherency analysis, assuming second-order dynamics, shows that the machines may be divided into two groups: those at buses 30, 31 and 39 in one group, and then all others.

With $\mathcal{B}^0 = \{30, 31, 39\}$ and $\mathcal{B}^1 = \mathcal{B}^{\text{G}} \setminus \mathcal{B}^0$, the optimal solution splits the system as shown in Tab. 7.4. Note that although buses 1–3 and 5–9 are included in the same section as 30, 31 and 39, no generators are present at these buses. The objective was to minimize the movement of generator real power outputs, *i.e.*, (7.10). To achieve this split and leave the islands balanced, the generator at bus 32 has to lower its output from 671 to 373 MW, while 311 MW is shed. It is worth stating that no other solution exists that splits these two groups but requires less total change in generator outputs.

Chapter 8

Conclusions and Future Work

In this chapter we summarise the results obtained in this thesis and give some future research directions.

8.1 Conclusions

There are three parts to this thesis: existence of local optima of OPF problems, methods for finding bounds on the solution of OPF problems, and an optimization framework for controlled islanding. In the first part on local optima of OPF problems, we have shown the existence of local solutions of OPF problems. All examples have either $\pm 5\%$ voltage bounds or the same bounds as standard cases from which they are derived. The data for the examples and the local solutions are publicly available at [38] so can be used in testing local and global optimization techniques for OPF problems. We have observed that cases of local solutions are hard to find: indeed none was found in any of the standard test cases. However after modifying load or generator bounds local optima were found for the 9-, 39-, 118- and 300-bus cases. The examples of local optima presented in this thesis are associated with either circulating flows, high line angles or an excess of reactive power. The local marginal prices (LMPs) for reactive power are then negative. An excess of reactive power can occur when load is reduced in a network that has been designed for peak loads. A related but less common situation that results in local optima is an excess of real power in the network. This results in negative LMPs for real power. Negative real power LMPs can occur as a result of real power generator ramping constraints. For example in multi period OPF if there is a reduction in demand between periods, or in islanding where there is an excess of generation in one island after the network is split. Rate of change limits give negative LMPs. We have observed this in the islanding work where we create and island with excess of generation and then try to rid of excess by line losses. We have shown that in some cases the local OPF solutions lie within a connected feasible region, and in

some cases they lie in different disconnected regions which result from the interaction of the nonlinear power flow equations with the bounds on voltage magnitudes, generator outputs or apparent power flows in lines. The SDP method of [26] worked in all except one of the standard test cases (which have no local optima), but failed in most cases in which there are local optima, but in most cases it then gave good bounds.

In the second part, a nonlinear relaxation of OPF problem is presented. The relaxation is found to be very accurate and more likely to converge to the global solution. The relaxed formulation does not come with a theoretical guarantee of lower bound but numerical test shows that with reasonable starting points, the relaxed formulation is accurate. The relaxation produces very good estimates of the lower bound of OPF problem. Also this formulation is useful to obtain good starting point for exact OPF formulation to overcome the problem of local optimization converging to infeasible point.

In the third part, an optimization-based approach to controlled islanding and intentional load shedding has been presented. The proposed method uses MILP to determine which lines to cut, loads to shed, and generators to switch or adjust in order to isolate an uncertain or failure-prone region of the network. The optimization framework allows linear network constraints—a loss-modified DC power flow model, line limits, generator outputs—to be explicitly included in decision making, and produces balanced, steady-state feasible DC islands. AC islanding solutions are found via the subsequent solving of an AC optimal load shedding problem.

The approach has been demonstrated through examples on a range of test networks, and the practicality of the method in terms of computation time has been demonstrated. Good feasible islanding solutions can be found very quickly. Furthermore, it was shown that these penalties had a small effect on the amount of load required to be shed. This approach is based on DC model of the power flow equations. We observe that using DC approximations sometime leads to AC infeasible cases.

Lastly, we improve our DC based islanding approach by incorporating more accurate model of power flow equations. This model is based on PWL approximations of the dominant nonlinear terms. It is shown that this model overcome the shortcomings of the DC model, by producing AC feasible islanding solutions.

8.2 Future Research Directions

In this section we will give brief description of the future research directions which naturally follow from our work.

8.2.1 Aggregation of Large Networks for the Islanding problem

The size of the power networks is huge and it is increasing over time. Often in power system, the disturbance initially affects small part of the network. In these cases it is advantageous to aggregate the rest of the network and reduce the size of the network to a manageable size. The idea of aggregation combines well with our islanding model and we hope to reduce the computational time by this approach.

8.2.2 Heuristics for Islanding

We are also interested in exploring the possibility of employing heuristics for power system islanding problem. The heuristics can start by an island around the troubled part of the network and then can explore possible islands around that bit of the network. Simulated annealing is a meta-heuristic technique which can be used for this purpose.

8.2.3 Using MILP Solution Pool

While solving MILP problems, CPLEX can return the pool of feasible solutions. It would be interesting to explore suboptimal MILP solutions if the optimal solution turns out to be AC infeasible. This approach has a promise of being parallelized. But unfortunately using CPLEX, there is no way to get a feasible solution as soon as it is found. CPLEX only returns the pool of solutions after it is done with the branching process. Another open source MILP solver SCIP [81], has the capability to return feasible solutions as soon as they are found. It would be interesting to parallelize this process using SCIP.

Appendices

Appendix A

Load shedding of IEEE 14 Bus System

b	v_b(p.u.)	θ_b(deg)	p_g^{G}(MW)	q_g^{G}(Mvar)	P_d^{D}(MW)	Q_d^{D}(Mvar)	α_d
1	1.053	0.00	153.8	4.1			
2	1.035	-3.10			21.7	12.7	0.00
3	1.025	-5.50	0.0	0.0	94.2	19.0	0.05
4	1.012	-7.10			47.8	-3.9	1.00
5	1.013	-6.22			7.6	1.6	1.00
6	1.060	-11.60	0.0	13.9	11.2	7.5	1.00
7	1.043	-10.30					
8	1.056	-10.30	0.0	7.6			
9	1.041	-11.97			29.5	16.6	1.00
10	1.037	-12.20			9.0	5.8	1.00
11	1.045	-12.03			3.5	1.8	1.00
12	1.045	-12.45			6.1	1.6	1.00
13	1.039	-12.50			13.5	5.8	1.00
14	1.022	-13.23			14.9	5.0	1.00

(a) Bus

l	*from(b)*	*to(b')*	$p_{bb'}^{\mathrm{L}}$(MW)	$q_{bb'}^{\mathrm{L}}$(Mvar)	$p_{b'b}^{\mathrm{L}}$(MW)	$q_{b'b}^{\mathrm{L}}$(Mvar)	MVA Limit	$(\theta_b - \theta_{b'})$
1	1	2	100.0	-98.2	-1.7	1.3	100	3.10
2	1	5	53.9	-52.4	5.8	-5.0	100	6.22
3	2	3	22.5	-22.3	-2.0	-1.7	100	2.40
4	2	4	41.9	-41.0	-0.4	-0.3	100	4.00
5	2	5	33.8	-33.2	1.1	-2.9	100	3..12
6	3	4	17.5	-17.3	0.8	-1.6	100	1.60
7	4	5	-34.9	-35.1	7.9	-7.4	100	-0.88
8	4	7	28.8	-28.8	-3.4	5.1	100	3.20
9	4	9	16.6	-16.6	1.3	0.1	100	4.87
10	5	6	42.9	-42.9	13.6	-9.3	100	5.38
11	6	11	6.6	-6.5	5.0	-4.9	100	0.43
12	6	12	7.7	-7.7	2.7	-2.6	100	0.85
13	6	13	17.4	-17.2	8.0	-7.5	100	0.90
14	7	8	0.0	0.0	-7.5	7.6	100	0.00
15	7	9	28.8	-28.8	2.4	-1.6	100	1.67
16	8	10	6.0	-6.0	2.8	-2.7	100	0.22
17	8	14	9.9	-9.8	2.7	-2.4	100	1.25
18	10	11	-3.0	3.0	-3.1	3.1	100	-0.17
19	12	13	1.6	-1.5	1.0	-1.0	100	0.05
20	13	14	5.2	-5.1	2.8	-2.6	100	0.73

(b) Line

Table A.1: Optimal AC OLS solution for 14-bus network with no line cuts and generator 2 switched off.

b	θ_b	p_g^{G}(MW)	P_d^{D}(MW)	α_d
1	0.00	154.6		
2	-3.75		21.7	0.00
3	-6.82	0.0	94.2	0.12
4	-8.41		47.8	1.00
5	-7.38		7.6	1.00
6	-12.93	0.0	11.2	1.00
7	-11.85			
8	-11.85	0.0		
9	-13.70		29.5	1.00
10	-14.06		9.0	1.00
11	-13.75		3.5	1.00
12	-14.24		6.1	1.00
13	-14.52		13.5	1.00
14	-15.65		14.9	1.00

(a) Bus

l	*from(b)*	*to(b')*	$p_{bb'}^{\mathrm{L}}$(MW)	PL,max$_{bb'}$(MW)	$(\theta_b - \theta_{b'})$(deg)
1	1	2	100.0	100	3.75
2	1	5	54.6	100	7.38
3	2	3	25.6	100	3.06
4	2	4	41.6	100	4.65
5	2	5	32.9	100	3.63
6	3	4	14.1	100	1.59
7	4	5	-38.6	100	-1.03
8	4	7	29.3	100	3.44
9	4	9	17.1	100	5.29
10	5	6	41.2	100	5.55
11	6	11	5.9	100	0.82
12	6	12	7.2	100	1.30
13	6	13	16.9	100	1.59
14	7	8	0.0	100	0.00
15	7	9	29.3	100	1.85
16	8	10	6.6	100	0.37
17	8	14	10.3	100	1.96
18	10	11	-2.4	100	-0.31
19	12	13	1.1	100	0.29
20	13	14	4.6	100	1.13

(b) Line

Table A.2: Optimal DC OLS solution for 14-bus network with no line cuts and generator 2 switched off.

b	v_b(p.u.)	θ_b(deg)	p_g^{G}(MW)	q_g^{G}(Mvar)	P_d^{D}(MW)	Q_d^{D}(Mvar)	α_d
1	1.060	0.00	198.1	13.0			
2	1.041	-3.04			21.7	12.7	0.00
3	0.984	-17.14	0.0	18.9	94.2	19.0	0.44
4	0.996	-12.57			47.8	-3.9	1.00
5	0.997	-11.48			7.6	1.6	1.00
6	1.060	-17.06	0.0	22.9	11.2	7.5	1.00
7	1.038	-15.78					
8	1.060	-15.78	0.0	13.5			
9	1.035	-17.44			29.5	16.6	1.00
10	1.032	-17.67			9.0	5.8	1.00
11	1.042	-17.49			3.5	1.8	1.00
12	1.044	-17.91			6.1	1.6	1.00
13	1.039	-17.96			13.5	5.8	1.00
14	1.018	-18.70			14.9	5.0	1.00

(a) Bus

l	*from(b)*	*to(b')*	$p_{bb'}^{\mathrm{L}}$(MW)	$q_{bb'}^{\mathrm{L}}$(Mvar)	$p_{b'b}^{\mathrm{L}}$(MW)	$q_{b'b}^{\mathrm{L}}$(Mvar)	MVA Limit	$(\theta_b - \theta_{b'})$(deg)
1	1	2	100.0	-98.3	0.2	-0.8	100	3.04
2	1	5	98.1	-93.3	12.8	1.6	100	11.48
3	2	4	98.3	-93.1	0.8	11.4	100	9.53
4	3	4	-41.2	42.5	10.6	-8.6	100	-4.57
5	4	5	-41.7	42.0	10.4	-9.6	100	-1.09
6	4	7	28.3	-28.3	-8.6	10.4	100	3.21
7	4	9	16.2	-16.2	-0.6	2.0	100	4.87
8	5	6	43.8	-43.8	6.4	-2.1	100	5.58
9	6	11	7.1	-7.0	6.1	-5.9	100	0.43
10	6	12	7.8	-7.8	2.8	-2.7	100	0.86
11	6	13	17.7	-17.4	8.5	-8.1	100	0.90
12	7	8	0.0	0.0	-13.2	13.5	100	0.00
13	7	9	28.3	-28.3	2.9	-2.0	100	1.66
14	8	10	5.5	-5.5	1.7	-1.7	100	0.22
15	8	14	9.5	-9.4	2.0	-1.8	100	1.26
16	10	11	-3.5	3.5	-4.1	4.1	100	-0.18
17	12	13	1.7	-1.6	1.1	-1.1	100	0.05
18	13	14	5.6	-5.5	3.4	-3.2	100	0.74

(b) Line

Table A.3: Optimal AC OLS solution for 14-bus network with line cuts and generator 2 switched off.

b	θ_b(deg)	p_g^{G}(MW)	P_d^{D}(MW)	α_d
1	0.00	200.0		
2	-3.75		21.7	0.00
3	-25.59	0.0	94.2	1.00
4	-14.94		47.8	0.36
5	-13.53		7.6	0.96
6	-18.83	0.0	11.2	0.95
7	-18.05			
8	-18.05	0.0		
9	-19.73		29.5	0.94
10	-20.00		9.0	0.86
11	-19.63		3.5	0.83
12	-20.05		6.1	0.91
13	-20.35		13.5	0.95
14	-21.48		14.9	0.93

(a) Bus

l	*from(b)*	*to(b')*	$p_{bb'}^{\mathrm{L}}$(MW)	PL,max$_{bb'}$(MW)	$(\theta_b - \theta_{b'})$(deg)
1	1	2	100.0	100	3.75
2	1	5	100.0	100	13.53
4	2	4	99.9	100	11.19
6	3	4	-94.2	100	-10.65
7	4	5	-53.3	100	-1.42
8	4	7	26.5	100	3.11
9	4	9	15.5	100	4.78
10	5	6	39.4	100	5.30
11	6	11	5.7	100	0.80
12	6	12	6.7	100	1.22
13	6	13	16.2	100	1.50
14	7	8	0.0	100	0.00
15	7	9	26.5	100	1.67
16	8	10	5.0	100	0.27
17	8	14	9.3	100	1.75
18	10	11	-2.8	100	-0.37
19	12	13	1.2	100	0.31
20	13	14	4.5	100	1.13

(b) Line

Table A.4: Optimal DC OLS solution for 14-bus network with line cuts and generator 2 switched off.

Appendix B

Test Archive for Local Solutions

Here we list test cases with known local optimal. The network data, diagrams and local solution details are available in the online archive[38].

Test Case	n_B[1]	n_L[2]	n_G[3]	Modifications	# of Local Optima	% Difference[4]
`WB2`	2	1	1	-	2	3.18
`WB3`	3	2	1	-	2	0.21
`WB5`	5	6	2	-	2	14.34
`LMBM3`	3	3	3	-	5	69.94
`case9mod`	9	9	3	Lower bounds on reactive power generations of all generators= -3 MVars, demand scaled to 60%	4	50.80
`case22loop`	30	30	15	-	2	33.69
`case39mod1`	39	46	10	Voltage bounds tightened by $\pm 5\%$	2	115.48
`case39mod2`	39	46	10	Voltage bounds tightened by $\pm 5\%$, only linear cost coefficients used	5	0.53
`case118mod`	118	186	54	Generators real and reactive power bounds scaled by 7	3	50.97
`case300mod`	300	411	69	Lower bounds on reactive power generations of all generators $= -3$ MVars, demand scaled to 60%	7	2.52

Table B.1: Test case archive for local solutions of OPF.

[1] n_B := # of Buses
[2] n_L := # of Lines
[3] n_G := # of Generators
[4] $\frac{\max(\text{Local Solution})}{\text{Global Solution}}$ Global Solution(%)

Appendix C

Network Data for real test networks

Here we list test cases collected from publicly available format and put together in a coherent format. The network data, and diagrams are available in an online archive [82].

Test Case	n_{B}	n_{L}	n_{G}	Comments
39 Bus Case	39	46	10	New England test case with realistic cost data
Iceland Network	118	206	35	Transmission network data of Iceland
Reduced GB Network	29	99	66	Reduced representative model of GB
GB Network	2224	3207	394	Complete transmission network of GB
European Network	21097	32112	2769	Anonymousized European network data

Table C.1: Network data for real transmission systems.

Bibliography

[1] P. Hines, J. Apt, and S. Talukdar, "Trends in the history of large blackouts in the united states," in *Power and Energy Society General Meeting - Conversion and Delivery of Electrical Energy in the 21st Century, 2008 IEEE*, pp. 1–8, 2008.

[2] C. H. C. J. Shortle, "What can lead to a wide-scale blackout?," *Sigma, 10(1), 11-15.*, 2010.

[3] "Investigation into transmission losses on UK electricity transmission system," tech. rep., Available Online on National Grid website, 2008.

[4] "Electricity distribution systems losses, non-technical overview," tech. rep., Sohn Associates and Ofgem, 2007.

[5] J. D. D. Kothari, *Power System Optimization.* PHI Learning, 2012.

[6] N.-Y. Chiang, *Structure-Exploiting Interior Point Methods for Security Constrained Optimal Power Flow Problems.* PhD thesis, School of Mathematics, 2013.

[7] J. Zhu, *Optimization of Power System Operation.* IEEE Press, 2009.

[8] K. Iba, H. Suzuki, M. Egawa, and T. Watanabe, "A method for finding a pair of multiple load flow solutions in bulk power systems," *IEEE Transactions on Power Systems*, vol. 5, pp. 582–591, 1990.

[9] A. Klos and J. Wojcicka, "Physical aspects of the nonuniqueness of load flow solutions," *International Journal of Electrical Power and Energy Systems*, vol. 13, pp. 268–276, 1991.

[10] A. Simsek, "Analysis of critical points for nonconvex optimization," Master's thesis, MIT Department of Electrical Engineering and Computer Science, 2005.

[11] A. Gopalakrishnan, A. U. Raghunathan, D. Nikovski, and L. T. Biegler, "Global optimization of optimal power flow using a branch & bound algorithm," in *50th Annual Allerton Conference on Communication, Control, and Computing*, 2012.

[12] D. T. Phan, "Lagrangian duality and branch-and-bound algorithms for optimal power flow," *Operations Research*, vol. 60, no. 2, pp. 275–285, 2012.

[13] K. Y. L. Mohamed A. El-Sharkawi, *Modern heuristic optimization techniques.* John Wiley, 2008.

[14] J. Carpentier, "Contribution a l'etude du dispacting economique," *Bull. Soc. Francaise des Electriciens*, vol. 3, pp. 431–447, 1962.

[15] W. Fu and J. McCalley, "Risk based optimal power flow," in *Power Tech Proceedings, 2001 IEEE Porto*, vol. 3, pp. 6 pp. vol.3–, 2001.

[16] R. Fourer, D. M. Gay, and B. W. Kernighan, *AMPL: A Modeling Language for Mathematical Programming.* Duxbury Press, Nov. 2002.

[17] R. P. O. Anya Castillo, "Computational performance of solution techniques applied to the acopf," tech. rep., Federal Regulatory Energy Commission.

[18] T. J. Overbye, "A power flow measure for unsolvable cases," *IEEE Transactions on Power Sys*, vol. 9, pp. 1359–1365, 1994.

[19] H. W. Dommel and W. F. Tinney, "Optimal power flow solutions," *IEEE Transactions on Power Apparatus and Systems*, vol. PAS-87, pp. 1866–1876, 1968.

[20] J. A. Momoh, R. Adapa, and M. E. El-Hawary, "A review of selected optimal power flow literature to 1993. i. nonlinear and quadratic programming approaches," *IEEE Transactions on Power Systems*, vol. 14, pp. 96–104, 1999.

[21] J. A. Momoh, M. E. El-Hawary, and R. Adapa, "A review of selected optimal power flow literature to 1993. ii. newton, linear programming and interior point methods," *IEEE Transactions on Power S*, vol. 14, pp. 105–111, 1999.

[22] P. E. Gill, W. Murray, and M. A. Saunders, "SNOPT: An SQP algorithm for large-scale constrained optimization," *SIAM Journal on Optimization*, vol. 12, pp. 979–1006, 2002.

[23] R. H. Byrd, J. Nocedal, and R. A. Waltz, *Large-Scale Nonlinear Optimization*, vol. 83 of *Nonconvex Optimization and Its Applications*, ch. KNITRO: An Integrated Package for Nonlinear Optimization, pp. 35–59. Springer US, 2006.

[24] A. Wächter and L. T. Biegler, "On the implementation of an interior-point filter line-search algorithm for large-scale nonlinear programming," *Mathematical Programming*, vol. 106, pp. 25–57, 2006.

[25] C. Coffrin and P. V. Hentenryck, "A linear-programming approximation of ac power flows," *CoRR*, vol. abs/1206.3614, 2012.

[26] J. Lavaei and S. H. Low, "Convexification of optimal power flow problem," in *48th Annual Allerton Conference on Communication, Control, and Computing*, 2010.

[27] B. Zhang and D. Tse, "Geometry of injection regions of power networks," *IEEE Transactions on Power Systems*, vol. 28, pp. 788–797, 2013.

[28] J. Lavaei, D. Tse, and B. Zhang, "Geometry of power flows in tree networks," in *IEEE Power and Energy Society General Meeting*, 2012.

[29] B. C. Lesieutre, D. K. Molzahn, A. R. Borden, and C. L. DeMarco, "Examining the limits of the application of semidefinite programming to power flow problems," in *49th Annual Allerton Conference on Communication, Control, and Computing*, 2011.

[30] J. Lofberg, "Yalmip : A toolbox for modeling and optimization in matlab," in *In Proceedings of the CACSD Conference*, 2004.

[31] J. F. Sturm, "Using sedumi 1.02, a matlab toolbox for optimization over symmetric cones," 1998.

[32] R. D. Zimmerman, C. E. Murillo-Sánchez, and R. J. Thomas, "Matpower: Steady-state operations, planning, and analysis tools for power systems research and education," *IEEE Transactions on Power Systems*, vol. 26, pp. 12–19, 2011.

[33] Z. Qiu, G. Deconinck, and R. Belmans, "A literature survey of optimal power flow problems in the electricity market context," in *IEEE/PES Power Systems Conference and Exposition*, 2009.

[34] M. R. AlRashidi and M. E. El-Hawary, "Applications of computational intelligence techniques for solving the revived optimal power flow problem," *Electric Power Systems Research*, vol. 79, pp. 694–702, 2009.

[35] I. A. Hiskens and R. J. Davy, "Exploring the power flow solution space boundary," *IEEE Transactions on Power Systems*, vol. 16, pp. 389–395, 2001.

[36] J. A. Momoh, R. Koessler, M. Bond, B. Stott, D. Sun, A. Papalexopoulos, and P. Ristanovic, "Challenges to optimal power flow," *IEEE Transactions on Power Systems*, vol. 12, pp. 444–455, 1997.

[37] K. I. M. W. A. Bukhsh, A. Grothey and P. A. Trodden, "Local solutions of optimal power flow," tech. rep., University of Edinburgh School of Mathematics, ERGO

11-017, [Online]. Available: http://www.maths.ed.ac.uk/ERGO/pubs/ERGO-11-017.html., 2011.

[38] W. A. Bukhsh, A. Grothey, K. McKinnon, and P. A. Trodden, "Test case archive of optimal power flow (opf) problems with local optima." [Online] Available:`http://www.maths.ed.ac.uk/optenergy/LocalOpt/`.

[39] A. J. Korsak, "On the question of uniqueness of stable load-flow solutions," *IEEE Transactions on Power Apparatus and Systems*, vol. PAS-91, pp. 1093–1100, 1972.

[40] N. Janssens and A. Kamagate, "Loop flows in a ring AC power system," *International Journal of Electrical Power and Energy Systems*, vol. 25, pp. 591–597, 2003.

[41] R. D. Christie, "Power systems test case archive," August 1999.

[42] S. Sojoudi and J. Lavaei, "Physics of power networks makes hard optimization problems easy to solve," in *IEEE Power and Energy Society General Meeting*, 2012.

[43] W. Bukhsh, A. Grothey, K. McKinnon, and P. Trodden, "Local solutions of the optimal power flow problem," *Power Systems, IEEE Transactions on*, vol. 28, no. 4, pp. 4780–4788, 2013.

[44] D. Molzahn, J. Holzer, B. Lesieutre, and C. DeMarco, "Implementation of a large-scale optimal power flow solver based on semidefinite programming," *Power Systems, IEEE Transactions on*, vol. 28, no. 4, pp. 3987–3998, 2013.

[45] P. V. H. Hassan L. Hijazi, Carleton Coffrin, "Convex quadratic relaxations of non-linear programs in power systems," *Optimization Online*, 2013.

[46] G. P. McCormick, "Computability of global solutions to factorable nonconvex programs: Part 1-convex underestimating problems," *Mathematical Programming*, vol. 10, pp. 146–175, 1976.

[47] F. Milano, *Documentation for PSAT version 2.0.0.* University of Castilla – La Mancha, February 2008.

[48] H. P. Williams, *Logic and Integer Programming.* International Series in Operations Research & Management Science, Springer, 2009.

[49] "Final Report of the Investigation Committee on the 28 September 2003 Blackout in Italy," final report, Union for the Coordination of the Transmission of Electricity (UCTE), April 2004.

[50] S. Larsson and A. Danell, "The black-out in southern Sweden and eastern Denmark, September 23, 2003," in *IEEE Power Systems Conference and Exposition*, 2006.

[51] U.S.-Canada Power System Outage Task Force, "Final Report on the August 14, 2003 Blackout in the United States and Canada: Causes and Recommendations," final report, April 2004.

[52] "Final Report System Disturbance on 4 November 2006," final report, Union for the Coordination of the Transmission of Electricity (UCTE), 2007.

[53] "Report of the National Grid Investigation into the Frequency Deviation and Automatic Demand Disconnection that occurred on the 27th May 2008," final report, National Grid, February 2009.

[54] "Report of the enquiry committee on grid disturbance in northern region," tech. rep., 2012.

[55] M. A. M. K. M. W. G. S. Michael Bruch, Volker MÃ$\frac{1}{4}$nch, "Power blackouts risks," *CRO Forum-Position Paper*, 2011.

[56] J. W. Bialek, "Are blackouts contagious?," *IEE Power Engineer*, vol. 17, p. 10, December/January 2003.

[57] J. W. Bialek, "Blackouts in the US/Canada and continental Europe in 2003: is liberalisation to blame?," in *IEEE PowerTech Conference*, (Russia), June 2005.

[58] G. Andersson, P. Donalek, R. Farmer, N. Hatziargyriou, I. Kamwa, P. Kundur, N. Martins, J. Paserba, P. Pourbeik, J. Sanchez-Gasca, R. Schulz, A. Stankovic, C. Taylor, and V. Vittal, "Causes of the 2003 major grid blackouts in North America and Europe, and recommended means to improve system dynamic performance," *IEEE Transactions on Power Systems*, vol. 20, pp. 1922–1928, November 2005.

[59] D. E. Newman, B. A. Carreras, M. Kirchner, and I. Dobson, "The impact of distributed generation on power transmission grid dynamics," in *44th Hawaii International Conference on System Science*, 2011.

[60] B. Yang, V. Vittal, and G. T. Heydt, "Slow-coherency-based controlled islanding—a demonstration of the approach on the August 14, 2003 blackout scenario," *IEEE Transactions on Power Systems*, vol. 21, pp. 1840–1847, 2006.

[61] K. Sun, D.-Z. Zheng, and Q. Lu, "Splitting strategies for islanding operation of large-scale power systems using OBDD-based methods," *IEEE Transactions on Power Systems*, vol. 18, pp. 912–923, 2003.

[62] H. You, V. Vittal, and X. Wang, "Slow coherency-based islanding," *IEEE Transactions on Power Systems*, vol. 19, pp. 483–491, February 2004.

[63] X. Wang and V. Vittal, "System islanding using minimal cutsets with minimum net flow," in *IEEE Power Systems Conference and Exposition*, 2004.

[64] G. Xu and V. Vittal, "Slow coherency based cutset determination algorithm for large power systems," *IEEE Transactions on Power Systems*, vol. 25, pp. 877–884, May 2010.

[65] L. Liu, W. Liu, D. A. Cartes, and I.-Y. Chung, "Slow coherency and angle modulated particle swarm optimization based islanding of large-scale power systems," *Advanced Engineering Informatics*, vol. 23, no. 1, pp. 45–56, 2009.

[66] M. R. Aghamohammadi and A. Shahmohammadi, "Intentional islanding using a new algorithm based on ant search mechanism," *International Journal of Electrical Power and Energy Systems*, vol. 35, pp. 138–147, 2012.

[67] M. Jin, T. S. Sidhu, and K. Sun, "A new system splitting scheme based on the unified stability control framework," *IEEE Transactions on Power Systems*, vol. 22, pp. 433–441, February 2007.

[68] C. G. Wang, B. H. Zhang, Z. G. Hao, J. Shu, P. Li, and Z. Q. Bo, "A novel real-time searching method for power system splitting boundary," *IEEE Transactions on Power Systems*, vol. 25, pp. 1902–1909, November 2010.

[69] L. Ding, F. M. Gonzalez-Longatt, P. Wall, and V. Terzija, "Two-step spectral clustering controlled islanding algorithm," *IEEE Transactions on Power Systems*, 2012.

[70] P. A. Trodden, W. A. Bukhsh, A. Grothey, and K. I. M. McKinnon, "MILP formulation for controlled islanding of power networks," *International Journal of Electrical Power & Energy Systems*, vol. 45, no. 1, pp. 501–508, 2013.

[71] E. B. Fisher, R. P. O'Neill, and M. C. Ferris, "Optimal transmission switching," *IEEE Transactions on Power Systems*, vol. 23, pp. 1346–1355, August 2008.

[72] D. Bienstock and S. Mattia, "Using mixed-integer programming to solve power grid blackout problems," *Discrete Optimization*, vol. 4, pp. 115–141, 2007.

[73] A. Khodaei and M. Shahidehpour, "Security-constrained transmission switching with voltage constraints," *International Journal of Electrical Power and Energy Systems*, vol. 35, pp. 74–82, 2012.

[74] P. A. Trodden, W. A. Bukhsh, A. Grothey, and K. I. M. McKinnon, "MILP formulation for islanding of power networks," Tech. Rep. ERGO 11-015, Edinburgh Research Group in Optimization, School of Mathematics, University of Edinburgh, October 2011.

[75] Reliability Test System Task Force of the Application of Probability Methods Subcommittee, "IEEE reliability test system," *IEEE Transactions on Power Apparatus and Systems*, vol. PAS-98, no. 6, pp. 2047–2054, 1979.

[76] B. Stott, J. Jardim, and O. Alsaç, "DC power flow revisited," *IEEE Transactions on Power Systems*, vol. 24, pp. 1290–1300, 2009.

[77] C. Coffrin, P. Van Hentenryck, and R. Bent, "Approximating line losses and apparent power in AC power flow linearizations," in *Proceedings of the 2012 IEEE Power & Energy Society General Meeting*, 2012.

[78] E. M. L. Beale and J. J. H. Forrest, "Global optimization using special ordered sets," *Mathematical Programming*, vol. 10, pp. 52–69, 1976.

[79] B. Avramovic, P. K. Kokotovic, J. R. Winkelman, and J. H. Chow, "Area decomposition for electromechnical models of power systems," *Automatica*, vol. 16, pp. 637–648, 1980.

[80] Reliability Test System Task Force of the Application of Probability Methods Subcommittee, "IEEE reliability test system – 1996," *IEEE Transactions on Power Systems*, vol. 14, no. 3, pp. 1010–1020, 1999.

[81] T. Achterberg, "SCIP: solving constraint integer programs," *Mathematical Programming Computation*, vol. 1, pp. 1–41, July 2009.

[82] W. A. Bukhsh, A. Grothey, K. McKinnon, and P. A. Trodden, "Network data for realistic power networks." [Online] Available:`http://www.maths.ed.ac.uk/optenergy/NetworkData/`.